8-2022

Radioluminescence Based Biochemical Sensing and Imaging Strategies to Measure Local Drug Release and pH

Gretchen B. Schober
gschobe@clemson.edu

Follow this and additional works at: https://tigerprints.clemson.edu/all_dissertations

Part of the Analytical Chemistry Commons, Bacterial Infections and Mycoses Commons, Biotechnology Commons, Chemicals and Drugs Commons, and the Therapeutics Commons

RADIOLUMINESCENCE BASED BIOCHEMICAL SENSING AND IMAGING
STRATEGIES TO MEASURE LOCAL DRUG RELEASE AND pH

_____

A Dissertation
Presented to
the Graduate School of
Clemson University

_____

In Partial Fulfillment
of the Requirements for the Degree
Doctor of Philosophy
Chemistry

_____

by
Gretchen B. Schober
August 2022

_____

Accepted by:
Dr. Jeffrey N. Anker, Committee Chair
Dr. Tzuen-Rong Jeremy Tzeng
Dr. George Chumanov
Dr. Joseph Kolis

ABSTRACT

In this dissertation we describe methods for measuring infection relevant biochemical analytes using radioluminescent and ultrasound luminescent materials. Films and nanoparticles fabricated with europium doped gadolinium oxysulfide ($Gd_2O_2S:Eu^{3+}$) are used to quantitatively measure radiolabeled pharmaceutical concentration, specifically tritium labeled vancomycin (^3H-vancomycin). Europium and dysprosium doped strontium aluminate is used to fabricate an ultrasound modulated, pH sensing film. These methods are indicated for theranostic evaluation of implant associated infection. Bacterial biofilms are inherently resistant to traditional antibiotic treatment and can coat biomedical implants. These biofilm related infections are difficult or impossible to eradicate non-invasively. As a result, implant coatings for early infection detection and prevention are a promising avenue of research. Non-invasive measurement of drug release is an important metric for development of effective treatment strategies because dosage must be sustained within a therapeutic window to be effective. *In vitro* methods of evaluating drug release are unable to replicate biological conditions and variability seen within patients. Furthermore, early detection of implant associated infection can aid early diagnosis and treatment to mitigate infection severity. For infection prevention, using a $Gd_2O_2S:Eu^{3+}$ film we are able to quantitatively measure antibiotic concentration at the implant surface, through 5 mm of tissue. We also demonstrate proof of principle for application of this technique with synthesized $Gd_2O_2S:Eu^{3+}$ nanoparticles. For early detection of infection, we have developed an ultrasound luminescent chemical imaging modality, and pH sensing film, to map local acidosis due to bacterial biofilm growth at the implant surface.

DEDICATION

This work is dedicated to my mother, **Elizabeth McKeon**, and grandmother, **Janice McCombs**. Thank you for your unwavering love and support.

ACKNOWLEDGMENTS

First, I would like to acknowledge and thank my PhD advisor, Dr. Jeffrey Anker. Throughout my years at Clemson, he has provided unwavering patience, support, and guidance. I also want to thank my PhD committee, Drs. George Chumanov, Joseph Kolis, and Tzuen-Rong Jeremy Tzeng.

I want to thank the undergraduate and graduate students (past and present) in Dr. Anker's research group. Specifically, I want to thank Dr. Melissa Rogalski and Donald Benza for their help and patience when I first started in the lab, and continued support thereafter (including all the wonderful lunches, coffee breaks, and laughs we shared). I want to thank Meenakshi Ranasinghe for the moral support and close collaboration on SARS-CoV-2 lateral flow assay development, and nanoparticle synthesis. Apeksha Rajamanthrilage, Sachindra Kiridena, and Uthpala Wijayaratna, provided much needed camaraderie as we all embarked on the goal of graduation in 2022. I also want to thank Vigjna Abbaraju, who worked diligently with me on the ultrasound luminescent chemical imaging project. I received helpful guidance from postdoctoral fellows in our lab throughout the years: Dr. Md. Arifuzzaman taught me various polymer syntheses, and Dr. Paul Millhouse helped fabricate 3D printed components for experiments.

Many of my research projects would not have been possible without the collaborative efforts of various research groups at Clemson. Specifically, Drs. Apparao Rao and Sriparna Bhattacharya, in the Clemson Nanomaterials Institute, have propelled the ultrasound luminescent chemical imaging project forward. Dr. Bhattacharya is also an incredible friend and cat-sitter, and I'm grateful to have met her. I want to acknowledge

4

TABLE OF CONTENTS

LIST OF FIGURES

9

List of Figures (Continued)

List of Figures (Continued)

List of Figures (Continued)

15

16

17

List of Figures (Continued)

Figure   **Page**

CHAPTER 1

INTRODUCTION

We describe methods for making chemical measurements, through biological tissue, using radioluminescent materials. Specifically, we use europium doped gadolinium oxysulfide (Gd_2O_2S:Eu) to monitor radiolabeled drug (^{3}H-vancomycin) release from a biomedical implant surface and demonstrate proof of principle to monitor release from nanoparticle surfaces. To monitor pH at the implant surface, we use europium and dysprosium doped strontium aluminate ($SrAl_2O_4$:Eu,Dy) paired with a pH sensitive dye. These methods are demonstrated in relation to a model of implant associated infection, as local acidosis is an indication of bacterial growth and vancomycin is a representative pharmaceutical for the treatment of biofilm related infection. However, the developed methods are intended for general application and depend on multiple factors for success. These considerations include the mechanism of radioluminescence (confined to discussion of inorganic crystals), the excitation source(s), interaction of luminescence with tissue, and collection optics.

1.1 Photon Generation: Radioluminescence Excitation and Emission

Radioluminescent materials convert ionizing radiation, such as X-Ray or beta-radiation, into visible light. These materials are used for a variety of applications that require radiation detection (e.g., biomedical diagnostics, dosimetry, industrial inspection) as well as for TV cathode-ray screens and fluorescent lighting.[1] The mechanism of

scintillator radiation conversion to visible light begins with generation of electron-hole pairs within a wide band gap material (inorganic crystal, in this case) following irradiation with high energy photon(s) (<1 MeV). This interaction occurs primarily through Compton scattering and the photoelectric effect. Compton scattered photons will often produce multiple electron-hole pairs until the energy of the photon is completely dissipated or the photon exits the crystal. The electron hole pairs then propagate throughout the crystal structure, and eventually luminescence occurs via radiative recombination of the electron and hole at luminescent centers (activators).[1] Activator ions introduce energy levels within the forbidden gap and permit more efficient radiative recombination, producing light in the visible range (**Figure 1.1**). Without luminescent activators, the return of an electron to the valence band is inefficient (due to large band gap) and energy is typically emitted via nonradiative recombination. If photons are emitted in this process, the energy is too high to be in the visible range.[2] Even when luminescent activators are present crystal defects (e.g., material point defects, grain boundaries, and surface flaws) can hinder scintillator luminescence efficiency. The scintillator crystals discussed in this work are Gd_2O_2S and $SrAl_2O_4$ doped with activators Eu^{3+}, and Eu^{2+}/Dy^{3+}, respectively.[3–5]

Imaging luminescence through tissue requires optimization of various parameters for success. Of the inherent radioluminescent material properties, some important parameters to consider include light yield (quantum efficiency), radiation stopping power (higher electron density=more stopping power), luminescence decay time, chemical stability, spectral matching between luminescence emission and photon detector, and
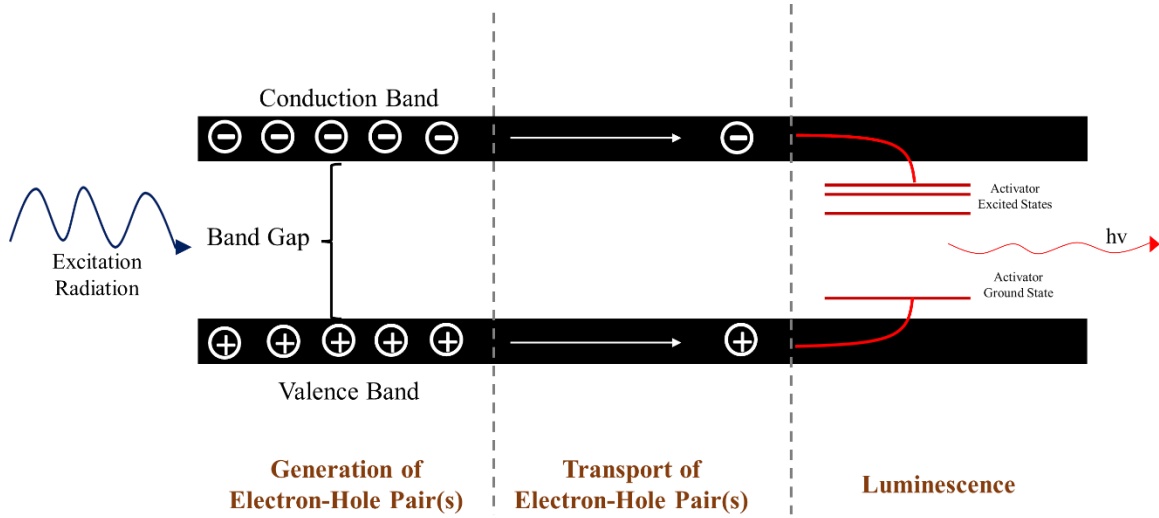
Figure 1.1. Scintillation process broken down into three steps: conversion of radiation to electron-hole pairs, transport of electron-hole pairs throughout the lattice, and radiative recombination resulting in visible luminescence.

linearity of response between incoming radiation and luminescence output. Of particular interest is light yield, which can be defined by the following equation[6,7]:

$$LY = 4.35 \times 10^5 \left(\frac{\beta SQ}{E_g[eV]} \right) \qquad (1)$$

Where β is the conversion efficiency of incoming radiation, E_g is the energy of forbidden band gap, S is the transport efficiency of electron-hole pairs through the crystal lattice, and Q is the efficiency of luminescence at emission centers. Typical band gap energies for scintillation crystals range from <1 eV to several eV. To optimize luminescence efficiency (Q), the activator ground electronic state must be above the valence band for the host crystal, and the activator excited state must be below the conduction band for the host crystal (see **figure 1.1**).[7] For example pure Gd_2O_2S crystal has a band gap energy (E_g) of 4.6 eV, and the Eu^{3+} dopant most prominent luminescence emission bands (electronic transitions $^5D_0 \rightarrow {}^7F_j$) occur due to 3.42 eV location of 4f states within that bandgap range.[8–10] The inorganic phosphors used for sensor design throughout

this dissertation emit luminescence with high efficiency (60,000 photons/MeV X-Ray for bulk $Gd_2O_2S:Eu^{3+}$). Overall, the luminescence efficiency and light yield is largely a function of the material.

The excitation sources used for the methods described in this dissertation are primarily beta-decay radiation (E_{max}=18 keV per decay for ^3H), UV light (3-30 eV per photon), and mechanical release of trapped electron-hole pairs after UV excitation via mechanical ultrasound stimulation. Beta-particles interact with matter primarily via ionization, electron orbital excitation, and bremsstrahlung X-Ray production (in cases with high-energy beta emission in high atomic number absorbers).[7] Because beta-particles and electrons have essentially equivalent mass, collisions result in significant transference of kinetic energy and electron scattering. The resulting ionization of electrons often produces secondary ionization by electrons ejected after primary collision with beta-particle.

For tritium (^3H) beta-decay, range is limited to the area immediately surrounding the radioactive isotope. For example, tritium decay is typically reported to carry a maximum energy (E_{max}) of 18 keV, but average beta emission energy is closer to $\frac{1}{3}E_{max}$ (~6 keV).[7] Given the energy of decay (E) in MeV, the range (R) in cm, of a beta particle in a given medium is governed primarily by the density of the absorber (d) in g/cm^3, and can be described by[7,11]:

$$R = \frac{0.11\left(\sqrt{1+22.4E^2}-1\right)}{d} \qquad \text{for } 0 < E < 3 \text{ MeV} \qquad (2)$$

For ^3H beta-decay in water, the range is expected to be between 0.4 and 4 μm. As a result, radioluminescence emission is dependent on the concentration and proximity of radiolabeled analyte (^3H-vancomycin) to radioluminescent material ($Gd_2O_2S:Eu^{3+}$).

22

For mechanoluminescent materials in this dissertation (i.e., $SrAl_2O_4{:}Eu^{2+}/Dy^{3+}$), UV light is used to "charge" the material. UV photons interact with the crystalline lattice, and electron clouds of the atoms, via Compton scattering and the photoelectric effect. This leads to ionization and production of electron-hole pairs (as described in section 1.1). The radiative recombination of electron-hole pairs can be slow, even in the presence of activator ions, when the absorbed photon exhibits intersystem crossing to an excited triplet state. These "trapped" electrons can be released via mechanical stimulation.[5,12,13] As a result, luminescence emission can be stimulated, point-by-point, using a focused ultrasound beam. The mechanoluminescent properties of $SrAl_2O_4{:}Eu^{2+}/Dy^{3+}$ are combined with pH sensitive dyes to map surface pH.

1.2 Photon Collection: Effect of Tissue and Optics for Light Detection

The first series of considerations for developing luminescence-based biosensors is based upon photon generation. However, even when using high energy excitation and materials that exhibit high quantum efficiency, the ability to collect and count emitted photons is another important consideration. Absorption and scattering of light by biological media detract from the overall luminescence intensity able to be collected. Once light passes through tissue to the point where it is collected, the efficiency of collection optics also has a dramatic effect.

Light interacts differently with different types of biological tissue. Tissues and fluids can be categorized as strongly scattering (skin, blood, muscle, brain, etc.) or weakly scattering (aqueous humor within the eye, cornea, etc.). Tissues containing intrinsic

chromophores are going to absorb more light, in a wavelength dependent manner. For example, tissue is most transparent to light within the near infrared region (NIR) because biological components do not strongly absorb this spectral range.[14] In short, there are a variety of factors that affect light propagation in tissue. The classical light propagation model for biological tissues is based on radiative transport theory, which depends largely on the total ballistic attenuation coefficient (μ_t) (**equation 3**) and angular distribution of scattering [15,16]:

$$\mu_t = \mu_a + \mu_s \tag{3}$$

Where μ_a (m^{-1}) represents the absorption coefficient, and μ_s (m^{-1}) is the scattering coefficient. However, despite consideration of various tissue types, it is difficult to generalize light behavior in tissue due to homogeneities inherent among living beings. As a result, luminescence based biosensors typically need to have a reference to account for tissue effects and non-uniformities, experimentally.[17–19] In addition, mechanical indentation of tissue is occasionally appropriate to minimize thickness and increase photon collection efficiency.[20]

Once luminescence has propagated through tissue, the collection efficiency of optics is the next important consideration. Spectral sensitivity of the photon detector needs to match the luminescence emission being collected. For example, traditionally a photodiode is considered optimum for wavelengths in the green-red, while photomultiplier detectors are more suitable for detection in the UV-blue spectral range. In recent years, there has been substantial development of back illuminated, cooled, charge coupled devices (CCD) that have wider wavelength range sensitivity.[1]

1.3 Description of Dissertation

Chapter 1 provides a brief introduction to the phenomenon of radioluminescence, which is important for the remainder of the dissertation, followed by a brief description of the research reported in the following chapters.

Chapter 2 describes a method to image and quantify radiolabeled drug release from biomedical implant surfaces using a radioluminescent, hydrophilic polyurethane composite film. The technique is used to quantify tritium labeled vancomycin (^{3}H-vancomycin) release from a film of Gd_2O_2S:Eu. The method is performed through 5 mm porcine muscle tissue to demonstrate feasibility for *in vivo* application. Luminescence images are acquired using a supercooled charge coupled device (CCD) camera (In Vitro Imaging System – small animal imager).

In chapter 3 we extended the work done in chapter 2 to provide proof of principle for monitoring drug release using radioluminescent, sodium fluoride doped Gd_2O_2S:Eu nanoparticles and radiolabeled vancomycin. Preliminary data is provided which demonstrates a linear correlation between concentration of radiolabeled drug and radioluminescent particles.

Chapter 4 describes the use of mechanoluminescent $SrAl_2O_4$:Eu/Dy polymer composite films for mapping pH in complex biological tissue mimic. Images are acquired as the sample is scanned, point-by-point, relative to a stationary pulsing ultrasound source and liquid light guide collection optics.

Chapter 5 contains overall conclusions and description of future directions for the work described herein. Namely the combination of mechanoluminescent and radioluminescent materials is proposed as an advantageous way to image drug release, and incorporation of radioactive material with the mechanoluminescent film may provide an alternative excitation source to UV for eventual *in vivo* application.

Finally, appendices A-C provide detailed explanation of the MATLAB scripts used for image analysis throughout this work.

References

[1]   M. Nikl, *Meas. Sci. Technol.* **2006**, *17*, R37.

[2]   G. F. Knoll, *Radiation Detection and Measurement, 4th Edition*, 4th ed., Wiley, **2010**.

[3]   J. Longjam, R. K. Singh, *Chem. Pap.* **2014**, *68*.

[4]   E. Brunet, O. Juanes, J. C. Rodriguez-Ubis, *Curr. Chem. Biol. 1*, 11.

[5]   Y. Jia, M. Yei, W. Jia, *Opt. Mater.* **2006**, *28*, 974.

[6]   G. Bressi, G. Carugno, E. Conti, C. D. Noce, D. Iannuzzi, *Nucl. Instrum. Methods Phys. Res. Sect. Accel. Spectrometers Detect. Assoc. Equip.* **2001**, *461*, 361.

[7]   M. L'Annunziata, *Handbook of Radioactivity Analysis*, 3rd ed., Elsevier Science & Technology, **2012**.

[8]   F. Wang, X. Chen, D. Liu, B. Yang, Y. Dai, *J. Mol. Struct.* **2012**, *1020*, 153.

[9]   P. A. Rodnyĭ, *Opt. Spectrosc.* **2009**, *107*, 270.

[10] M. Raukas, K. C. Mishra, C. Peters, P. C. Schmidt, K. H. Johnson, J. Choi, U. Happek, *J. Lumin.* **2000**, *87–89*, 980.

[11] W. Paul, H. Steinwedel, *Beta- Gamma-Ray Spectrosc.* **1955**.

[12] A. Feng, P. F. Smet, *Materials* **2018**, *11*, 484.

[13] B. P. Chandra, A. S. Rathore, *Cryst. Res. Technol.* **1995**, *30*, 885.

[14] V. V. Tuchin, In *Biomedical Photonics Handbook: Fundamentals, Devices, and Techniques*, CRC Press, **2019**, pp. 123–167.

[15] S. L. Jacques, *Phys. Med. Biol.* **2013**, *58*, R37.

[16] W. F. Cheong, S. A. Prahl, A. J. Welch, *IEEE J. Quantum Electron.* **1990**, *26*, 2166.

[17] T. L. Moore, F. Wang, H. Chen, S. W. Grimes, J. N. Anker, F. Alexis, *Adv. Funct. Mater.* **2014**, *24*, 5815.

[18] F. Wang, Y. Raval, T.-R. J. Tzeng, J. N. Anker, *Adv. Healthc. Mater.* **2015**, *4*, 903.

[19] F. Wang, Y. Raval, H. Chen, T.-R. J. Tzeng, J. D. DesJardins, J. N. Anker, *Adv. Healthc. Mater.* **2014**, *3*, 197.

[20] A. A. Gurjarpadhye, W. C. Vogt, Y. Liu, C. G. Rylander, *Int. J. Biomed. Imaging* **2011**, *2011*, 1.

CHAPTER 2

RADIOLUMINESCENCE IMAGING OF DRUG ELUTION
FROM BIOMEDICAL IMPLANTS

2.1 Abstract

We describe a method to noninvasively measure the concentration of radiolabeled pharmaceuticals on modified drug-eluting biomedical implant surfaces. The implants are coated with microphosphors and radiolabeled pharmaceuticals in a hydrophilic polyurethane film. The drug molecules emit radiation which excites radioluminescence in nearby phosphors; for drug released from the film, the radiation is absorbed by the surrounding media and generates no light. We applied the technique to measuring beta-emitting tritium-labeled vancomycin (^{3}H-vancomycin) concentration on the surface of an orthopedic plate. Bacteria can coat orthopedic implant surfaces and form biofilms which are resistant to antibiotics and the host's immune system. Antibiotic eluting implant coatings are thus promising candidates for infection prevention and treatment. Radioluminescence imaging permits surface-specific, noninvasive measurement of drug concentration on implant surfaces, which is an important metric for developing effective drug eluting coatings. The radioluminescence signal increases linearly with ^{3}H-vancomycin concentration, with a limit of detection (LOD) of 9.6 nCi (0.35 pmol) without tissue. We also monitored biomedically relevant drug release concentrations by spiking unlabeled vancomycin with ^{3}H-vancomycin. Using this technique, we achieve an LOD of 5.7 nmol through 0 mm of porcine tissue slices, and 38.7 nmol vancomycin through 5 mm

porcine tissue slices. Despite light scattering, drug release and reference regions are resolvable for non-invasive quantification.

2.2 Introduction

Over half of hospital acquired infections are associated with implanted medical devices, and infections are hard to treat because bacteria can form biofilms on the device surface that are resistant to antibiotics.[1,2] For example, around 5-10% of fracture fixation surgeries result in infection with variation depending largely on injury severity, location, time to surgery, diabetes, smoking, immune compromised states, revision of previously infected implant, and other risk factors.[3] Hypothesized mechanisms for antibiotic resistance in biofilms include a combination of nutrient limitation and slow growth, quorum sensing, formation of persister cells, and poor antibiotic penetration.[1,2,4–6] The minimum bactericidal concentration (MBC) for bacterial biofilms can be 10-1000 times higher than that required to eradicate planktonic bacterial infections, which is difficult or impossible to achieve *in vivo*.[7] As a result, there has been much research done to develop infection-specific imaging techniques[8–11], as well as antibiotic-releasing implants for prevention and treatment of bacterial biofilms on biomedical implants.[3,12–15] It is important that the release profile be controlled to keep local drug concentration in the therapeutic window and below toxic doses. A variety of methods are available to control the release, and there is also interest in "smart" systems with release controlled by pH and exogenous signals.[16] However, these techniques are typically difficult to evaluate *in vivo*, especially with heterogeneous environments during infection at the implant surface.
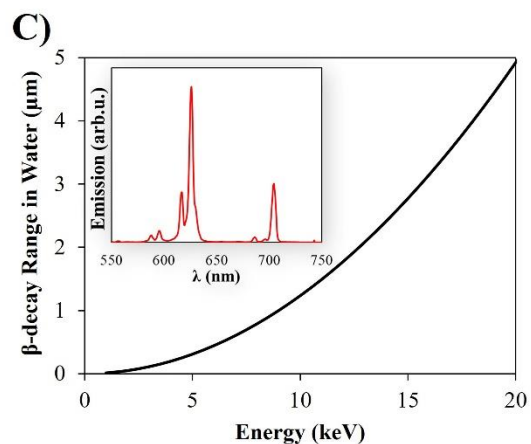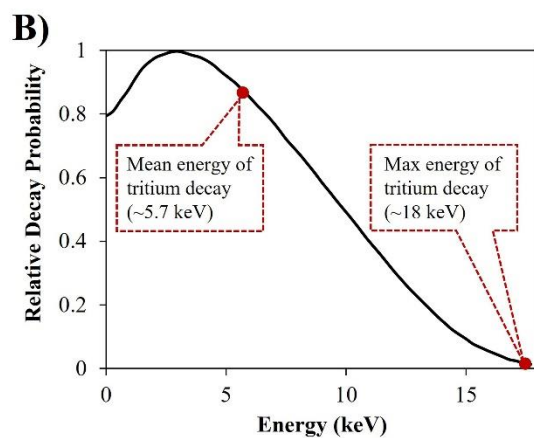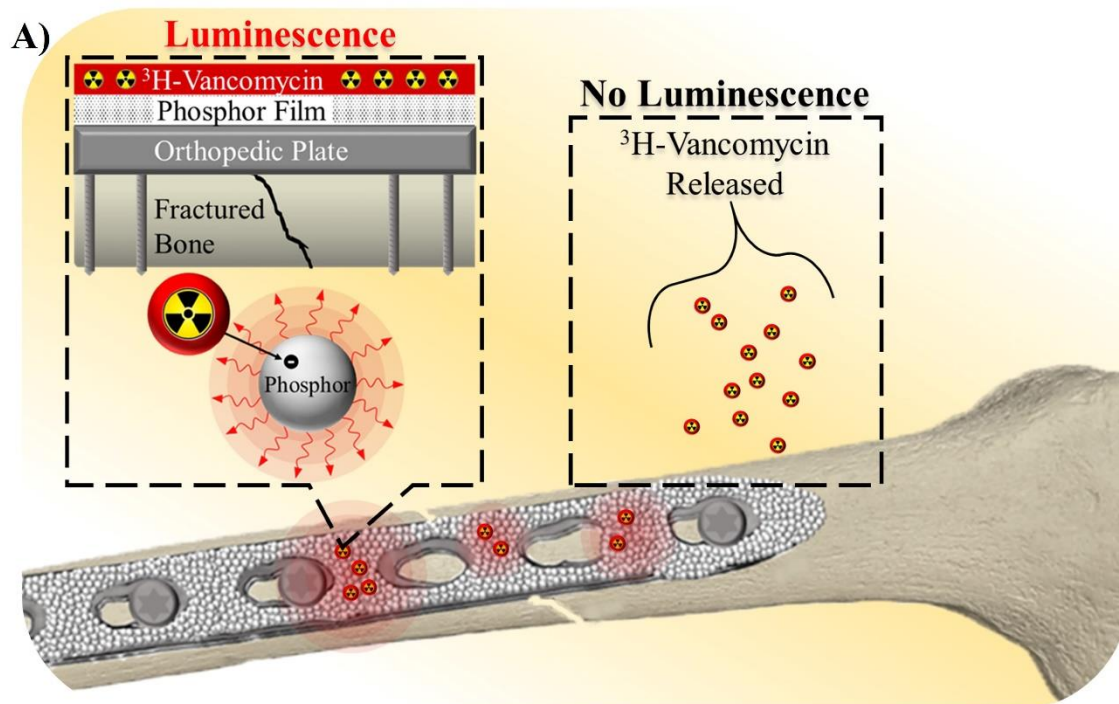
Figure 2.1. Radiopharmaceutical detection method using radioluminescent phosphors. A) Illustration of fracture fixation plate coated with radioluminescent phosphor particles. B) Relative decay probability vs energy of associated ^{3}H beta particle emission. Mean energy of tritium decay is roughly 5.7 keV but can be as high as 18 keV. C) Beta-decay range for ^{3}H in water, calculated based on E_{max}.[38] Indicates required proximity of radionuclide to radioluminescent phosphor particle for excitation and subsequent luminescence emission spectrum of $Gd_2O_2S:Eu^{3+}$ radioluminescent phosphors (inset).

Assessing local drug release and/or accumulation is quite challenging for *in vivo* applications. There have been numerous advances in non-invasive drug monitoring techniques, including use of nanomaterials as therapeutic and diagnostic drug carriers [16–19], electrical impedance[20], optical imaging[16,17,21–23], and magnetic resonance imaging (MRI)[24,25]. However, many of these techniques, particularly nanomaterial and optical techniques, rely on the use of photoactive drugs or fluorophores. This becomes challenging for technique generalization, as few pharmaceuticals are optically active especially in the tissue penetrating red/near infrared spectral region, and fluorophore labeling may interfere with drug activity *in vivo*. MRI based techniques are advantageous for imaging through deep tissue but are generally unsuitable for quantitative measurements, which is an important factor when examining drug delivery. In addition, current approaches are not capable of providing surface specific resolution in cases where drug is released from a fixed biomedical implant.

The most common methods for infection specific imaging use radiolabeled pharmaceuticals imaged with positron emission tomography (PET) or single-photon emission computed tomography (SPECT), but these require expensive instrumentation and they do not generally distinguish between drug in nearby tissue and on the implant.[10,16] ^{18}F-fluorodeoxyglucose positron emission tomography (FDG-PET) has been applied in the detection of infection, as FDG accumulates in infected tissue, thereby permitting infection specific imaging.[7,26,27] Similarly, ^{111}In or ^{99m}Tc labeled leucocyte imaging (WBC imaging), and ^{99m}Tc-Infecton (Ciprofloxacin) have been paramount for inflammation, and infection specific imaging.[9,28] SPECT, particularly SPECT/CT, has been used in

conjunction with bone scintigraphy for identification of inflammatory and infectious processes in soft tissues as well.[29,30] However, these approaches do not provide implant surface specific information. PET radioisotope contrast agents also typically have short half-lives, which requires close proximity to cyclotron and chemical synthesis facilities.[31]

Radioluminescence is a promising candidate for biomedical application and has recently been used in nanoparticle-based molecular imaging and radioluminescence imaging (RLI).[32] Cerenkov radiation luminescence has been used for luminescence tomography, and tumor monitoring, but the phenomenon generates low light yield. Typically, longer exposure times (3-5 minutes minimum) and higher energy radioisotopes are required (>219 keV), and obtaining quantitative results using Cerenkov luminescence is challenging.[33,34] Alternatively, flexible RLI has recently been done with ^{18}F-FDG, using a flexible terbium doped gadolinium oxysulfide film in order to improve signal to noise ratio when imaging tumors, as compared to traditional RLI.[35] However these techniques have similar drawbacks to PET and SPECT imaging with regard to short half-life radioisotopes, and lack of surface specificity.

The use of scintillators to quantify radiolabeled analytes is well-documented in a technique called scintillation proximity assay (SPA).[36] However application has typically been confined to radioimmunoassays, enzyme assays, and ligand-receptor binding assays.[37] We describe a method to image surface-specific drug release and/or accumulation at the biomedical implant surface. We coated an implant with a radioluminescent phosphor film and radiolabeled a fraction of vancomycin (a representative antibiotic often used to treat implant infection) as a tracer to monitor release

32

near the implant surface. The presence or absence of that drug at the implant surface is indicated by the presence or absence of luminescence signal (**Figure 2.1**). In this study we have used tritium labeled vancomycin (^{3}H-vancomycin), which decays via beta-radiation, and $Gd_2O_2S:Eu^{3+}$ radioluminescent phosphors. The energy of an emitted beta particle affects its range in any given medium; higher energy particles travel farther. The range can be calculated by considering the energy of the beta-particle, and the density of the medium.[38] In water, for example, ^{3}H beta-particles decay with a relatively low energy (~6 keV average), and will travel a maximum of ~4 μm, with an average range closer to ~0.4 μm. If the ^{3}H-Vancomycin can excite a phosphor film immobilized on the surface of an implant, then the drug is within 4 μm of that implant. This permits unprecedented surface specificity in monitoring drug release or accumulation. To translate the technique for imaging through biological tissue, rare earth doped gadolinium oxysulfide phosphors (e.g. $Gd_2O_2S:Eu^{3+}$) are selected due to the high quantum efficiency (60,000 photons MeV^{-1} X-ray in bulk gadolinium oxysulfide), distinct and narrow emission peaks, high optical penetration depth of red emission, low toxicity, and robust photostability of the material.[16,31] These particles emit light with narrow spectral peaks when excited by blue light, X-Rays, or alpha/beta radiation. $Gd_2O_2S:Eu^{3+}$ has emission peaks between 560 nm and 750 nm due to $^5D_0 \rightarrow {}^7F_j$ (j = 0-4) transitions of Eu^{3+} ions.[39] This region of visible light is ideal for *in vivo* imaging because blood and tissue will absorb and scatter less light at longer wavelengths. Using the combination of ^{3}H-Vancomycin and $Gd_2O_2S:Eu^{3+}$, we can detect drug release from an implant surface with inherent micrometer resolution, permitting unprecedented surface specificity in quantitative drug monitoring. Tritium

labeling does not interfere with the structure or action of the labeled drug and does not rely on photoactive properties of the drug itself. As a result, this technique may be expanded for use with other implant types and pharmaceuticals with relative ease.
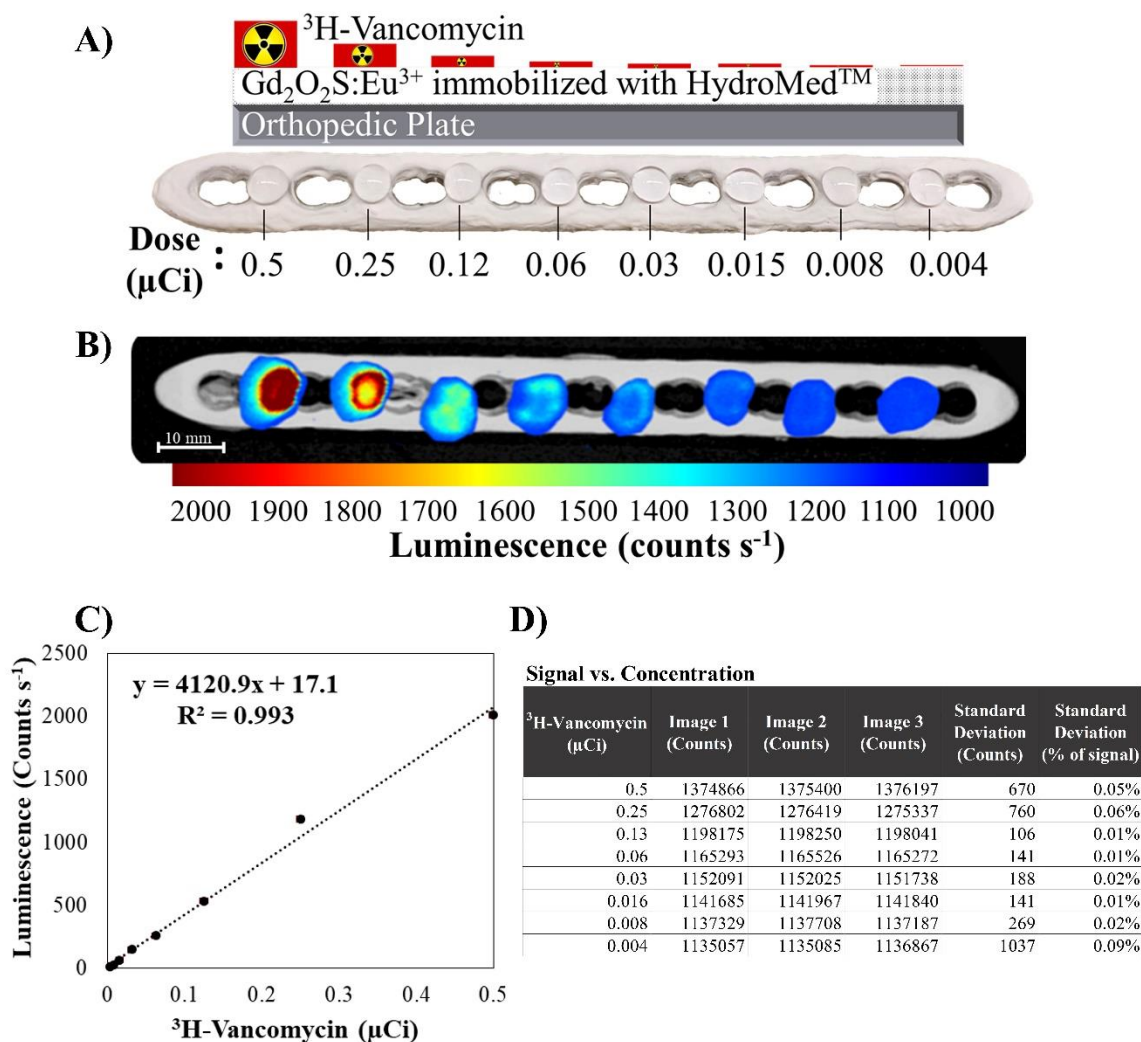
Figure 2.2. A) Fracture fixation plate coated with Hydromed D3^{TM} and $Gd_2O_2S:Eu^{3+}$ microparticles. ^{3}H-Vancomycin deposited with decreasing activity left to right. B) Superimposed pseudo-colored luminescence intensity image overlayed with reflected light image taken with IVIS Lumina. Regions of luminescence indicated with color gradient map, generated in MATLAB. Background manually removed to show regions of interest. C) Luminescence intensity plotted against ^{3}H-Vancomycin activity. D) Raw luminescence intensity values (without blank or background correction) for each 30 x 30 px region in the concentration gradient. Standard deviation values shown in both "counts" and "% of signal."

2.3 Results and Discussion

We developed an implant coating and imaging technique to detect drug release. First, we demonstrated the linear dependance of luminescence signal on ^{3}H-Vancomycin concentration using a concentration gradient. Next, we demonstrated the ability to monitor drug release, and examined the effect of biological tissue on the emission signal.

2.3.1 Signal vs. Concentration/Dose

As shown in **Figure 2.2A-C**, the luminescence spots become brighter with increasing ^{3}H-Vancomycin concentration. The luminescence vs. ^{3}H-Vancomycin plot depicts an average of 3 images captured consecutively (raw luminescence data and standard deviation values found in **Figure 2.2D**). The integrated luminescence intensity in any spot is proportional to the activity/amount of radiolabeled vancomycin deposited, demonstrated by the highly linear correlation between photon emission and activity deposited (R^2=0.99). This is expected because the luminescence depends upon the number of beta emissions near the phosphors, provided that all the vancomycin is deposited within ~2 μm of the phosphor surface (since the average decay range for ^{3}H is ~0.4 μm in water and similar density materials such as HydroMed D3^{TM}).[40] ^{3}H-vancomycin generates 3.7×10^4 decays s^{-1}μCi^{-1} and, theoretically, if each decay deposits all its energy in the microphosphors, produces 342 photons per decay (5.7 keV average decay energy for ^{3}H * 60 photons per keV bulk Gd_2O_2S:Eu^{3+} radioluminescence quantum efficiency with X-ray excitation), then we expect ~1.7×10^7 photons s^{-1} μCi^{-1} to be generated.[16,41] In our experiment we expect fewer photons μCi^{-1} for five reasons: 1) not all tritium decay energy is absorbed by the phosphors (i.e. some of the energy is deposited in the water and

HydroMed D3^{TM}); 2) the beta luminescence efficiency may be lower than X-ray efficiency since energy is preferentially deposited near the microphosphor surface – which is quenched compared to bulk[35,36]; 3) Some of the luminescence is absorbed in the phosphor film, especially for thick samples with much internal scattering, or scattering and absorption in tissue (if present); 4) only 5% of the 4π steradian solid angle is collected by the objective at maximum f-number of 1; 5) There is light loss in lenses and imperfect detector quantum efficiency.

In our experiment without tissue, we detected 5×10^3 photons s^{-1} μCi^{-1} (~1 photon per 8 beta emission events), which is 0.04% of the maximum number of photons we expect could be generated. Adding the ^{3}H-vancomycin directly to the microphosphors (without any HydroMed D3^{TM}) in a white microwell plate increases the signal (**Figure 2.3**); at low particle concentrations with well-washed particles the signal is 5x brighter than in the HydroMed D3^{TM} (0.2% of maximum theoretical number), although it decreases with increasing particle concentration especially for unwashed particles, presumably due to scattering and optical absorption by the microphosphors. In principle, we expect the efficiency could be increased by 1-2 orders of magnitude using a light guide with less loss and higher numerical aperture, and the last 1-2 orders of magnitude might be improved by reducing surface quenching (e.g., using more deeply penetrating, higher energy beta-emitters, or by embedding and annealing the emitters in the phosphors). However, even

A) Unwashed Gd₂O₂S:Eu³⁺ **B)** Washed Gd₂O₂S:Eu³⁺ **C)**
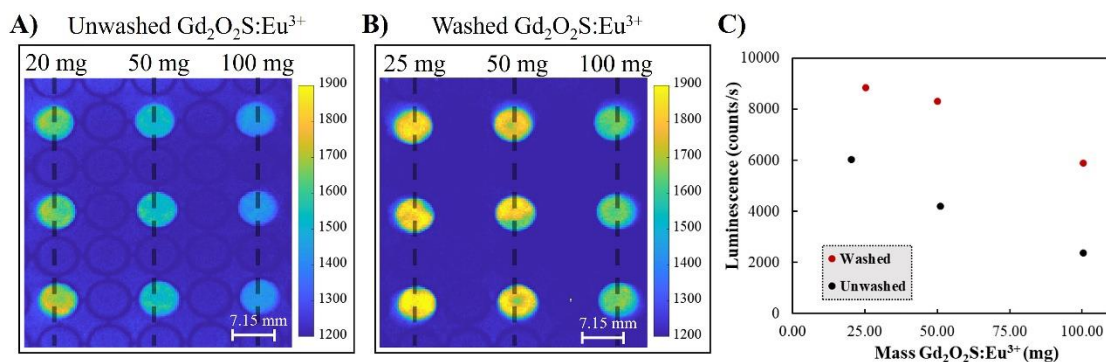
Figure 2.3. Radioluminescence images of white microwell plates containing 0.25 µCi ^{3}H-vancomycin and A) unwashed Gd$_2$O$_2$S:Eu^{3+} microphosphors; B) washed Gd$_2$O$_2$S:Eu^{3+} microphosphors. Samples are dried of solvent, and do not contain Hydromed D3. C) The luminescence increase obtained by washing the particles and reducing phosphor mass. This experiment is done to assess the effect of Hydromed D3, a pre-wash step, and Gd$_2$O$_2$S:Eu^{3+} self-quenching, on β- excitation and particle emission efficiency.

with its inefficiencies, the current system provides a clear linear increase in luminescence with ^{3}H-vancomycin concentration using relatively low activity.

Based on standard deviation of the blank intensity (s_b), and the slope of the linear regression line from the concentration gradient (m) we find a concentration LOD ($3*s_b/m$ = 9.6 nCi = 0.35 pmol vancomycin) and a limit of quantification ($10*s_b/m$ = 32 nCi or 1.2 pmol vancomycin). This is sufficient for the application: the minimum vancomycin inhibitory dose (MIC) is 1.5 mg L^{-1} [42], and typical drug loading concentrations, intended for localized release over time, are on the milligram scale. [43,44] Since picomoles of ^{3}H-vancomycin can be measured with this technique, ^{3}H-vancomycin can be added as a tracer to therapeutic, un-labeled vancomycin to track release. These images are acquired using a 2 min exposure time, but longer exposure time would increase the signal-to-noise ratio, thereby improving sensitivity. In practice, exposure time is likely limited to ~30 minutes

or eventual applications in animal or human subjects due to need for keeping subject still and issues relating to cosmic spike removal.

2.3.2 Monitoring Drug Release

To demonstrate that the technique can be used to track drug release, we measure luminescence as the plate, coated with unlabeled Vancomycin and ^{3}H-Vancomycin as a tracer, is periodically submerged in DI water. Unlabeled Vancomycin is spiked with ^{3}H-Vancomycin to monitor biologically relevant concentrations of drug while keeping the radioactivity as low as reasonably achievable for the technique. Specifically, in the signal vs. concentration experiment, only ^{3}H-Vancomycin is used with an activity of 1.9×10^4 μCi/mg (i.e. we used ~53 ng total ^{3}H-Vancomycin at the highest activity). For the subsequent drug release study, the ^{3}H-Vancomycin is mixed with unlabeled Vancomycin in a mass ratio of 1:5000 (i.e., we used ~210 ng of tritium labeled vancomycin and 1 mg of unlabeled vancomycin). A recent study found that a mixture of 0.1 mg vancomycin and 0.2 mg of chitosan plasma deposited on a tibial plate prevented infection in a *staph aureus* challenge rabbit study.[45] The blank and constant drug reference region are encapsulated in PDMS to prevent any changes in drug concentration at the surface to have a constant region for comparison through tissue section. As drug is dissolved by the water and released from the drug release region, the luminescence intensity goes down proportionally while the blank and constant drug reference regions maintain constant luminescence intensity (**Figure 2.4A**). The luminescence vs. Vancomycin released plots depict an average of 3 images captured consecutively for 0 mm tissue, and 1 image captured
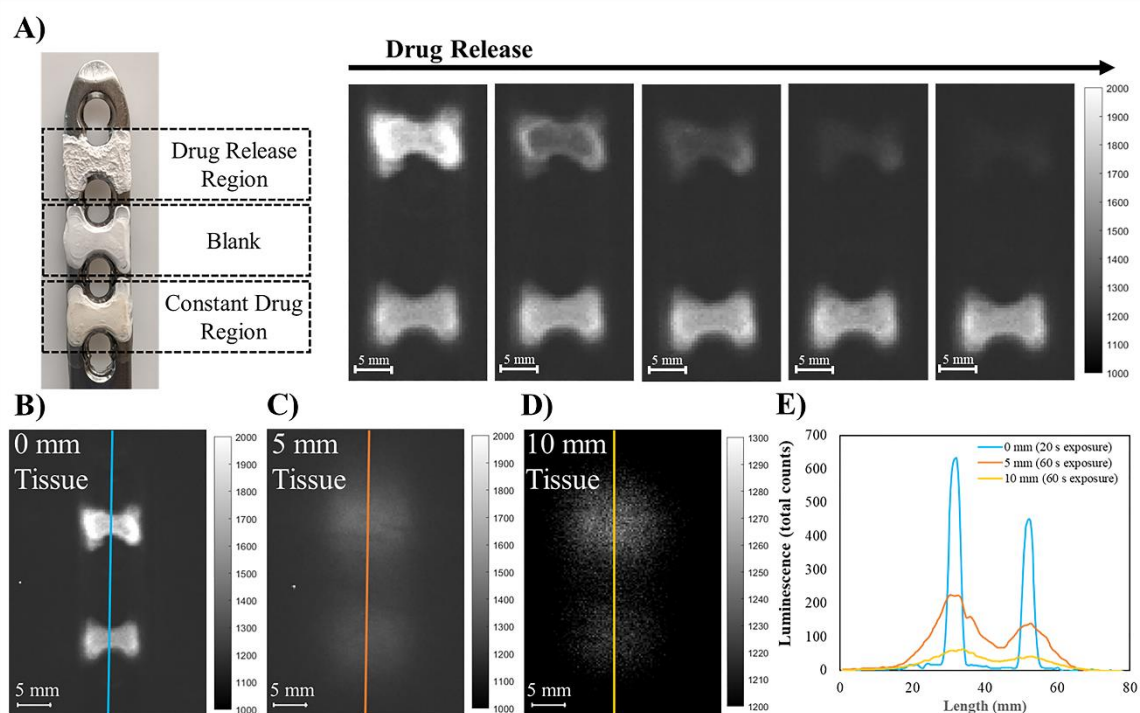
Figure 2.4. A) Fracture fixation plate coated with HydroMed D3™ in three regions. Drug release region and constant drug reference region contain ^{3}H-Vancomycin. Blank and constant region are encapsulated using PDMS. Images demonstrate luminescence decrease in drug release region as drug elutes from surface. Images captured using IVIS Lumina, with color map representing luminescence intensity B, C, and D) Luminescence regions of interest are imaged through 0 mm, 5 mm, and 10 mm of porcine tissue. Vertical line through each indicates the line used for the intensity profile in E. E) Intensity profile plotting signal intensity vs. location for vertical line through each image.

for 5 mm tissue (raw luminescence data and standard deviation values for 0 mm tissue experiment can be found in **Figure 2.6C**).

The plate is imaged through 0 mm, 5 mm, and 10 mm of porcine tissue (**Figure 2.4 B, C, D**). Light scattering in the tissue causes the image to blur so that features are poorly resolved. Previous studies have shown that the point spread function is about 20 mm for 650-800 nm light through 10 mm of tissue (in slab geometry).[46] The intensity profile of vertical lines through the center of each image demonstrates the signal decrease and spread for the drug release region (left-most peak) and constant drug reference region (right-most

peak) (**Figure 2.4E**). The full-width half-max (FWHM) for the signal through 5 mm, and

10 mm of tissue, calculated after four iterations of gaussian smoothing (**Figure 2.5A-B**) to

reduce image noise, is 13.1 mm, and 16.5 mm, respectively. If the reference region is

separated by >16.5 mm, it can be resolved from the drug eluting region through 10 mm

tissue. If they are closer, the reference may need to be distinguished from the sensor region,

e.g., using spectrally distinct scintillators.
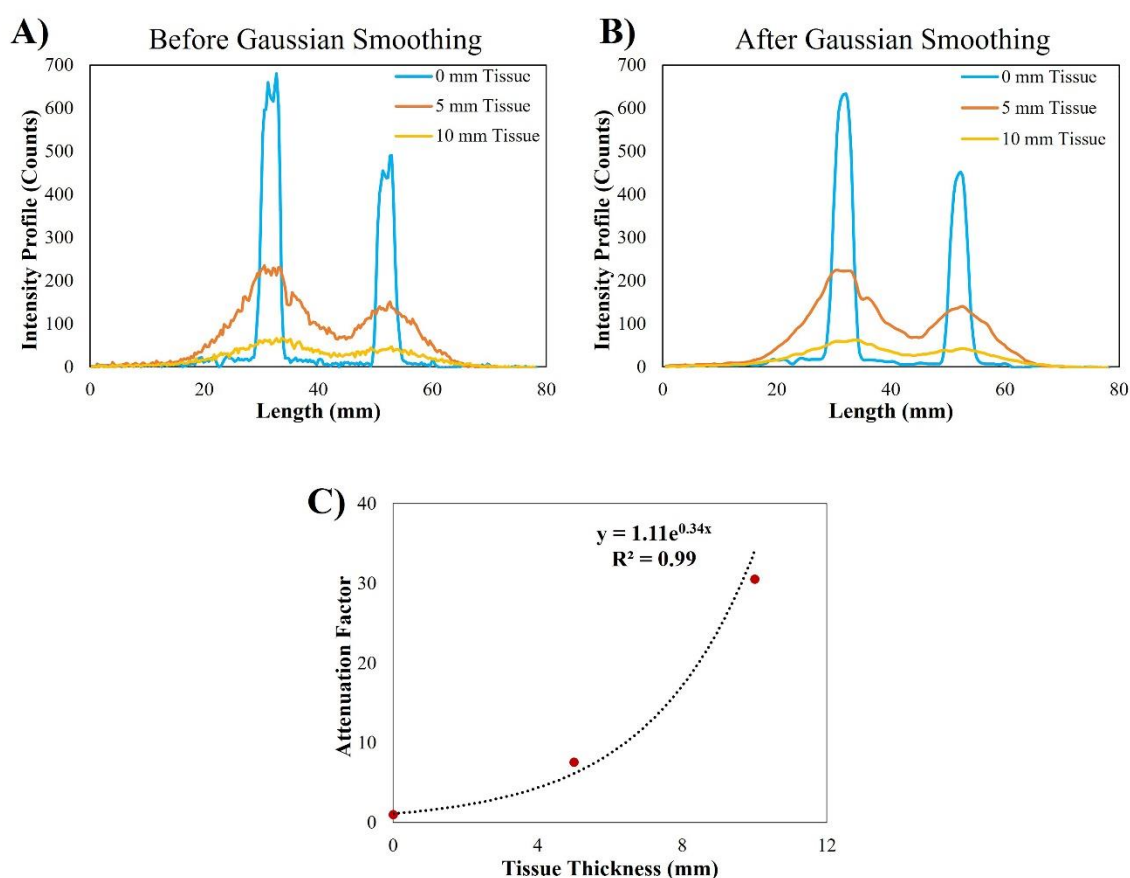
Figure 2.5. Intensity profile of a vertical line drawn through the center of the implant, from images taken through 0, 5, and 10 mm of porcine tissue. The left-most peak represents the drug release region and the right-most peak represents the constant drug reference region. A) The plot before gaussian smoothing. FWHM of left-most peak for 0 mm tissue is 3.36 mm. B) The plot after four iterations of gaussian smoothing. FWHM of left-most peak for 0 mm tissue is 3.66 mm. C) Luminescence signal attenuation factor vs tissue thickness. The luminescence signal is attenuated exponentially with tissue thickness. Signal decreases by an attenuation factor of ~7.6 through 5 mm tissue, and a factor of 30 through 10 mm of tissue. The exponential fit is useful for determining how much the luminescence signal is expected to decrease through larger tissue depths.

In addition to reduced spatial resolution, the total signal intensity decreases when imaged through tissue due to a combination of absorption and scattering. The integrated signal decreases by a factor of ~7.6 through 5 mm of tissue, and a factor of ~30 through 10 mm of tissue in the range of reported effective attenuation coefficients.[47] The attenuation coefficient increases exponentially with tissue thickness, as shown in **Figure 2.5C**. Despite tissue signal scattering and absorption, the drug release region and constant drug reference luminescence can be resolved due to the spatial separation of the regions (**Figure 2.4C, D**). Since the tissue thickness is roughly constant over the region imaged, the ratio between drug release and reference regions accounts for common mode attenuation in the tissue. After an initial equilibration period, as HydroMed D3™ absorbs water, the drug release profile is highly linear, with R^2 values of 0.99 without tissue, and 0.98 with 5 mm of porcine tissue (**Figure 2.6**). Despite equal amounts of ^{3}H-vancomycin being deposited, the constant drug reference exhibits lower luminescence intensity compared to the initial drug release region intensity. This is due to the PDMS layer deposited on the blank and constant drug reference. The deposited PDMS interferes with the ^{3}H-vancomycin coating, likely placing >2 μm distance between the phosphor film and some of the ^{3}H-vancomycin molecules, thereby inhibiting efficient excitation. Nonetheless, the signal remains constant after coating (HydroMed D3™) equilibration.

A)

0 mm Tissue

B)
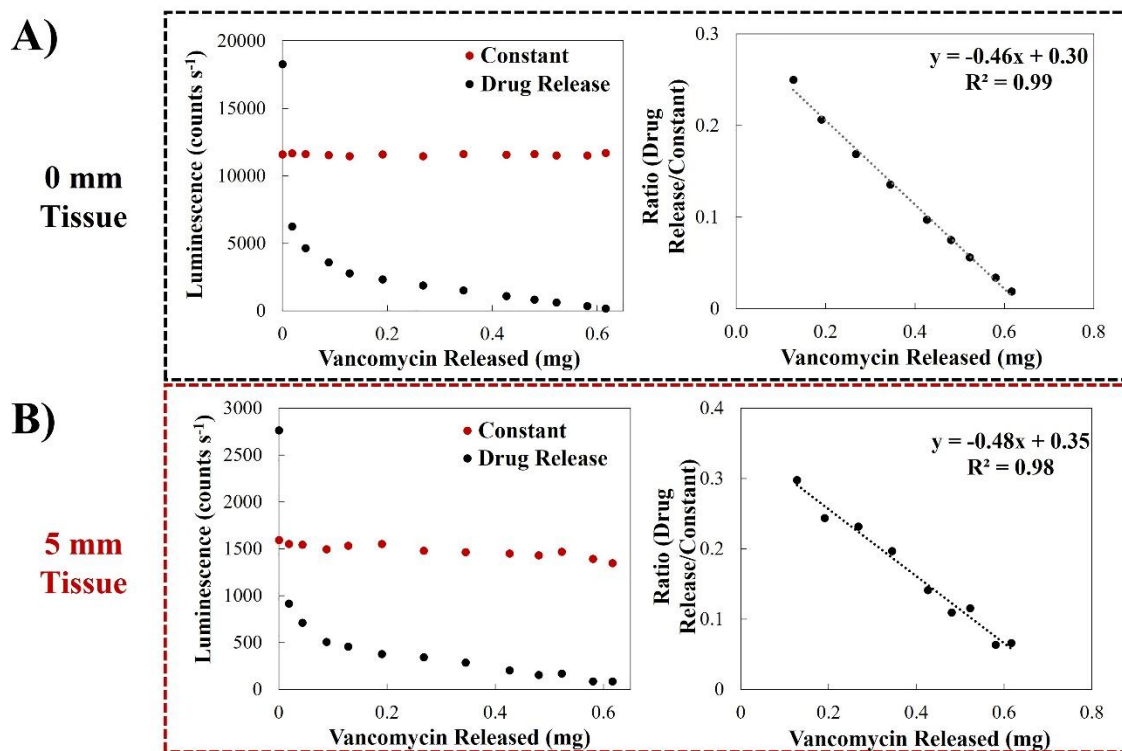
5 mm Tissue

C) **Drug Release (0 mm Tissue)**

Drug Release Point	Image 1 (Counts)	Image 2 (Counts)	Image 3 (Counts)	Standard Deviation (Counts)	Standard Deviation (% of signal)
0	1510714	1512634	1511931	971	0.06%
1	1268640	1262438	1261348	3933	0.31%
2	1235932	1230210	1229180	3638	0.30%
3	1213099	1207972	1207829	3002	0.25%
4	1194906	1191784	1192631	1615	0.14%
5	1184519	1183116	1183003	845	0.07%
6	1174783	1173904	1174178	450	0.04%
7	1166927	1166780	1167081	151	0.01%
8	1158023	1158430	1158022	235	0.02%
9	1152723	1152721	1152209	296	0.03%
10	1148127	1148408	1148411	163	0.01%
11	1143223	1143291	1143094	100	0.01%
12	1153824	1151351	1150116	1888	0.16%

Figure 2.6. A) Luminescence vs ^{3}H-Vancomycin without tissue. Left graph shows constant drug reference and drug release region. Right graph shows the ratio of the linear region of drug release/constant drug reference, after Hydromed D3 equilibration. B) Same as A) except images acquired through 5 mm porcine tissue. C) Raw luminescence intensity values of the 30 x 30 px drug release region (without blank or background correction) for each drug release point. Standard deviation values shown in both "counts" and "% of signal."

The blank region between the drug release and constant drug reference could not be resolved through tissue due to scattering. This can be remedied by coating the blank region a sufficient distance away from the drug release and constant reference regions (>13.1 mm for 5 mm porcine tissue). The blank region is useful for background subtraction because $Gd_2O_2S:Eu^{3+}$ generates a background from long-lived afterglow following earlier exposure to room light, even in the absence of ^{3}H-vancomycin. Consequently, a blank region must be subtracted to account for background luminescence not caused by ^{3}H-betaluminescence (this especially affects measurements with low concentrations of ^{3}H-vancomycin). Because the blank region could not be resolved through tissue, the blank is estimated using the value of the blank without tissue adjusted using the attenuation factor determined from the constant drug reference. Additionally, in **Figure 2.7** we show a correction that can be done to account for light emission crosstalk between the drug release and constant drug reference when imaged through tissue. Crosstalk is estimated to be ~5%, although deconvolution of the intensity profile (**Figure 2.4E**) would be required to determine the exact value. The effect is minimal but permits correction of the artificially high signal of the drug release plot through 5 mm tissue relative to the same plot with 0 mm tissue. Nonetheless, using only a 4 µCi spike of ^{3}H-vancomycin in an otherwise unlabeled sample of vancomycin, we find a LOD of 38.6 nmol (56 µg) vancomycin through 5 mm of tissue. For tissue depths >10 mm, exponential attenuation of luminescence signal with tissue thickness presents a challenge with signal intensity decreasing by a factor of 30 per centimeter (**Figure 2.5C**). However, the decreased signal can be compensated for by increasing exposure time past 60 s, improving optical collection efficiency, and/or using a
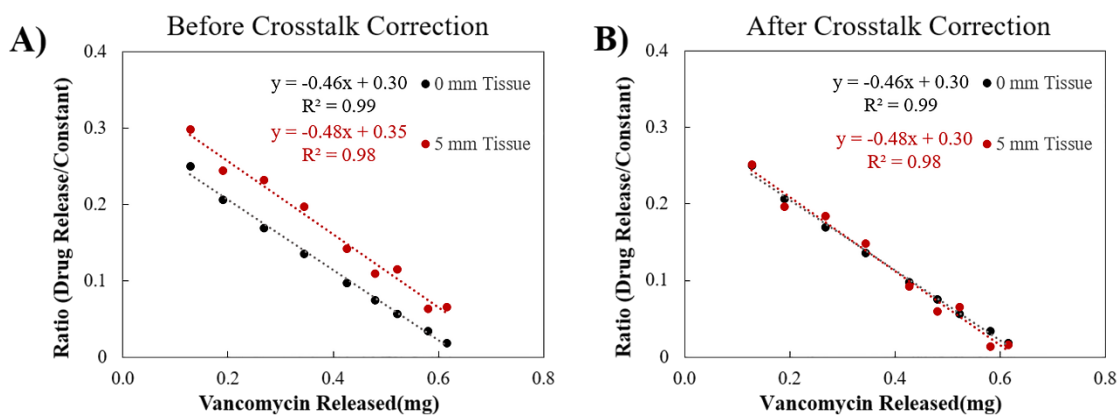
Figure 2.7. A) Drug release intensity ratio plots through 0 mm and 5 mm porcine tissue, A) before crosstalk correction, and B) with an additional correction for 5% signal crosstalk. When imaged through tissue, some of the signal from the drug release region bleeds in to the constant drug reference region due to scattering (and vice versa). This causes the drug release plot to have an artifically higher signal than the plot without tissue.

higher ^{3}H-vancomycin activity. Additionally, the effective tissue thickness can be decreased by mechanical indentation to the region of interest when imaging.[48]

2.3.3 Radiation Dose Concerns

Our technique could have medical or pre-clinical applications. Medical procedures should use doses as low as feasible but must balance the potential risks from extra radiation (especially long-term potential for oncogenesis) against immediate medical needs. Risks depend on many factors, including patient age, radioisotope chemical form, route of entry, and clearance half-life. The most commonly employed linear no-threshold model suggests that incidence of deadly cancers increases by 5.5% per 1 Sievert (Sv) effective full-body radiation dose (1 Sv represents the equivalent biological effect of 1 Gray (Gy), or 1 joule kg^{-1}).[49] For routine imaging studies, effective doses are typically between 0.1-20 mSv. As a contrast, when tissue ablation is desired (e.g. in high dose rate brachytherapy and to treat

ectopic bone) doses are typically >12 Gray (Gy).[50] Nuclear medicine techniques to image bone healing and infection diagnostics typically use ^{18}F PET and ^{99m}Tc SPECT administered intravenously at dosages between 5-10 mCi, and 20-30 mCi, respectively.[51,52] Although tritium is not used in imaging studies because the beta emission is not energetic enough to penetrate through the tissue (except if a nearby scintillator converts the energy to light), the ICRP estimates that a 20 mSv effective full body dose would require 30 mCi for tritiated water, 24 mCi for ^{99m}Tc, and 11 mCi for [18]F.[53]. Tritium labeled pharmacokinetic studies in patients typically use 200 µCi doses.[54]

Less than 1 µCi of ^{3}H-vancomycin is used in the signal vs. concentration/dose experiment, and the drug release portion of our study uses a maximum of 8 µCi ^{3}H-Vancomycin. We note that tritium has a much longer radioactive half-life than most imaging radionuclides such as ^{99m}Tc and [18]F (12.3 years, 6 hours, and 1.8 hours, respectively).[40,55,56] Dose is thus limited by biological clearance rather than physical half-life. The ICRP estimate is based upon a 10-day circulation half-life for tritiated water. The vancomycin has an even shorter circulation half-life (6 hours).[57] Although the implant increases the amount of time the radioactive drug is in the body (with release programmed over days or weeks), while drug is in the implant coating it primarily irradiates the polymer coating rather than the tissue. Specifically, radiation exposure is localized to tissues at the interface within ~0.4 µm of the coating surface (average beta decay range average 5.7 keV ^{3}H beta particle in tissue), although a smaller fraction of energy is deposited within 5 µm from the surface (maximum 18.6 keV beta emission when normal to the surface).[58] For a drug-eluting coating several hundred micrometers thick which releases drug over days or

weeks, the radiation dose to the tissue from the interface is small compared to the dose from released drug. For the constant drug region, which is encapsulated with several hundred μm of PDMS, only the polymer experiences radiation, not the tissue. Although leakage of ^{3}H-Vancomycin from the encapsulated region is not expected to occur, any leakage will be cleared from the body at the same rate as the ^{3}H-Vancomycin released from the drug release region.

As a final reference point, the EPA declares a Maximum Contaminant Level (MCL) of 14 μCi per year (assuming an intake of 2 L water per day at 20,000 pCi/L tritium activity) for beta radiation in drinking water.[59] Although these dose limits specifically do not apply to medical exposures which can be much higher, the dose we employed in our experiment is below this level too. In summary, radiation used should be as low as feasible, and the radiation used in these experiments was quite low by most medical standards.

2.4 Methods

2.4.1 Fracture Fixation Plate Preparation

A 9-hole, 3.5 mm Small Fragment Locking Compression Plate (LCP™ part number 223.591, DePuy Synthes USA Products, LLC, West Chester, PA, USA) is coated with $Gd_2O_2S:Eu^{3+}$ microphoshor particles (8 μm median diameter, part number UKL63/N-R1, Phosphor Technology LTD, Stevenage, UK) using HydroMed™ D3 polyurethane (AdvanSource Biomaterials Corp, Wilmington, MA, USA). The HydroMed™ D3 and $Gd_2O_2S:Eu^{3+}$ microphoshor particles are combined in a 1:30 ratio, in dichloromethane. Characterization of the phosphor particles is performed by Phosphor Technologies using a

Coulter Counter with 100 μm aperture: 95 volume % below 13.2 μm diameter (**Figure 2.8B**). The LCP™ is coated with the mixture via drop wise deposition and solvent evaporation. 3 layers are deposited to ensure uniform coating. **Figure 2.8A** depicts an example of one layer, imaged using Nikon Eclipse TE2000-U microscope (Nikon
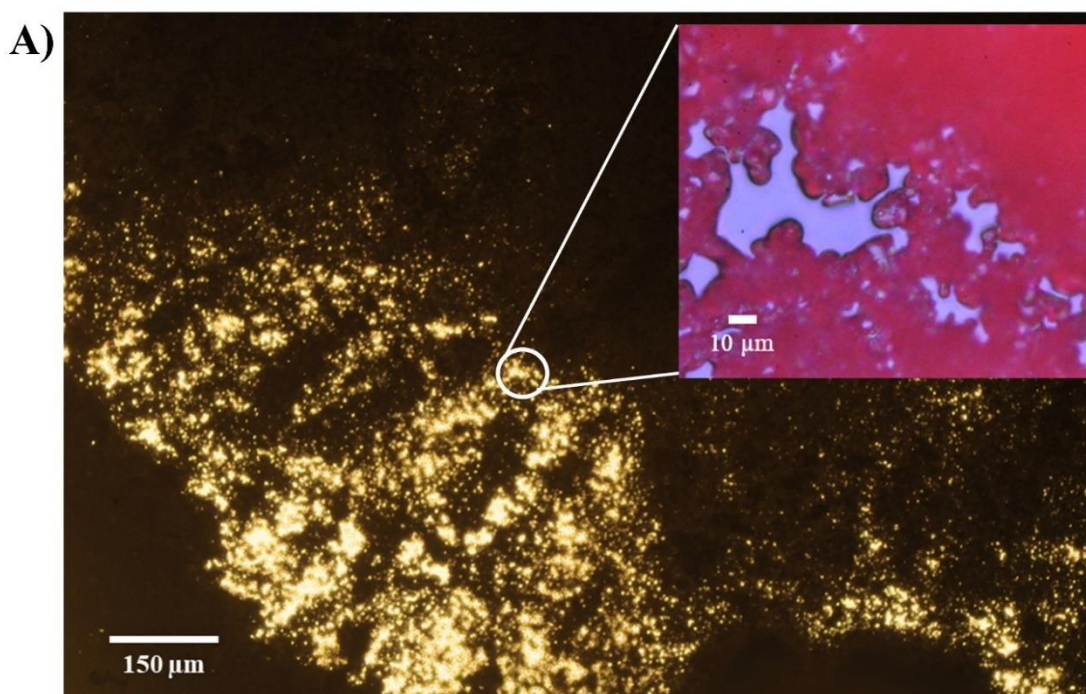
B) Particle size distribution – by Coulter Counter (100 μm Aperture)

Ultrasonic Disperson. Sizes at listed Volume %

Vol %	5	25	50	75	95
μm	4.7	6.5	8.0	10.0	13.2

Quartile Deviation: 0.21

Figure 2.8. A) Microscope images of $Gd_2O_2S:Eu^{3+}$ microphosphors in a thin layer of Hydromed™ spread over a glass slide (a thin region at the edge was selected so that the particles could be distinguished). Three layers are deposited onto the LCP™ to ensure uniformity. Primary image shows brightfield light transmission image taken at 4X plus 1.5X magnification (scale bar 150 μm). Inset image is taken at 40X plus 1.5X magnification, with UV excitation to demonstrate luminescence and packing. B) $Gd_2O_2S:Eu^{3+}$ microphosphor characterization performed by Phosphor Technologies LTD.

Instruments Inc, Melville, NY, USA). The HydroMed™ D3 permits immobilization of the microparticles on LCP™ surface.

2.4.2 Vancomycin Deposition – Signal vs. Concentration/Dose

^{3}H-Vancomycin (27.5 Ci mmol^{-1}, ViTrax Radiochemicals, Placentia, CA) is prepared via serial dilution using deionized water and deposited in 8 spots on $Gd_2O_2S:Eu^{3+}$ coated LCP™. The deposited ^{3}H-Vancomycin spots contain 0.5, 0.25, 0.12, 0.06, 0.03, 0.015, 0.008, and 0.004 μCi ^{3}H (26.8, 13.4, 6.7, 3.4, 1.7, 0.8, 0.4, and 0.2 ng Vancomycin). Following ^{3}H-vancomycin deposition, LCP™ is dried at room temperature (~23°C), to evaporate any remaining solvent.

2.4.3 Vancomycin Deposition – Drug Release

This technique involves the use of three regions, one drug release region, one blank region, and one constant drug reference region. The drug release and constant drug reference regions must be sufficiently separated to visually distinguish after emission signal blurring and point spread as it passes through tissue. The fracture fixation plate is prepared using the drop coating and solvent evaporation method of 1:30 HydroMed™ D3 and $Gd_2O_2S:Eu^{3+}$ microphoshor particles in dichloromethane. An X-Acto Precision Knife is used to cut the uniform coating into three distinct regions (the drug release region, blank region, and constant drug reference region) before Vancomycin deposition. To slow drug release, the deposited vancomycin mixture is prepared with 10 mg mL^{-1} unlabeled Vancomycin, 0.04 mCi mL^{-1} ^{3}H-vancomycin, and 5 mg mL^{-1} chitosan, in 1 M acetic acid. 100 μL of mixture (4 μCi ^{3}H) is deposited on the drug release region and constant drug

reference regions. The constant drug reference region is sealed using polydimethylsiloxane (PDMS), in order to prevent drug elution and produce a consistent emission signal.

2.4.4 Image Acquisition

Radioluminescence images are acquired on a small animal imager (IVIS Lumina XR, Perkin Elmer, Waltham, MA) under luminescence photograph mode (no external light source). For signal vs. concentration experiment, 3 images are acquired consecutively with 120 s exposure time, medium binning, field of view "C", and an aperture f-stop of 1. The experiment is performed 1 time. For drug release experiment, 3 images are acquired consecutively with 20 s exposure time (0 mm tissue), and 1 image is acquired with 60 s exposure time (5- and 10-mm tissue) at each drug release point. The experiment is performed 1 time. For limit of detection and limit of quantification, the LCP™ is imaged consecutively 10 times with an exposure time of 120 s each (0 mm tissue). Other settings: medium binning, field of view "C", and f-stop of 1. The sample holder is manufactured using a 3D printer (MAKEiT, Inc, Alhambra, CA, USA) and white, acrylonitrile butadiene styrene (ABS) filament. The sample holder is attached to the IVIS stage using double-sided tape to ensure consistent placement of the implant in the imaging chamber. Raw

luminescence images are collected and analyzed via custom MATLAB scripts [**appendices A-C**].

2.4.5 Tissue Preparation

Porcine tissue (pork, center cut loin chops, boneless) is acquired from the supermarket (Walmart Neighborhood Market, Clemson, SC, USA) and sliced into sections of controlled thickness using a Gourmet Electric Food Slicer (Model 630, Chef's Choice International, Avondale, PA, USA). These sections are placed over the plate to observe the effect of increasing tissue thickness on the signal. 5 mm and 10 mm sections are used for the drug release experiment.

2.4.6 Image Analysis

Raw luminescence images are analyzed using custom MATLAB scripts. For concentration vs. signal experiment, 8 regions are analyzed for the concentration gradient (0.5, 0.25, 0.12, 0.06, 0.03, 0.015, 0.008, and 0.004 µCi ^{3}H-vancomycin), and 1 blank region, containing HydroMed™ D3 and Gd_2O_2S:Eu^{3+} microphoshor particles, is analyzed to correct for background and phosphor afterglow. Each region is 30 x 30 px (**Figure 2.9**), and the coordinates are kept consistent for each image. The blank region counts are subtracted from each concentration gradient region to obtain luminescence signal contributed by ^{3}H-vancomycin.
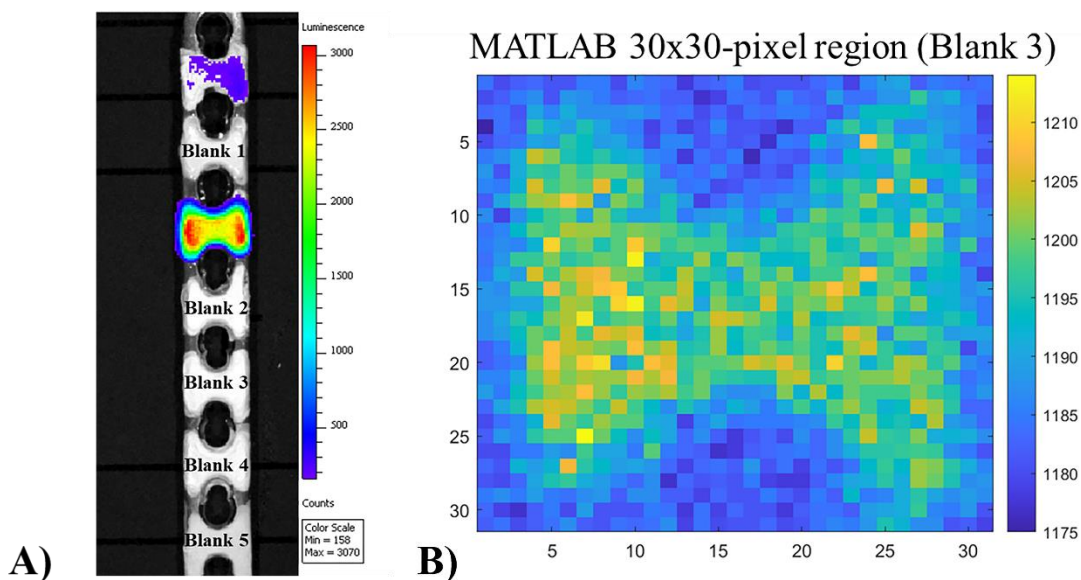
Figure 2.9. A) Reflected light and radioluminescence image of LCP™ plate coated with Gd$_2$O$_2$S:Eu^{3+} microphosphors, and HydroMed™ D3. From top to bottom, the first and third region also contain ^{3}H-vancomycin. Five blank regions are used to determine the standard deviation of the blank for LOD calculations. B) Example 30x30 pixel region generated from IVIS luminescence image, analyzed for LOD and LOQ determination.

For the drug release experiment, 4 regions of interest are analyzed for each photo: Drug Release, Blank, Constant Drug Reference, and Background. Each region is 30 x 30 px, and the coordinates are kept consistent for each image. The sum-total counts are obtained for each region and exported to excel. The blank region counts are subtracted from the drug release and constant drug reference signals to obtain the luminescence signal for each drug release point (this is also done for signal vs. concentration images). Each drug release point is imaged 3 times, and the luminescence value for the drug release and constant drug reference regions are averaged. There are 13 drug release points, each imaged 3 times, for an analysis of 39 photos. For the images acquired through tissue, a similar analysis is performed using the same 30 x 30 px regions described above.

Since light emitted from the drug release and constant drug reference regions both scatter into the blank region between them, the blank is difficult to calculate directly. In principle, we could use regions where there are no nanophosphors, but such blanks would not account for the significant afterglow signal we observe after exposing the plate to an overhead light during the imaging and drug elution procedure. This afterglow artifact varies between 2% and 7% of the constant drug reference region and would be both dramatically lower and more predictable in a live system after implantation, not periodically opened and exposed to light (especially blue and ultraviolet excitation). We corrected for the artifact by measuring the intensity for the blank without tissue and adjusting using the tissue attenuation factor (A) determined from the change in signal intensity in the constant drug reference region without tissue and with 5 mm tissue. A is calculated by first subtracting the background (a 30 x 30 px region next to the plate without phosphors) from the 30 x 30 px constant drug reference region for the data sets without tissue and with 5 mm tissue. Specifically, the constant drug reference region with 0 mm tissue (C_{t0}) is corrected using a background region from the image taken with 0 mm tissue (BG_{t0}), and the constant drug reference with 5 mm tissue (C_{t5}) is corrected using a background region from the image taken with 5 mm tissue (BG_{t5}). The ratio of the background corrected constant drug reference with 0 mm tissue ($C_{t0} - BG_{t0}$) to the background corrected constant drug reference with 5 mm tissue ($C_{t5} - BG_{t5}$) is calculated for each drug release point, using Equation (1), to determine A. The blank values (B_{t0}) obtained from the images without tissue are then divided by A to estimate the blank values through 5 mm tissue (B_{t5}) using Equation (2).

$$A = \frac{C_{t0} - BG_{t0}}{C_{t5} - BG_{t5}} \qquad (1)$$

$$B_{t5} = \frac{B_{t0}}{A} \qquad (2)$$

These blank values and background values are then subtracted from the drug release (DR_{i5}) and constant drug reference (C_{i5}) values obtained through 5 mm tissue to estimate and correct for luminescence from afterglow. Equation (3) and (4) yield the final corrected drug release (DR_{f5}) and constant drug reference (C_{f5}) regions through 5 mm tissue.

$$DR_{f5} = DR_{i5} - BG_{t5} - B_{t5} \qquad (3)$$

$$C_{f5} = C_{i5} - BG_{t5} - B_{t5} \qquad (4)$$

To correct for the 5% crosstalk observed between radioluminescence at the drug release and constant reference region (based upon the intensity profile), we multiply the observed values by the inverse matrix giving a final crosstalk corrected drug release value (DR_f) and constant drug reference value (C_f) (equations 5 and 6). This correction is shown in **Figure 2.7** and had a small but measurable effect on the calibration.

$$Crosstalk\ Corrected\ DR_f = (\frac{1}{1 - 0.05^2})(DR_f - (0.05 * C_f)) \qquad (5)$$

$$Crosstalk\ Corrected\ C_f = (\frac{1}{1 - 0.05^2})(C_f - (0.05 * DR_f)) \qquad (6)$$

To calculate LOD and LOQ, the LCP™ is coated with an additional 4 blank regions, for a total of 5 blank regions (**Figure 2.9**). The plate is imaged 10 times, with an exposure of 120 s each. The blank regions (30 x 30 pixels) in each image are analyzed in MATLAB and exported to excel, as described above. To determine variation in the blank, the luminescence counts from blank region 1 are subtracted from each of the additional blank regions. The standard deviation of these values (S_b) is used along with the slope of the regression line (m), taken as an average of 3 analyzed images of the concentration gradient, each with a 120 s exposure and no tissue, to calculate LOD and LOQ in Equation (7) and (8).

$$LOD \ = \ 3 \ * \ \left(\frac{S_b}{m}\right) \tag{7}$$

$$LOQ \ = \ 10 \ * \ \left(\frac{S_b}{m}\right) \tag{8}$$

To evaluate effect of tissue on signal spread and attenuation, an average of the intensity profile of three vertical lines through the center of 0 mm, 5 mm, and 10 mm images, prior to submersion in water for drug release, are co-plotted. The full width half maximum (FWHM) from these intensity profiles is used to estimate signal spread through 5 mm and 10 mm tissue. The maximum signal intensity value from the 0 mm tissue image is divided by the maxima from 5 mm and 10 mm tissue images to estimate attenuation factors.

2.4.7 Liquid Scintillation Counting

To verify the amount of ^{3}H-Vancomycin eluted during drug release, each drug release image is taken after dipping the plate into 10 mL of DI water. Each 10 mL sample of water is analyzed by drawing a 100 µL aliquot and adding it to 15 mL of Ultima Gold uLLT liquid scintillation cocktail (Perkin Elmer, Waltham, MA). The samples are counted three times each, for one minute, using a liquid scintillation counter (Beckman Coulter LS 6500, Brea, CA), yielding the count rate of sample before addition of internal standard (C_s). Internal standard of known disintegration rate (D_i) and concentration (10 µL of 5 µCi mL$^-$^{1}) is then added to each vial and counted again for one minute, three times each, yielding the count rate after addition of internal standard (C_{s+i}). The samples are shaken, then light adapted for 30 minutes before counting. The counting efficiency (E) is first calculated using Equation (9). The activity of ^{3}H-Vancomycin (D_s) is then extrapolated from the values of E and C_s, using Equation (10).[38]

$$E = \frac{(C_{s+i} + C_s)}{D_i} \tag{9}$$

$$D_s = \frac{C_s}{E} \tag{10}$$

2.4.8 Evaluation of Gd$_2$O$_2$S:Eu^{3+} Amount and Wash Step

Gd$_2$O$_2$S:Eu^{3+} microphoshor particles (8 µm median diameter, part number UKL63/N-R1, Phosphor Technology LTD, Stevenage, UK) are washed 3x in DI water, and 1x in ethanol. Washing is done by immersing 2 g of phosphor particles in 50 mL of

solvent, agitating, centrifuging at 10,000 rcf, and discarding supernatant. After washing, particles are placed in the oven to dry at 90°C for 1 hour. Unwashed particles are used directly from original packaging, with no prior treatment step. 2 Optiplate-96, opaque white 96-well microplates (Perkin Elmer, Waltham, MA) are used. For unwashed particle plate, 20 mg $Gd_2O_2S:Eu^{3+}$ is placed into wells D2, D4, and D6, 50 mg is placed into wells F2, F4, and F6, and 100 mg is placed into wells H2, H4, and H6. For washed particle plate, 25 mg $Gd_2O_2S:Eu^{3+}$ is placed into wells D2, D4, and D6, 50 mg is placed into wells F2, F4, and F6, and 100 mg is placed into wells H2, H4, and H6. 0.25 μCi ^{3}H-vancomycin is also deposited into each well, with excess solvent evaporated in the oven at 50°C for 1 hour. Radioluminescence images (**Figure 2.3**) are acquired on a small animal imager (IVIS Lumina XR, Perkin Elmer, Waltham, MA) under luminescence photograph mode (no external light source).

2.5 Conclusion

We demonstrate a method to visualize and quantify ^{3}H-vancomycin escaping from the surface of a biomedical implant using a CCD camera (IVIS Lumina). Our work demonstrates this technique applied in detecting trace concentrations of radiolabeled antibiotics on the surface of an orthopedic implant. Orthopedic implants are susceptible to colonization by bacterial biofilms, which often require aggressive, and invasive treatment for eradication. Antibiotic eluting implant coatings are a promising candidate for both prevention and treatment. The present method permits surface specific evaluation of drug concentration on biomedical implants, which is an important metric for development of

effective drug release coatings. ^{3}H labeling is not expected to interfere with drug molecule activity, which makes this an attractive approach for concentration measurements of other analytes near the implant surface using simple cameras.

LOD and LOQ calculations were performed based on the results of each experiment, where noise was acquired from the same sample measured sequentially, and slope was determined with respect to the difference between the blank and constant reference. The values do not reflect reproducibility between separate experiments using different implants and different days or instruments, which would be expected to show less reproducibility especially with respect to the background. Nonetheless, they do provide an indication of a minimum under the conditions used. LOD and LOQ calculations are performed based on standard deviation of the blank intensity (s_b), and the slope of the linear regression line from the concentration gradient or drug release gradient (m), respectively. The standard deviation of the blank (s_b) was based on 10 images of 5 blank regions (each with only $Gd_2O_2S:Eu^{3+}$ and HydroMed^{TM} D3), acquired consecutively. The standard deviation in the blank regions was found to be 1729 average counts. Error bars are not reported in the signal vs. concentration linear regression plot (**Figure 2.2C**) or drug release linear regression plots (**Figure 2.6 A/B**) because the standard deviation of these measurements was less than 0.1% and 0.35% of the total luminescence signal, respectively (**Figure 2.2D and 2.6C**). The standard deviation of these measurements was determined from the variation in three separate images of the same film, acquired consecutively.

The primary sources of noise for a CCD imaging system are dark noise, read noise and shot noise. Dark noise is calculated to be 0.2 e$^-$/pixel based on the dark current

57

($I_d < 3 \times 10^{-4}$ e$^-$/pixel/s) of the CCD camera and the integration time (t_i=120 s for the signal vs. concentration experiment) using **equation 11**.

$$Dark\ Noise = \sqrt{I_d \times t_i} \qquad\qquad (11)$$

Read noise for the CCD camera is reported to be better than 5 electrons. The shot noise is proportional to the square root of the average number of events. For example, if we examine the average of 3 images in the 0.5 μCi region for the signal vs. concentration experiment, N=268,560 photons. Theoretical shot noise, then, is 518 photons. The experimental standard deviation in the signal for this region, amongst the three images, is 845 photons. This trend is seen throughout the data, so the signal appears to be shot noise dominant at reasonably high signal intensities. At low analyte concentrations, a major source of noise is variation in long lived phosphorescence afterglow after exposure to visible light. This can be decreased by preventing blue and UV light exposure for hours or days prior to luminescence imaging, as would likely be the case in a real implant experiment.

As this method is repeated, and individual experiments are compared, we expect the standard deviation to increase and the LOD/LOQ to increase accordingly. However, as previously described, we can increase the concentration of radiolabel and increase exposure time to improve signal to noise ratio and sensitivity; improving the optical collection efficiency and scintillator betaluminescence efficiency would also help.

2.6 References

[1]   H.-C. Flemming, J. Wingender, U. Szewzyk, P. Steinberg, S. A. Rice, S. Kjelleberg, *Nat. Rev. Microbiol.* **2016**, *14*, 563.

[2]   N. Høiby, O. Ciofu, H. K. Johansen, Z. Song, C. Moser, P. Ø. Jensen, S. Molin, M. Givskov, T. Tolker-Nielsen, T. Bjarnsholt, *Int. J. Oral Sci.* **2011**, *3*, 55.

[3]   C. Pan, Z. Zhou, X. Yu, *J. Orthop. Surg.* **2018**, *13*.

[4]   P. S. Stewart, *Int. J. Med. Microbiol.* **2002**, *292*, 107.

[5]   P. S. Stewart, *Microbiol. Spectr.* **2015**, *3*.

[6]   N. Høiby, T. Bjarnsholt, M. Givskov, S. Molin, O. Ciofu, *Int. J. Antimicrob. Agents* **2010**, *35*, 322.

[7]   H. Wu, C. Moser, H.-Z. Wang, N. Høiby, Z.-J. Song, *Int. J. Oral Sci.* **2015**, *7*, 1.

[8]   D. Wareham, J. Michael, S. Das, *Braz. Arch. Biol. Technol.* **2005**, *48*, 145.

[9]   A. V. Hall, K. K. Solanki, S. Vinjamuri, K. E. Britton, S. S. Das, 6.

[10]   M. Salouti, A. Fazli, In *Medical Imaging in Clinical Practice* (Ed.: Erondu, O. F.), InTech, **2013**.

[11]   S. Basu, T. Chryssikos, S. Moghadam-Kia, H. Zhuang, D. A. Torigian, A. Alavi, *Semin. Nucl. Med.* **2009**, *39*, 36.

[12]   D. Campoccia, L. Montanaro, C. R. Arciola, *Biomaterials* **2013**, *34*, 8533.

[13]   A. Bekmurzayeva, W. J. Duncanson, H. S. Azevedo, D. Kanayeva, *Mater. Sci. Eng. C* **2018**, *93*, 1073.

[14]   I. Francolini, G. Donelli, *FEMS Immunol. Med. Microbiol.* **2010**, *59*, 227.

[15]   N. J. Hickok, I. M. Shapiro, *Adv. Drug Deliv. Rev.* **2012**, *64*, 1165.

[16] H. Chen, T. Moore, B. Qi, D. C. Colvin, E. K. Jelen, D. A. Hitchcock, J. He, O. T. Mefford, J. C. Gore, F. Alexis, J. N. Anker, *ACS Nano* **2013**, *7*, 1178.

[17] T. L. Moore, F. Wang, H. Chen, S. W. Grimes, J. N. Anker, F. Alexis, *Adv. Funct. Mater.* **2014**, *24*, 5815.

[18] X. Zhu, J. Li, P. Peng, N. Hosseini Nassab, B. R. Smith, *Nano Lett.* **2019**, *19*, 6725.

[19] D. Losic, G. J. Atkins, P. Pivonka, D. Findlay, M. S. Aw, K. A. Khalid, K. Gulati, *Int. J. Nanomedicine* **2012**, 4883.

[20] P. Arpaia, U. Cesaro, N. Moccaldi, *Sci. Rep.* **2017**, *7*, 44647.

[21] J. R. Mourant, T. M. Johnson, G. Los, I. J. Bigio, *Phys. Med. Biol.* **1999**, *44*, 1397.

[22] I. J. Bigio, J. R. Mourant, G. Losh, *J. Gravitational Physiol.* **1999**, *6*, 3.

[23] G. Normand, M. Maker, J. Penraat, K. Kovach, J. G. Ghosh, C. Grosskreutz, S. Chandra, *Commun. Biol.* **2020**, *3*, 16.

[24] T. Moore, H. Chen, R. Morrison, F. Wang, J. N. Anker, F. Alexis, *Mol. Pharm.* **2014**, *11*, 24.

[25] F. Alexis, J. N. Anker, *Ther. Deliv.* **2014**, *5*, 97.

[26] H. Zhuang, A. Alavi, *Semin. Nucl. Med.* **2002**, *32*, 47.

[27] P. A. G. T. Jurrius, M. R. Grootendorst, M. Krotewicz, M. Cariati, A. Purushotham, M. Turska-d'Amico, *EJNMMA Res.* **2021**, *11*.

[28] F. Y. Lambrecht, *Ann. Nucl. Med.* **2011**, *25*, 1.

[29] P. A. Erba, O. Israel, *Clin. Transl. Imaging* **2014**, *2*, 519.

[30] R. Berber, J. Henckel, M. Khoo, S. Wan, J. Hua, J. Skinner, A. Hart, *J. Arthroplasty* **2015**, *30*, 687.

[31] H. Chen, D. C. Colvin, B. Qi, T. Moore, J. He, O. T. Mefford, F. Alexis, J. C. Gore, J. N. Anker, *J. Mater. Chem.* **2012**, *22*, 12802.

[32] J. S. Klein, C. Sun, G. Pratx, *Phys. Med. Biol.* **2019**, *64*, 04TR01.

[33] A. E. Spinelli, *Phys. Med.* **2015**, 10.

[34] M. T. King, C. M. Carpenter, C. Sun, X. Ma, Q.-T. Le, J. B. Sunwoo, Z. Cheng, G. Pratx, L. Xing, *Journal of Nuclear Medicine* **2015**, *56*, 7.

[35] M. T. King, C. H. Jenkins, C. Sun, C. M. Carpenter, X. Ma, K. Cheng, Q.-T. Le, J. B. Sunwoo, Z. Cheng, G. Pratx, L. Xing, *Med. Phys.* **2016**, *43*, 5298.

[36] J. F. Glickman, A. Schmid, S. Ferrand, *ASSAY Drug Dev. Technol.* **2008**, *6*, 433.

[37] S. Wu, B. Liu, *BioDrugs* **2005**, *19*, 383.

[38] M. L'Annunziata, *Handbook of Radioactivity Analysis*, 3rd ed., Elsevier Science & Technology, **2012**.

[39] S. Som, A. Choubey, S. K. Sharma, *J. Exp. Nanosci.* **2015**, *10*, 350.

[40] W. L. Pillinger, J. J. Hentges, J. A. Blair, *Phys. Rev.* **1961**, *121*, 232.

[41] W. Van Schaik, G. Blasse, *Chem. Mater.* **1992**, *4*, 410.

[42] T. P. Lodise, J. Graves, A. Evans, E. Graffunder, M. Helmecke, B. M. Lomaestro, K. Stellrecht, *Antimicrob. Agents Chemother.* **2008**, *52*, 3315.

[43] T. E. Swanson, X. Cheng, C. Friedrich, **2011**, *97*, 10.

[44] D. Li, P. Lv, L. Fan, Y. Huang, F. Yang, X. Mei, D. Wu, *Biomater Sci* **2017**, *5*, 2337.

[45] S. M. Helms, L. O'Neill, S. B. Behbahani, J. Tzeng, K. Jeray, M. S. Kennedy, A. W. Cross, S. L. Tanner, J. D. DesJardins, *Materialia* **2021**, *17*, 101122.

[46] U. Uzair, C. Johnson, S. Beladi-Behbahani, A. C. Rajamanthrilage, Y. S. Raval, D. Benza, M. Ranasinghe, G. Schober, T.-R. J. Tzeng, J. N. Anker, *ACS Appl. Mater. Interfaces* **2020**, *12*, 52343.

[47] S. Mosca, P. Lanka, N. Stone, S. Konugolu Venkata Sekar, P. Matousek, G. Valentini, A. Pifferi, *Biomed. Opt. Express* **2020**, *11*, 1697.

[48] A. A. Gurjarpadhye, W. C. Vogt, Y. Liu, C. G. Rylander, *Int. J. Biomed. Imaging* **2011**, *2011*, 1.

[49] J. Valentin, Ed., *The 2007 Recommendations of the International Commission on Radiological Protection. ICRP Publication 103.*, Vol. 37, Elsevier, **2007**.

[50] L. C. Mendez, G. C. Morton, *Transl. Androl. Urol.* **2018**, *7*, 357.

[51] G. Segall, D. Delbeke, M. G. Stabin, E. Even-Sapir, J. Fair, R. Sajdak, G. T. Smith, *J. Nucl. Med.* **2010**, *51*, 1813.

[52] C. J. Palestro, H. F. Hospital, L. A. Forstrom, M. Clinic, B. S. Green, *Soc. Nucl. Med. Proced. Guidel.* **2004**, 6.

[53] K. Eckerman, J. Harrison, H.-G. Menzel, C. H. Clement, *Compendium of Dose Coefficients based on ICRP Publication 60. ICRP Publication 119.*, Vol. 41, Elsevier, **2012**.

[54] N. Penner, L. J. Klunk, C. Prakash, *Biopharm. Drug Dispos.* **2009**, *30*, 185.

[55] M. M. Alauddin, *Am J Nucl Med Mol Imaging* **2012**, *2*, 55.

[56] D. Papagiannopoulou, *J. Label. Compd. Radiopharm.* **2017**, *60*, 502.

[57] J. C. Rotschafer, K. Crossley, D. E. Zaske, K. Mead, R. J. Sawchuk, L. D. Solem, *Antimicrob. Agents Chemother.* **1982**, *22*, 391.

[58] D. Alloni, C. Cutaia, L. Mariotti, W. Friedland, A. Ottolenghi, *Radiat. Res.* **2014**, *182*, 322.

[59] Radionuclides in Drinking Water: A Small Entity Compliance Guide, United States Environmental Protection Agency, **2002**.

CHAPTER 3

MONITORING ^{3}H-VANCOMYCIN CONCENTRATION USING RADIOLUMINESCENT NANOPARTICLES

3.1 Abstract

Nanoparticles are a useful biomedical tool for imaging and targeted drug release, but drug release pharmacokinetics are generally investigated and characterized *in vitro*. Due to patient heterogeneity, and variable drug release behavior in different biological tissue environments, there remains a need for quantitative *in vivo* tracking strategies. In this chapter we provide proof of concept for using radioluminescent nanophosphors to measure radiolabeled drug release *in vivo*. We present a functionalization strategy for synthesized $Gd_2O_2S:Eu^{3+}$ nanoparticles with anti-vancomycin IgM antibodies, which permits binding of tritium labeled vancomycin (^{3}H-vancomycin). Successful binding of ^{3}H-vancomycin to radioluminescent $Gd_2O_2S:Eu^{3+}$ nanoparticles in aqueous suspension is expected to produce a luminescent signal that would not be present if unbound. Initial experiments demonstrate a linear relationship between nanoparticle luminescence emission and concentration of vancomycin (LOD=7.8 nCi) using only 1 mg dry nanoparticles. $Gd_2O_2S:Eu^{3+}$ emits red light with high quantum efficiency, which has been demonstrated to penetrate biological tissues sufficiently for quantitative imaging applications.[1–5] Monitoring decrease in luminescence emission intensity as a function of radiolabeled drug release from nanoparticles is a conceptually simple, promising avenue for development of a novel theranostic imaging strategy.

3.2 Introduction

Nanoparticles, most commonly defined as being 10-100 nm in diameter[6], are heavily investigated for imaging and therapeutic biomedical application. The 10-100 nm size range is appealing because particles are large enough to avoid renal clearance, but small enough to avoid rapid clearance by the reticuloendothelial system (RES).[7] This permits a long blood circulation time which gives the particles more time to bind specific targets. Additional factors that affect particle circulation and clearance include surface charge, functional groups, protein corona, morphology, and mechanical properties. In addition, nanomaterials in this size range have a large surface-to-volume ratio, which provides high surface area for drug loading (in cases where drug is surface loaded). Besides high surface area, nanoparticle drug carriers are often able to impart selective and targeted release pharmacokinetics.[1] This is useful when drug is needed in a specific location and may increase drug potency with a lower overall dose. Depending on the material used, nanoparticles also have potential for use in combinatory imaging and therapy.[3,8]

The list of nanomaterials for drug delivery application is extensive and includes a variety of different nanomaterials, pharmaceutical drugs, and biological targets. For example, cancer is a popular target for nanotherapeutics because traditional chemotherapy wreaks havoc on the body due to non-specific targeting that results in severe side effects and ineffective treatment. Biomimetic nanoparticles[9,10], nanogels[11,12], and inorganic nanoparticles[13,14] have been investigated for cancer immunotherapy.[15] Many types of metal, and metal oxide nanoparticles have been used to add imaging capability to drug delivery. For example, "smart" europium doped gadolinium oxysulfide ($Gd_2O_2S:Eu^{3+}$)

nanocapsules have been developed to release photoactive doxorubicin (a chemotherapeutic) at pH values found in tumor tissue.[1] $Gd_2O_2S:Eu^{3+}$ is radioluminescent and paramagnetic, so these nanocapsules can be monitored both optically (as doxorubicin release affects the emission spectrum of $Gd_2O_2S:Eu^{3+}$) and by MRI.[3]

Despite the exponential increase in nanomaterials for biomedical application, there is still a lack of systematic methodology to evaluate drug release pharmacokinetics and pharmacodynamics *in vivo*. For materials with appropriate magnetic properties and electron density, magnetic resonance imaging (MRI) and computed tomography (CT) are useful for imaging nanoparticle localization through deep tissue, but are generally unable to provide quantitative information about drug release.[16] A variety of *in vitro* techniques are used to study fundamental information about drug release and behavior in biological conditions and are usually relied upon to predict *in vivo* behavior.[7] These methods include, but are not limited to, sample and separate (SS), dialysis, and continuous flow (CF). While *in vitro* evaluation of pharmacokinetics is useful, treatment efficacy also depends largely on factors that must be evaluated *in vivo*. There is significant variation among patients, which includes disease progression, drug biodistribution, and drug release kinetics in different tissue environments. Multimodal theranostic nanomaterials, which combine therapeutic and diagnostic modalities in the treatment of disease, are lucrative for evaluating drug release and therapeutic efficacy in real time.[4,17] Gd_2O_2S nanoparticles are a promising candidate for multimodal imaging application due to low toxicity, MRI contrast, and luminescence properties.[16,18,19]

$Gd_2O_2S:Eu^{3+}$ radioluminescent phosphors exhibit high quantum efficiency (60,000 photons per MeV X-Ray in bulk phase) with narrow, highly penetrating red emission.[19] Specifically, emission peaks are located in the region between 560-750 nm (due to $^5D_0$ $\rightarrow^7F_j$, where j=1-4, electronic transitions). For *in vivo* optical applications, using light in the visible wavelength range, red light emission is ideal because penetration depth in tissue increases as wavelength increases.[20] Luminescence emission can be stimulated by X-Ray, UV, and radioactive decay such as beta-radiation. As a result, by radiolabeling an analyte of interest, $Gd_2O_2S:Eu^{3+}$ can be used to measure analyte concentration as a function of luminescence intensity.[2] In addition to appealing optical properties, various toxicological studies demonstrate that gadolinium based contrast agents are safe at clinically indicated doses (except in patients with advanced renal insufficiency).[21,22] More specifically, according to a comprehensive biodistribution, elimination, and toxicological study, Gd_2O_2S nanoparticles are well tolerated, with the majority of injected product eliminated through the feces within five months.[23]

Tritium (^3H) is an appealing radiolabel because it should not interfere with the pharmaceutical action of a drug, and the associated energy of decay (~5.7 keV) is sufficient to stimulate significant luminescence emission in $Gd_2O_2S:Eu^{3+}$, but low enough to minimize stochastic effects *in vivo* (see 2.3.3 "Radiation Dose Concerns"). In addition, the decay range of ^3H (0.4-4 μm in water) means excitation of phosphors in an aqueous suspension will only occur if the ^3H-analyte is attached to the phosphor (or closely associated). This concept is well-documented for quantification of radiolabeled analytes in scintillation proximity assays (SPA). This assay methodology typically requires plastic

(polyvinyl toluene and polystyrene with diphenyl anthracene) or inorganic (cerium doped yttrium silicate and yttrium oxide) scintillator beads, scintillation cocktail, and a liquid scintillation counter.[24,25] Application of SPA has been confined to radioimmunoassays, ligand-receptor binding assays, and enzyme assays. Monitoring drug release using phosphorescent $Gd_2O_2S:Eu^{3+}$ is a novel application. The previous chapter describes measuring radiolabeled drug concentration on the surface of a locking compression plate using 8 μm commercially synthesized particles in an immobilized film (Chapter 2). This chapter aims to demonstrate the feasibility of measuring drug concentration on in-house synthesized and functionalized nanoparticles in an aqueous suspension. Specifically, we investigate the ability of ^{3}H-vancomycin, a representative antibiotic in the treatment of implant associated infection, to excite $Gd_2O_2O:Eu^{3+}$ nanoparticles.[26] This technique is a promising step toward monitoring nanoparticle drug release, quantitatively, *in vivo*.

3.3 Nanoparticle Synthesis and Characterization

3.3.1 Gd$_2$O$_2$S:Eu^{3+} Nanoparticle Synthesis

There are a variety of synthetic strategies to produce rare earth based luminescent nanomaterials, and the selected method depends largely on desired size range. Uniform crystal lattice structure, and high luminescence efficiency are ubiquitously desired, but intended application determines the target size range. Solid-state synthetic flux routes are used to generate larger particles (2.5-25 μm diameter), for application in biomedical X-Ray scintillator screens or TV cathode-ray screens.[19,27,28] For example, $Gd_2O_2S:Tb^{3+}$ can

be synthesized from Gd_2O_3 commercial precursor via an alkaline polysulfide formed *in situ* using an alkaline-carbonate flux. Luminescent activator Tb^{3+} ions are incorporated into the host lattice during this process as well.[29] However, traditional solid-state flux methods have not been shown to produce particles on the nanoscale. The most common solution based synthetic routes for lanthanide nanomaterials are thermal decomposition[30,31], solvothermal[32,33], and coprecipitation in either aqueous or organic solution.[34]
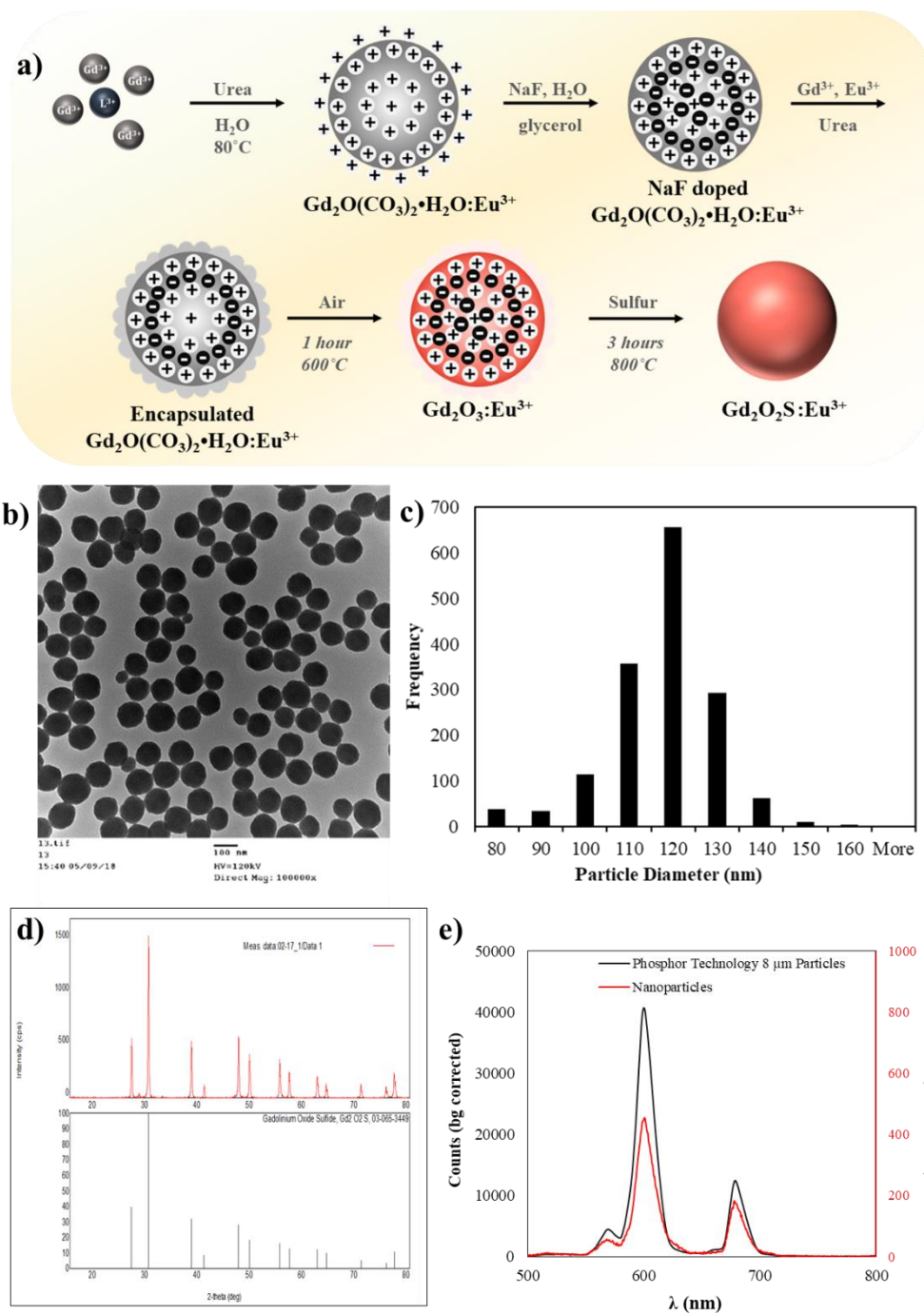
Figure 3.1. A) Synthesis schematic for $Gd_2O_2S:Eu^{3+}$ nanoparticles. B) TEM image of synthesized particles. Image taken at 100,000x magnification. C) Size analysis of 18 TEM images, and 1565 individual particles. Number of particles is plotted vs. bins according to diameter in nm. D) Powder XRD of synthesized particles (top) plotted in comparison to GOS standard (bottom). E) X-Ray excited optical luminescence spectrum of synthesized particles compared to commercial microparticles.

Coprecipitation of gadolinium and europium nitrate salts, in aqueous solution under decomposition of urea, is a simple synthetic strategy that can yield monodisperse particles with high luminescence intensity.[19] Urea decomposes into ammonium and carbonate ions in aqueous media. Basicity imparted by ammonia helps trigger initial spontaneous nucleation, which then reduces the precursor (carbonate) concentration below the nucleation threshold as the particles grow. The continued slow production of carbonate precursor from urea decomposition, using temperatures above 70°C but below 100°C, permits controlled growth of gadolinium oxycarbonate ($Gd_2O(CO_3)_2 \cdot H_2O$) amorphous particles (general mechanism elucidated in **equations 1-4**), while avoiding secondary nucleation events. Previous work has shown that lower urea concentrations ($[urea]/[Gd^{3+}]<45$) generally results in fewer individual nuclei, and polydisperse size distribution. As the concentration increases ($[urea]/[Gd^{3+}]>90$), there is a larger number of individual seeds formed via burst nucleation, and a smaller average diameter after the growth period.[35] In this reaction scheme there is a ~240x molar excess of urea to $Eu(NO_3)_3$ and $Gd(NO_3)_3$ combined.

$$H_2N - CO - NH_2 \xrightarrow{k} NH_3 + HCNO \leftrightarrow NH_4^+ + NCO^- \tag{1}$$

$$NCO^- + 2H_2O \leftrightarrow NH_4^+ + CO_3^{2-} \tag{2}$$

$$M(H_2O)_n^{3+} + H_2O \leftrightarrow [M(OH)(H_2O)_{n-1}]^{2+} + H_3O^+ \tag{3}$$

$$[M(OH)(H_2O)_{n-1}]^{2+} + CO_3^{2-} \rightarrow [M(OH)CO_3(H_2O)] + (n-2)H_2O \tag{4}$$
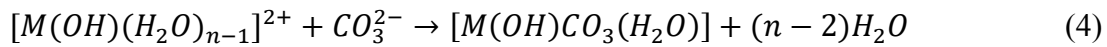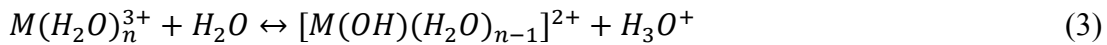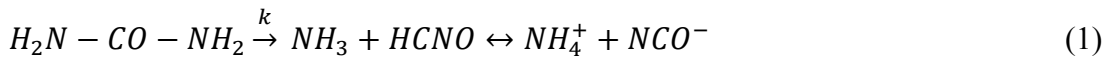
Where $M = Eu^{3+}, Gd^{3+}$

The $Gd_2O(CO_3)_2 \cdot H_2O{:}Eu^{3+}$ can be directly converted to $Gd_2O_3{:}Eu^{3+}$ via calcination under atmosphere at 600°C, then converted to $Gd_2O_2S{:}Eu^{3+}$ via sulfidation with

elemental sulfur under argon flow at 700°C. However, the brightness of these particles can be substantially increased by first encapsulating a sintering agent.[36] Sodium fluoride (NaF) is incorporated into the crystal structure to act as a sintering agent, minimize defects, and increase crystal domain size after initial precipitation and growth of particles. To prevent particle fusion during calcination and sulfidation, a protective shell of $Gd_2O(CO_3)_2$ • $H_2O:Eu^{3+}$ is co-precipitated on the surface after incorporation of fluoride ions.[19] The target $Gd_2O_2S:Eu^{3+}$ is obtained by oxidation of the precursor in air at 600°C, followed by sulfidation of the oxide under inert argon atmosphere at 700°C, which is a typical synthetic strategy.[19,28]

3.3.2 $Gd_2O_2S:Eu^{3+}$ Nanoparticle Characterization

Size analysis of nanoparticle samples is done via transmission electron microscope image analysis. A total of 18 TEM images and 1565 individual nanoparticles are measured and grouped into bins according to diameter in **Figure 3.1c**. Based on this analysis, the mean particle diameter is approximately 120 nm, with a distribution of sizes between 6-157 nm. Despite efforts to reproduce previous reported synthetic methods[19], our particles are polydisperse with average diameter is over 100 nm. This could be due to additional nucleation events occurring during the encapsulation step after incorporation of NaF. The second co-precipitation step is intended to deposit a protective amorphous shell onto the surface of previously synthesized particles, but it is probable that some of the precursor is nucleating as $Gd_2O(CO_3)_2$ • $H_2O:Eu^{3+}$ particles (without the NaF dopant).

X-Ray excited optical luminescence emission of synthesized particles is ~1.4% commercial particles, determined via comparison of 30 mg samples of each material. The crystalline domain average size is estimated from the powder XRD data using the Scherrer equation (**equation 5**):

$$D = \frac{K\lambda}{\beta \times \cos\theta} \tag{5}$$

Where D is the mean crystal domain size, K is a dimensionless shape factor (0.90), λ is the wavelength for X-Ray (~0.154 nm), β is the peak broadening (in radians) at full width half maximum (FWHM), and θ is the diffraction angle. Based on analysis of peaks with local maxima at $2\theta=26.8°$, $30.0°$, and $38.2°$, the average crystal domain size is determined to be 56.2 nm. With average particle diameter being ~120 nm, luminescence efficiency is likely hindered by crystal defects at grain boundaries within individual particles, in addition to point defects and site defects on particle surface.[19] Nonetheless, particles synthesized by this method are visibly luminescent, and appropriate for subsequent functionalization.

3.4 Nanophosphor Functionalization

Nanophosphors used in this study, for functionalization and imaging, are from a more recent synthesis performed by Dr. Sriparna Bhattacharya and Basanta Ghimire. XEOL and XRD characterization are unavailable, but luminescence is verified qualitatively via UV excitation. TEM images confirm spherical, nanoscale morphology (**Figure 3.2**).
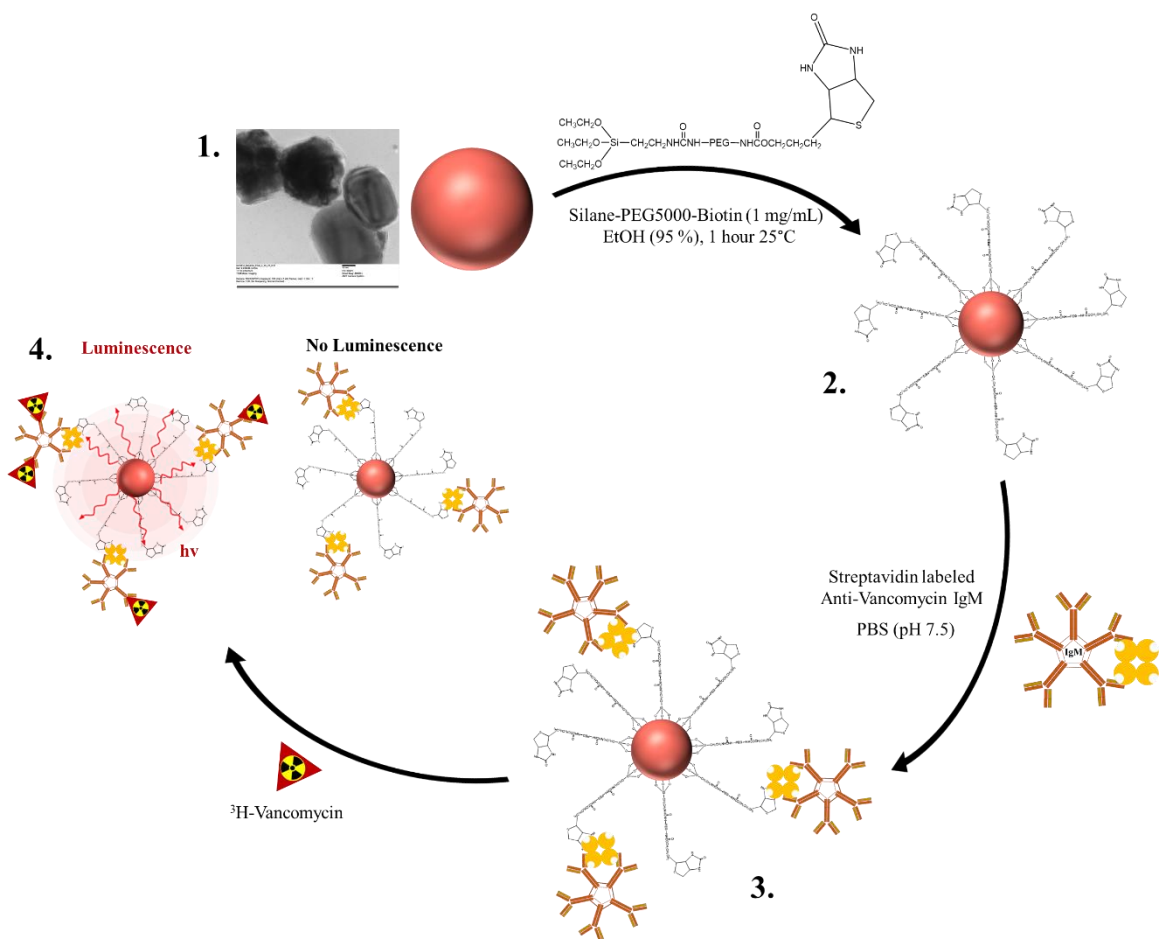
Figure 3.2. Schematic illustrating the functionalization of synthesized nanoparticles. First step is Silane-PEG5000-Biotin conjugation to the nanoparticle surface. Second step is the attachment of streptavidin labeled anti-vancomycin IgM via streptavidin-biotin bond. Third step is the addition of ^{3}H-vancomycin. Fourth step illustrates the concept that, in solution, bound ^{3}H-vancomycin will excite luminescence in $Gd_2O_2S:Eu^{3+}$ particles, while particles in the absence of ^{3}H-vancomycin will not luminesce.

3.4.1 Silane-PEG5000-Biotin Functionalization and Verification

The goal of this functionalization procedure is to attach anti-vancomycin IgM to the surface of $Gd_2O_2S:Eu^{3+}$ nanoparticles (**Figure 3.2**). IgM functionalized nanoparticles will bind free vancomycin (and ^{3}H-vancomycin) stimulate luminescence emission. First, silane-PEG5000-biotin is attached to the surface of synthesized $Gd_2O_2S:Eu^{3+}$

74

nanoparticles. Particles have previously been coated with tetraethyl orthosilicate (TEOS), in a solution of ethanol and distilled water, as an intermediate step for amine functionalization of $Gd_2O_2S:Eu^{3+}$ and $Y_2O_2S:Yb/Er$.[19] A similar reaction approach is used to attach the silicate moiety to the positively charged $Gd_2O_2S:Eu^{3+}$ nanoparticles, in step one of the functionalization procedure. This attachment is verified using streptavidin labeled microbubbles (**Figure 3.3**). Streptavidin labeled microbubbles bind the free biotin moieties on synthesized nanoparticles, causing the labeled nanoparticles to float to the top of the buffer solution. When illuminated with UV (~395 nm), the red luminescence from nanophosphors is visible by eye in the microbubble layer at the top of the centrifuge tube. By contrast, when unlabeled particles are added to a solution of streptavidin labeled microbubbles, the nanoparticles form a pellet at the bottom of the centrifuge tube.
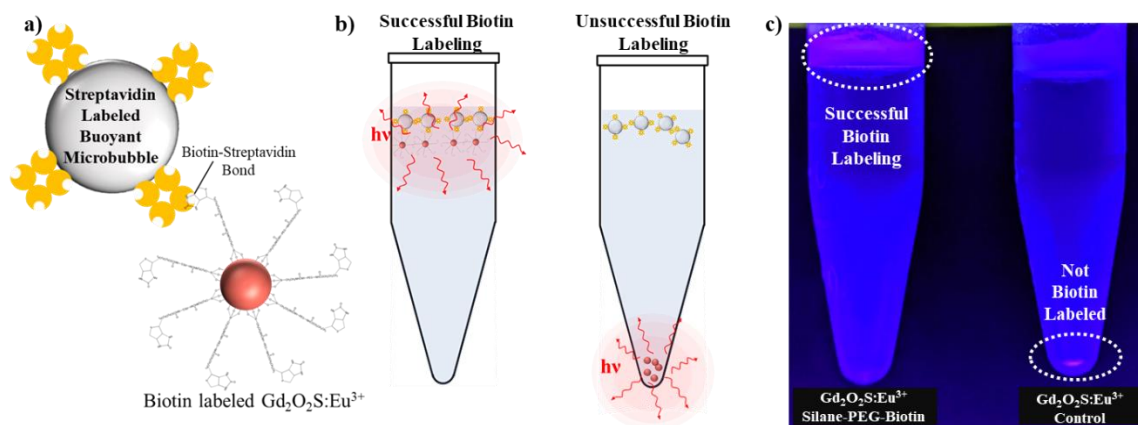
Figure 3.3. a) Illustration of streptavidin labeled buoyant microbubble (Akadeum Life Sciences) bound to biotin labeled $Gd_2O_2S:Eu^{3+}$ nanoparticle. b) Experimental design for verification of biotin labeling. Successfully labeled nanoparticles will bind buoyant microbubbles and float along the top of buffer filled centrifuge tube. Unlabeled particles should form a pellet at the bottom of the tube. c) Photograph of biotin labeled particles in left-most tube, and unlabeled control particles in right-most tube. Luminescence is evidence in the microbubble layer of the left-most tube, indicating successful conjugation of biotin to nanoparticles. Control tube exhibits luminescent pellet at the bottom.

3.4.2 Anti-Vancomycin IgM Functionalization

Streptavidin has an incredibly high binding affinity for biotin, exhibiting a dissociation constant of $\sim10^{-14}$ mol/L, and is a common motif in bio-nanotechnology due its ease of application in functionalization strategies.[37–39]   For this reason, our functionalization strategy aims to conjugate streptavidin to anti-vancomycin IgM antibody for easy attachment to biotin labeled nanoparticles. Streptavidin labeling of anti-vancomycin IgM is performed using a streptavidin labeling kit that acts upon the amine group in lysine residues (details are proprietary information from Abcam). Based on the calculated area of an IgM molecule, which has an approximate extended diameter of ~30 nm, approximately 64 antibodies can fit within the surface area of a 120 nm diameter nanoparticle.[40] This functionalization protocol aimed to add ~16 IgM per particle, which is well under the maximum feasible amount. IgM is a pentameric antibody, with the ability to bind 10 antigens (vancomycin, in this case). As a result, roughly 150 ^{3}H-vancomycin molecules should be able to bind to each particle.

3.5 Nanoparticle Luminescence Signal vs ^{3}H-Vancomycin Concentration

To evaluate anti-vancomycin IgM conjugation, 1 mg of silane-PEG5000-biotin functionalized particles are added to 5 separate wells in a 96-microwell plate. In each 1 mg sample, if 150 ^{3}H-vancomycin molecules bind each particle, then the addition of 2.4×10^{13} vancomycin molecules would theoretically saturate all available epitope binding sites. The commercially obtained ^{3}H-vancomycin has an activity of 27.5 Ci/mmol, so 2.4×10^{13} vancomycin molecules corresponds to an activity of 1.1 µCi. Therefore, the concentration

gradient added to the wells is 0, 0.05, 0.1, 0.25, and 0.5 µCi, to prevent saturation of binding sites and ensure that a change in luminescence would be visible with increasing ^{3}H-vancomycin concentration.

Initially the plate is imaged with 200 µL of buffer present in each well, but there is not a significant luminescence signal when the particles are suspended in liquid. As a result, the buffer solution was evaporated from the wells and imaged again (**Figure 3.4**). When the wells are dried, the nanoparticles exhibit a linear increase in luminescence signal with increase in ^{3}H-vancomycin concentration (R^2=0.99). This demonstrates the feasibility of imaging changes in radiolabeled drug concentrations using radioluminescent nanoparticles. The lack of luminescence signal in nanoparticle suspension is currently under investigation. When there is liquid present, if vancomycin is not directly bound to anti-vancomycin functionalized nanoparticles, the free ^{3}H-vancomycin beta-decay range is too short (~0.4 µm average path length in water) to excite luminescence from nanoparticles.[41,42] Biotin labeling of particles appears to have been successful, so the subsequent streptavidin labeling of anti-vancomycin IgM and attachment to biotin labeled particles may not have been successful.

Though no tissue was present for initial experiments, we can detect changes in drug concentration on the order of nanograms, using only 1 mg nanoparticles, and 300 s exposure time. Luminescence is evident only in the presence of ^{3}H-vancomycin, confirmed by the lack of luminescence in well containing only 1 mg nanoparticles. Based on standard deviation of background (S_b), and the slope of the linear regression line from the concentration gradient (m) we find a limit of detection (LOD) of 7.8 nCi (LOD = 3*S_y/m

= 7.8 nCi = 0.4 ng vancomycin). Our previous study, using tritium excited microphosphors to detect drug release from an immobilized $Gd_2O_2S:Eu^{3+}$ film, demonstrates that the integrated luminescence signal decreases by a factor of ~7.6 when imaging through 5 mm porcine muscle tissue.[2] As a result, we expect the limit of detection for this method to increase when imaging through tissue, but signal decrease can be partially mitigated by using longer exposure time, higher luminescence efficiency nanoparticles, and higher concentrations of both nanoparticles and drug.
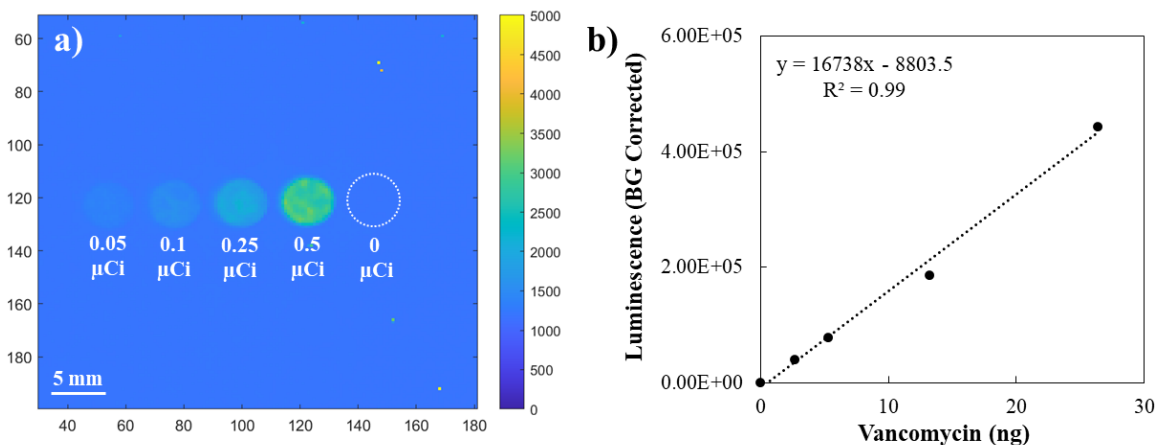
Figure 3.4. a) Luminescence image of synthesized $Gd_2O_2S:Eu^{3+}$ nanoparticles with increasing ^{3}H-Vancomycin concentration from left to right. Each well contains 1 mg particles. Image collected with IVIS Lumina using an exposure time of 300 s and plotted as pseudo-color image using MATLAB. Color bar represents relative luminescence intensity. b) Luminescent regions of interest (ROIs) plotted vs. amount of vancomycin (ng).

3.6 Methods

3.6.1 $Gd_2O_2S:Eu^{3+}$ Nanoparticle Synthesis

1. Synthesis of $Gd_2O(CO_3)_2$ Precursor: Gadolinium (III) nitrate ($Gd(NO_3)_3 \cdot 6H_2O$) and europium nitrate ($Eu(NO_3)_3 \cdot 6H_2O$) solutions are prepared with DI water at concentrations of 1 M and 80 mM, respectively (Alfa Aesar, Haverhill, MA). 2 mL of 1M $Gd(NO_3)_3$, 625 µL 80 mM $Eu(NO_3)_3$, and 1.2 g polyvinylpyrrolidone (PVP K-30, MW 40,000, Spectrum Chemicals, Gardena, CA) added to a 2 L DI water in a round bottom flask. Flask is placed in an appropriately sized (2 L) heating mantle and heated to 80 °C using an Inkbird temperature controller and thermocouple (Shenzhen, China) with constant stirring (using a magnetic stir bar). Once solution reaches 80 °C, 30 g urea is added to the solution (4111-05, J.T. Baker, Phillipsburg, NJ). Reaction is removed from heat as soon as solution becomes cloudy (approximately 30 minutes) and placed immediately in an ice water bath to quench reaction. Once cooled to 25°C, particles are collected by centrifugation at 15,000 RCF for 10 minutes. Particles are washed 3x with DI water and 1x with ethanol.

2. Sodium Fluoride (NaF) Doping: Particles are resuspended in 10 mL DI water and sonicated with 5 mg NaF for five minutes (A13019, Alfa Aesar, Haverhill, MA). 30 mL glycerol (BDH1172, BDH Chemicals, Poole, UK) is added and the mixture is subsequently heated to 120°C for 2 hours to evaporate water. The mixture is then heated to 170°C for 1 hour under nitrogen in a vacuum oven to calcine and encapsulate NaF. Once cool, particles are collected by centrifugation at 15,000 RCF and washed 3 x with DI water.

3. Preparation of Protective Shell on NaF Doped Precursor: Amorphous particles are resuspended in 200 mL DI water with 1.2 g PVP and heated to 80°C. 2 mL 1M $Gd(NO_3)_3$, 1 mL 80 mM $Eu(NO_3)_3$, and 12 g urea are then added to the solution. Solution is kept stirring for 1 hour, then quenched with an ice bath. Particles are collected via centrifugation at 15,000 RCF, washed 3x with DI water, and 1x with ethanol. Dry particles in an oven for 3 hours at 80°C to evaporate remaining solvent.

4. Conversion to $Gd_2O_3:Eu^{3+}$, then $Gd_2O_2S:Eu^{3+}$: Dry particles are transferred to a ceramic combustion boat and calcined in a muffle furnace for 2 hours at 600°C. This process converts $Gd_2O(CO_3)_2$ precursor to $Gd_2O_3:Eu^{3+}$. Sample, still in the combustion boat, is then placed in a high purity quartz process tube (OD 60 mm, L 1000 mm, open both ends, Across International, Livingston, NJ) with excess sulfur powder (10785, Alfa Aesar, Haverhill, MA). Tube is placed in a tube furnace at 700°C for 1 hour, with argon flow. Once cool, particles are incubated in 200 mL DI water to remove residual sulfur and gadolinium sulfide. Particles collected using centrifugation (15,000 RCF).

Nanoparticles used for the following functionalization steps are synthesized using an identical co-precipitation method. The sulfidation step, however, is performed using molar equivalent of sodium thiosulfate ($Na_2SO_3•5H_2O$), as opposed to elemental sulfur in excess . Nanoparticles are ground together with $Na_2SO_3•5H_2O$, transferred to a combustion boat, and placed in a muffle furnace at 1000°C for 1 hour. Once cool, particles are washed 3x with DI and collected via centrifugation (15,000 RCF).

3.6.2 Nanoparticle Characterization

Transmission electron microscopy (TEM) was performed using an H7600 with an accelerating voltage of 120 kV. 18 Images (1565 total particles) collected at 100,000x magnification were analyzed using ImageJ software. Images are first converted to binary (black and white) via threshold adjustment. "Watershed" feature is used to separate particles that are touching, although images with minimal particle overlap are selected for size analysis. "Analyze Particles" is used to estimate diameter. Particle diameters are plotted as a histogram in Excel.

Powder X-Ray diffraction (XRD) is performed using a Rigaku diffractometer (40 kV, 40 mA, $Cu_{K\alpha}$ X-Ray target and radiation). Measurements collected at 2θ values between 15-80°. Crystal domain size is calculated using the Scherrer equation, based on XRD peak full-width half-max.

X-Ray excited optical luminescence characterization performed using a Leica DMI 5000 microscope (Wetzlar, Germany), coupled with a DNS 300 spectrometer (DeltaNu, Laramie, WY). X-Ray source operated at a voltage of 40 kV and current of 99 µA (Mini-X X-Ray tube, Amptek Inc., Bedford, MA). For comparison of commercial particles ($Gd_2O_2S:Eu^{3+}$ 8 µm median diameter, part number UKL63/N-R1, Phosphor Technology LTD, Stevenage, UK), 30 mg of synthesized and commercial particles are deposited into separate wells in a transparent 96-microwell plate, and spectra are collected using an exposure time of 1 s.

3.6.3 Biotin Functionalization of Nanoparticles

20 mg of $Gd_2O_2S:Eu^{3+}$ particles first washed 3x in 50 mL DI water, and 1x in 50 mL 95% ethanol (UN1170, Pharmco by Greenfield Global, Brookfield, CT, USA). For wash steps, particles are centrifuged at 5000 RCF for 10 minutes, and supernatant is removed using an electronic pipette controller (MSP3000, MedSupply Partners, Atlanta, GA, USA). Particles are then resuspended in 40 mL 1x phosphate buffered saline (PBS) to a final concentration of 2 mg/mL, at pH 7.5 (P4417-50TAB, Sigma-Aldrich, St. Louis, MO, USA). Measurement of pH is performed using pH indicator strips (Indicator Paper pH 4.5-10,2614-991, Whatman™ GE Healthcare Companies, Buckinghamshire, UK).

PEGylation solution is made using 95% ethanol, at a concentration of 1 mg/mL (Silane-PEG-Biotin MW5000, 10285-5000-1g, Nanosoft Polymers, Winston-Salem, NC, USA). 10 mL of 1mg/mL washed $Gd_2O_2S:Eu^{3+}$ 2.5 μm diameter particles, and 30 μL of 1 mg/mL PEG solution are added to a 15 mL Teflon centrifuge tube for PEGylation of particles. Sample tube is placed on a 360° sample rotator for 1 hour at room temperature (~25°C) (VWR® Tube Rotator, 10136-084, Radnor, PA, USA). The particles are washed 3x with DI water, with centrifugation at 500 RCF for 10 minutes per cycle, then resuspended in 10 mL of pH 7.5 1x PBS buffer (concentration 1 mg/mL).

PEG to particle ratio was determined by calculating the surface area of a particle and supposing ~1 silane-PEG-biotin molecule could bind per nm^2. The surface area for 1 particle, based on a mean diameter of 120 nm, is calculated to be $4.52x10^4$ nm^2. This corresponds to $4.52x10^4$ PEG molecules per particle, which stoichiometrically converts to $7.5x10^{-20}$ mol PEG per particle. Based on the density of Gd_2O_2S (7.34 g/cm^3)[43], and the

calculated volume of a single particle (9.0×10^{-16} cm^3), each particle has an approximate mass of 6.5×10^{-15} g. Therefore, in a sample of 10 mg, there are approximately 1.5×10^{12} individual particles. Knowing the moles of PEG required per particle (7.5×10^{-20}), the number of Gd$_2$O$_2$S:Eu^{3+} particles in a 10 mg sample (1.5×10^{12}), and the approximate molecular weight of silane PEG biotin (5000 g/mol), we calculate that 574 µg of silane PEG biotin will provide enough surface coverage. Therefore, we add 600 µL of 1 mg/mL PEG solution to 10 mL of 1 mg/mL Gd$_2$O$_2$S:Eu^{3+}.

3.6.4 Buoyant Microbubble Verification of Biotin Functionalization

Streptavidin microbubbles and separation buffer purchased from Akadeum Life Sciences (SKU: 1110-000, Akadeum Life Sciences, Ann Arbor, MI). 50 µL of 1 mg/mL biotin labeled Gd$_2$O$_2$S:Eu^{3+}, and 50 µL microbubbles are added to 1 mL separation buffer. Control is made using same proportions of microbubbles, separation buffer, and nanoparticles (unlabeled). Solutions are placed on 360° rotator for 5 minutes, then allowed to separate for 30 minutes. Image (**figure 3.3**) taken from the side using standard phone camera, with UV illumination (~395 nm) positioned ~15 cm above open centrifuge tubes.

3.6.5 Streptavidin Labeling of Anti-Vancomycin
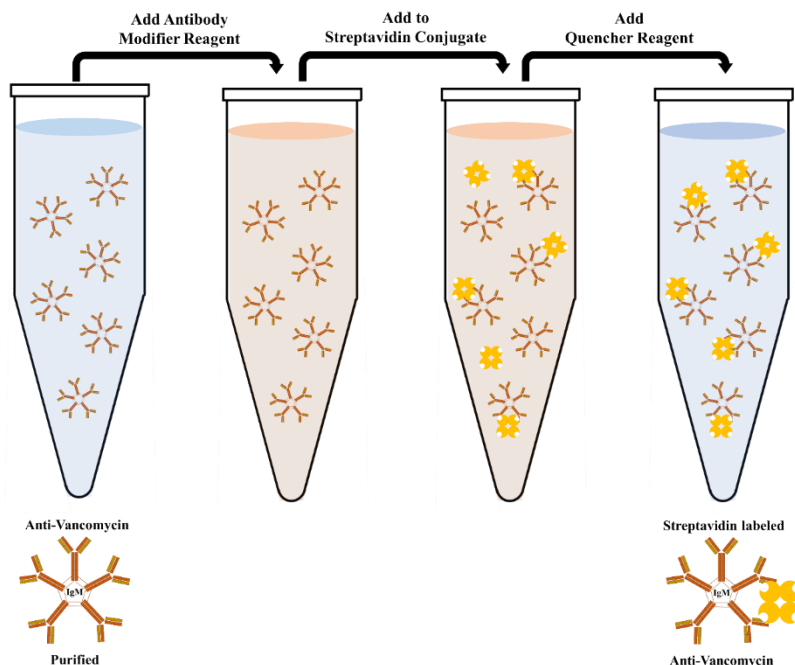
Figure 3.5. Schematic illustration for streptavidin conjugation to anti-vancomycin IgM. Figure adapted from Abcam instructional booklet.

Mouse Anti-Vancomycin antibodies (IgM) (MCA5746G, BIO-RAD, Hercules, CA, USA) are labeled with streptavidin using a streptavidin conjugation kit (ab102921, Abcam, Cambridge, MA, USA). Frozen materials are first brought to room temperature (~25°C). 100 µg (1 mg/mL) anti-vancomycin IgM is transferred to a 2 mL, low-binding, centrifuge tube. 10 µL of "modifier" are added to the solution and gently agitated. The solution is transferred to the vial of streptavidin conjugation mix and combined via drawing solution into the pipette and dispensing 3 times. The vial is wrapped in foil and left at room temperature for 3 hours to complete conjugation. 10 µL of "quencher" are added to the solution to stop reaction. The solution is ready to use after 30 minutes.

3.6.6 Anti-Vancomycin IgM Labeling of Nanoparticles

10 mg silane-PEG-biotin coated microparticles from section 3.6.2 are transferred to a fresh 15 mL centrifuge tube. 20 µL (1 mg/mL) of streptavidin labeled anti-vancomycin IgM is the added to the tube. Sample is gently inverted three times then placed in the fridge at 4°C for 12 hours. Amount of anti-vancomycin IgM to add is determined by estimating the number of particles in a 10 mg sample. Number of particles is estimated using the volume of a single particle ($V=4/3\pi r^3$) and density of gadolinium oxysulfide (7.34 g/cm^3). A target value of 16 antibody molecules per 120 nm particle is used. This is based on the calculated area of an IgM antibody (~707 nm^2), of which approximately 64 fit within the surface area of a single 120 nm particle (4.5×10^4 nm^2) . Number of antibodies is converted to mass using the average molecular weight for IgM antibodies (~900 kDa).[44] After 12 hours, particles settle naturally. Supernatant is carefully removed using a graduated plastic pipette. Functionalized particles are reconstituted in pH 7.5 PBS at a concentration of 5 mg/mL.

3.6.7 ^{3}H-Vancomycin Gradient Preparation, Imaging, and Analysis

200 µL (5 mg/mL) nanoparticles from section 3.6.5 are deposited into neighboring wells (D4-D8) in a an Optiplate-96, opaque white 96-well microplate (Perkin Elmer, Waltham, MA). 0, 10, 20, 50, and 100 µL (5 µCi/ mL) ^{3}H-vancomycin standard are then deposited to create concentration gradient. Radioluminescence images are acquired on a small animal imager (IVIS Lumina XR, Perkin Elmer, Waltham, MA) under luminescence collection only (no photograph). F/stop of 1, medium binning, field of view (FOV) B, and

300 s exposure acquisition settings are used. Luminescence image is then processed and analyzed using custom MATLAB scripts. 20x25 pixel regions of interest (ROIs) are identified, using "Data Tips" feature, for each of the five wells in the concentration gradient. 10 background ROIs (20x25 pixels) are also measured from regions within the same image surrounding the luminescent wells. Standard deviation of the blank/background (S_y) is calculated based on these values. Slope of the linear regression line (m) of total, background corrected, luminescence intensity vs. concentration of vancomycin is used, along with S_y, to calculate limit of detection according to **equation 6**:

$$LOD = 3 \times \frac{S_y}{m} \tag{6}$$

3.7 Conclusions

The goal of this work is to establish proof of concept for using radioluminescent $Gd_2O_2S:Eu^{3+}$ nanoparticles to monitor radiolabeled drug loading and release. First, radioluminescent $Gd_2O_2S:Eu^{3+}$ doped nanoparticles (~120 nm) have been synthesized via coprecipitation of gadolinium and europium nitrate salts under decomposition of urea. Characterization of nanoparticles indicates that the average crystal domain size is 56.2 nm, and X-Ray excited optical luminescence is approximately 1.4% of commercial microparticle luminescence intensity, based on spectra acquired under the same conditions.

Particles synthesized using a nearly identical method (alternative sulfidation step) are functionalized with silane-PEG5000-biotin. Functionalization is confirmed using buoyant streptavidin labeled microbubbles. Anti-vancomycin IgM is conjugated with streptavidin and intended to attach to biotin labeled nanoparticles via streptavidin-biotin

bond. Conjugation step appears to be unsuccessful because addition of ^{3}H-vancomycin to nanoparticles suspended in buffer solution do not result in a luminescence signal. However, when suspension is dried, we observe a linear relationship between luminescence intensity and concentration of radiolabeled drug. Successful streptavidin labeling of anti-vancomycin IgM, and subsequent attachment to biotin labeled particles, is expected to generate a similar response in aqueous suspension.

This method is intended for use in monitoring drug loading and release, *in vivo*. While this study demonstrates the concept for application with the antibiotic vancomycin, the approach is generalizable for any pharmaceutical appropriate for delivery via nanocarrier. For imaging *in vivo*, X-Ray luminescence tomography (XLT) can be a used to calibrate nanoparticle luminescence signal in tandem with radiolabeled analyte luminescence.[45,46] Imaging radiolabeled drug release from radioluminescent nanoparticles is more complicated than imaging drug release from a stationary, implanted film of radioluminescent $Gd_2O_2S:Eu^{3+}$. An immobilized film can be characterized prior to implantation, and a reference region can be incorporated into the sensor design to account for luminescence perturbations due to tissue.[2] Part of the advantage of nanomedicine is the ability to non-invasively achieve local drug delivery. However, this also means that the number of nanoparticles that reach the target location is dependent on a variety of factors that largely depend on individual patient biology. To achieve quantitative drug measurements, the luminescence signal due to presence of radiolabeled drug will need to be calculated ratiometrically in comparison to the luminescence signal evident under X-

Ray of known energy. To achieve this, the luminescence signal can be collected via XLT with and without X-Ray excitation.

3.8 References

[1] H. Chen, T. Moore, B. Qi, D. C. Colvin, E. K. Jelen, D. A. Hitchcock, J. He, O. T. Mefford, J. C. Gore, F. Alexis, J. N. Anker, *ACS Nano* **2013**, *7*, 1178.

[2] G. B. Schober, J. N. Anker, *Adv. Funct. Mater.* **2022**, *32*, 2106508.

[3] T. L. Moore, F. Wang, H. Chen, S. W. Grimes, J. N. Anker, F. Alexis, *Adv. Funct. Mater.* **2014**, *24*, 5815.

[4] T. Moore, H. Chen, R. Morrison, F. Wang, J. N. Anker, F. Alexis, *Mol. Pharm.* **2014**, *11*, 24.

[5] F. Wang, Y. Raval, H. Chen, T.-R. J. Tzeng, J. D. DesJardins, J. N. Anker, *Adv. Healthc. Mater.* **2014**, *3*, 197.

[6] V. J. Mohanraj, Y. Chen, *Trop. J. Pharm. Res.* **2006**, *5*, 561.

[7] S. D'Souza, *Adv. Pharm.* **2014**, *2014*, 1.

[8] X. Zhu, J. Li, P. Peng, N. Hosseini Nassab, B. R. Smith, *Nano Lett.* **2019**, *19*, 6725.

[9] P. Zhao, Y. Wang, X. Kang, A. Wu, W. Yin, Y. Tang, J. Wang, M. Zhang, Y. Duan, Y. Huang, *Chem. Sci.* **2018**, *9*, 2674.

[10] H. Wang, Y. Liu, R. He, D. Xu, J. Zang, N. Weeranoppanant, H. Dong, Y. Li, *Biomater. Sci.* **2020**, *8*, 552.

[11] T. Wu, Q. Qiao, X. Qin, D. Zhang, Z. Zhang, *Nanomedicine Nanotechnol. Biol. Med.* **2019**, *18*, 66.

[12] H. Jin, C. Wan, Z. Zou, G. Zhao, L. Zhang, Y. Geng, T. Chen, A. Huang, F. Jiang, J.-P. Feng, J. F. Lovell, J. Chen, G. Wu, K. Yang, *ACS Nano* **2018**, *12*, 3295.

[13] T. Jiang, W. Sun, Q. Zhu, N. A. Burns, S. A. Khan, R. Mo, Z. Gu, *Adv. Mater.* **2015**, *27*, 1021.

[14] D.-W. Zheng, J.-L. Chen, J.-Y. Zhu, L. Rong, B. Li, Q. Lei, J.-X. Fan, M.-Z. Zou, C. Li, S.-X. Cheng, Z. Xu, X.-Z. Zhang, *Nano Lett.* **2016**, *16*, 4341.

[15] W. Mu, Q. Chu, Y. Liu, N. Zhang, *Nano-Micro Lett.* **2020**, *12*, 142.

[16] H. Chen, M. M. Rogalski, J. N. Anker, *Phys. Chem. Chem. Phys.* **2012**, *14*, 13469.

[17] F. Alexis, J. N. Anker, *Ther. Deliv.* **2014**, *5*, 97.

[18] H. Chen, D. C. Colvin, B. Qi, T. Moore, J. He, O. T. Mefford, F. Alexis, J. C. Gore, J. N. Anker, *J. Mater. Chem.* **2012**, *22*, 12802.

[19] H. Chen, F. Wang, T. L. Moore, B. Qi, D. Sulejmanovic, S.-J. Hwu, O. T. Mefford, F. Alexis, J. N. Anker, *J. Mater. Chem. B* **2017**, *5*, 5412.

[20] C. Ash, M. Dubec, K. Donne, T. Bashford, *Lasers Med. Sci.* **2017**, *32*, 1909.

[21] T. J. Fraum, D. R. Ludwig, M. R. Bashir, K. J. Fowler, *J. Magn. Reson. Imaging* **2017**, *46*, 338.

[22] J. Ramalho, R. C. Semelka, M. Ramalho, R. H. Nunes, M. AlObaidy, M. Castillo, *Am. J. Neuroradiol.* **2016**, *37*, 1192.

[23] J. S. PhD, S. Lechevallier, D. Calise, D. Marsal, A. Siegfried, M. Vincent, C. Martinez, D. Cussac, R. Mauricot, M. Verelst, *Multimodal Gadolinium Oxysulfide Nanoparticles for Bioimaging: A Comprehensive Biodistribution, Elimination and Toxicological Study*, Social Science Research Network, Rochester, NY, **2019**.

[24] J. F. Glickman, A. Schmid, S. Ferrand, *ASSAY Drug Dev. Technol.* **2008**, *6*, 433.

[25] S. Wu, B. Liu, *BioDrugs* **2005**, *19*, 383.

[26] L. Zhang, J. Yan, Z. Yin, C. Tang, Y. Guo, D. Li, B. Wei, Y. Xu, Q. Gu, L. Wang, *Int. J. Nanomedicine* **2014**, *9*, 3027.

[27] G. A. Kumar, M. Pokhrel, A. Martinez, R. C. Dennis, I. L. Villegas, D. K. Sardar, *J. Alloys Compd.* **2012**, *513*, 559.

[28] C. Larquet, S. Carenco, *Front. Chem.* **2020**, *8*, 179.

[29] E.-J. Popovici, L. Muresan, A. Hristea-Simoc, E. Indrea, M. Vasilescu, M. Nazarov, D. Y. Jeon, *Opt. Mater.* **2004**, *27*, 559.

[30] Y.-P. Du, Y.-W. Zhang, L.-D. Sun, C.-H. Yan, *J. Phys. Chem. C* **2008**, *112*, 405.

[31] H.-X. Mai, Y.-W. Zhang, R. Si, Z.-G. Yan, L. Sun, L.-P. You, C.-H. Yan, *J. Am. Chem. Soc.* **2006**, *128*, 6426.

[32] C. Li, Z. Quan, J. Yang, P. Yang, J. Lin, *Inorg. Chem.* **2007**, *46*, 6329.

[33] C. Li, J. Yang, P. Yang, H. Lian, J. Lin, *Chem. Mater.* **2008**, *20*, 4317.

[34] H. Dong, S.-R. Du, X.-Y. Zheng, G.-M. Lyu, L.-D. Sun, L.-D. Li, P.-Z. Zhang, C. Zhang, C.-H. Yan, *Chem. Rev.* **2015**, *115*, 10725.

[35] E. Matijević, W. P. Hsu, *J. Colloid Interface Sci.* **1987**, *118*, 506.

[36] Rare-Earth Nanoparticles with Enhanced Upconversion Emission and Suppressed Rare-Earth-Ion Leakage, .

[37] P. C. Weber, D. H. Ohlendorf, J. J. Wendoloski, F. R. Salemme, *Science* **1989**, *243*, 85.

[38] C.-C. You, A. Chompoosor, V. M. Rotello, *Nano Today* **2007**, *2*, 34.

[39] N. M. Green, In *Advances in Protein Chemistry* (Eds.: Anfinsen, C. B.; Edsall, J. T.; Richards, F. M.), Academic Press, **1975**, pp. 85–133.

[40] R. R. Akhouri, S. Goel, H. Furusho, U. Skoglund, M. Wahlgren, *Cell Rep.* **2016**, *14*, 723.

[41] W. L. Pillinger, J. J. Hentges, J. A. Blair, *Phys. Rev.* **1961**, *121*, 232.

[42] D. Alloni, C. Cutaia, L. Mariotti, W. Friedland, A. Ottolenghi, *Radiat. Res.* **2014**, *182*, 322.

[43] E. I. Gorokhova, V. A. Demidenko, S. B. Mikhrin, P. A. Rodnyi, **2004**, 4.

[44] T. Klaus, K. Stalińska, D. Czaplicki, P. Mak, B. Skupien-Rabian, S. Kedracka-Krok, K. Wiatrowska, M. Bzowska, M. Machula, J. Bereta, *Sci. Rep.* **2018**, *8*, 519.

[45] C. M. Carpenter, G. Pratx, C. Sun, L. Xing, *Phys. Med. Biol.* **2011**, *56*, 3487.

[46] X. Liu, Q. Liao, H. Wang, *Opt. Lett.* **2013**, *38*, 4530.

CHAPTER 4

DEVELOPMENT OF PH SENSITIVE FILM FOR OPTICAL DETECTION OF IMPLANT ASSOCIATED INFECTION VIA ULTRASOUND LUMINESCENT CHEMICAL IMAGING (ULCI)

4.1 Abstract

We have developed an ultrasound luminescent, pH sensitive film and imaging method for early detection of implant associated bacterial infection. The film consists of mechanoluminescent europium and dysprosium doped strontium aluminate ($SrAl_2O_4$:Eu, Dy) microphosphors immobilized in a polymer film (either polydimethyl siloxane or hydrophilic polyurethane). After brief excitation with UV (~395 nm) light, a focused ultrasound beam generates an ~18x increase in luminescence intensity of the $SrAl_2O_4$:Eu, Dy film at the ultrasound focal point. By pulsing the ultrasound ON and OFF, the luminescence can be modulated and exploited for imaging. To impart pH sensitivity, first Krylon™ spray paint, and eventually nile red fluorescent dye, is used to shift $SrAl_2O_4$:Eu, Dy luminescence emission to overlap with pH sensitive dye, bromothymol blue, absorption at pH 8. As pH decreases from pH 8.0 to pH 6.0, bromothymol blue transmits more $SrAl_2O_4$:Eu, Dy excited nile red fluorescence emission. Decrease in pH manifests as an increase in luminescence intensity, which is first characterized using a spectrometer, then imaged using a novel Ultrasound Luminescent Chemical Imaging (ULCI) technique. Results demonstrate that our film(s) are sensitive to biologically relevant changes in pH, and can be imaged through tissue mimicking, light scattering media.

4.2 Introduction

In the past 10 years, there has been an upsurge in development and application of implanted medical devices, including heart valves, pacemakers, stents, orthopedic rods, screws, plates, hernia mesh, and prosthetic joints. Biomedical implants have improved and extended the quality of life for patients, but implant associated infection continues to be a concern. About 5-10% of the 2 million fracture fixation surgeries performed each year result in implant associated infection.[1] In war trauma related fractures and treatment scenarios, infection is reported to be as high as 40%.[2] The severity of infection depends on a multitude of risk factors including smoking, diabetes, immunosuppressed states, and revision surgeries for previously infected implants.[3,4] Early detection of implant associated infection is of paramount importance for maximizing treatment efficacy. For example, if infection is diagnosed within four weeks of device implantation, surgical debridement of the implant surface and administration of antibiotics is often sufficient to eradicate infection. Infections diagnosed after this initial timeframe commonly require device removal to eradicate infection, which is because bacterial biofilms exhibit increased resistance to antibiotics the longer they are permitted to grow.[5–7] Device removal is expensive and painful for patients, and there is an increased risk of re-infection from additional surgery and hospitalization. Earlier detection of implant infection may reduce the need for invasive treatment. In addition, probing the biochemical environment at the implant surface can guide efforts to develop therapeutics capable of targeting biofilms with reduced antibiotic susceptibility.

Infection specific imaging has been done using radiolabeled probes, imaged with either positron emission tomography (PET) or single-photon emission computed tomography (SPECT). However, these techniques are expensive, and require close proximity to radiochemical synthesis facilities containing a cyclotron.[8] Alternative imaging modalities that do not use radiopharmaceutical contrast agents, such as computed tomography (CT), magnetic resonance imaging (MRI), ultrasound, and X-Ray projection imaging, can provide excellent spatial resolution but lack the chemical sensitivity required for early diagnosis of infection.[9]

One promising avenue for early detection of infection is to monitor pH at the implant surface. Surface pH is a promising analyte because inflammation and infection can cause local acidosis. Acidosis is a well-documented product of bacterial metabolic fermentation and respiration (i.e., lactic and carbonic acid produced in glycolysis) , and bacterial colonies have been shown to produce a local acidic environment *in vitro*.[10] This acidic environment is suspected to play a role in reduced antibiotic susceptibility of biofilms, along with other factors such as nutrient limitation and insufficient antibiotic penetration.[5] As a result, there has been a concerted effort to develop methods to detect pH at the biomedical implant surface, *in vivo*. One such optical method is X-Ray Excited Luminescent Chemical Imaging (XELCI). This imaging modality exploits scintillators that emit visible light when excited by ionizing radiation (e.g., X-Rays). In this approach, light from X-Ray luminescent scintillators passes through a pH sensitive film that alters the spectrum and can be detected through tissue. Mapping of pH is done by scanning the sample, point-by-point, relative to a stationary X-Ray source and light collection optics.

The spectrum at each point is used to generate an image. The spatial resolution of this technique is limited, primarily, by the X-Ray beam width. This approach produces high resolution images that contain local biochemical information about the implant surface. Some drawbacks of this technique, however, are the necessity of a relatively expensive focused X-Ray source, and the associated radiation dose that limits repeated measurements.[8]

Herein we describe Ultrasound Luminescent Chemical Imaging (ULCI), which is designed for monitoring pH, *in vivo*, as an early indication of implant associated infection (**Figure 4.1**).[11] The scanning technique and image generation is similar to XELCI but uses a pulsed ultrasound source to excite a mechanoluminescent pH sensor instead of a focused X-Ray beam. Traditionally ultrasound imaging is used as a complementary diagnostic tool to capture structural images through biological tissues. Ultrasound is a lucrative optical excitation source because it is non-ionizing, and scatters less than light in biological tissues.[12] However, ultrasound alone does not provide the biochemical information necessary to measure pH, and monitor local infection. To impart biochemical sensitivity, an ultrasound luminescent film is paired with a pH sensitive dye. Specifically, $SrAl_2O_4$: Eu, Dy is a mechanoluminescent material that emits luminescence, with a maximum at ~522 nm, in response to mechanical stimulation such as ultrasound. This emission is attributed to the *$4f^65d$-$4f^7$* electronic transition of Eu^{2+} ions in $SrAl_2O_4$: Eu.[13] This emission is red shifted using, first, fluorescent spray paint, and later nile red fluorescent dye. After shifting the emission to >605 nm, the mechanoluminescence overlaps with absorption of pH sensitive bromothymol blue at pH 8 (~627 nm). As a result, pH is mapped

by scanning the UL film relative to a fixed ultrasound source and light collection optics. As pH becomes more acidic, the bromothymol blue film transmits more luminescence, manifesting as an increase in luminescence with decreasing pH.
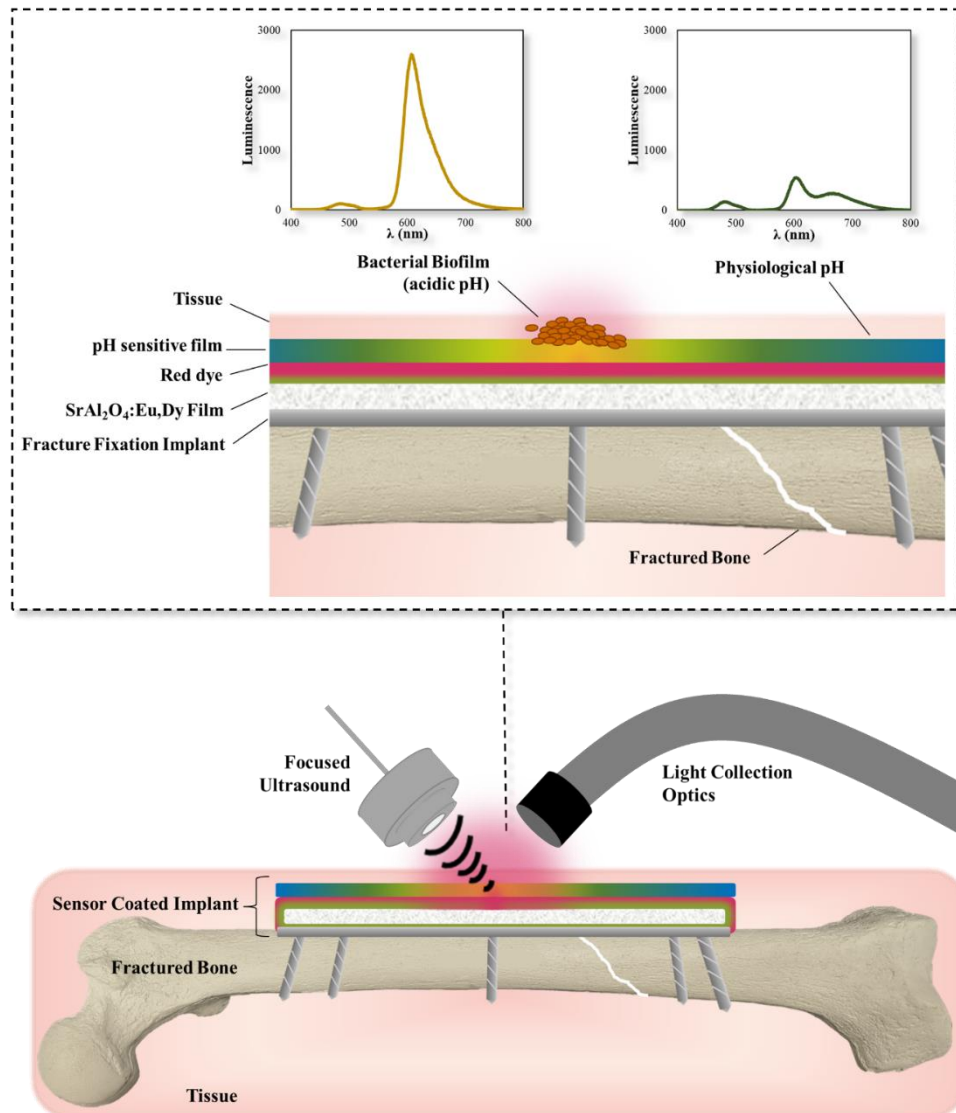
Figure 4.1 Illustration of ULCI pH sensor design and application. Sensor is attached to fracture fixation implant on a fractured bone. Focused ultrasound excites the film, point-by-point, and light is collected by a liquid light guide. Sensor Design: Green luminescence of SrAl$_2$O$_4$:Eu,Dy is shifted, using red dye, to overlap absorption of pH sensitive dye. As a result, phosphorescence is modulated by pH sensitive dye. Growth of bacterial biofilm generates an acidic environment, which causes the pH sensitive film to turn yellow. Yellow film transmits more luminescence, resulting in higher transmittance of luminescence emission. Blue/green color film, associated with physiological and basic pH, transmits less luminescence emission. pH is monitored as a function of luminescence emission intensity.

4.3. Optical Characterization of Ultrasound Modulated Mechanoluminescent Film

After exciting a polydimethyl siloxane (PDMS) encapsulated $SrAl_2O_4$:Eu, Dy microphosphor film with UV light, an ultrasound beam pulse produces a bright spot in the film (**Figure 4.2a**). $SrAl_2O_4$:Eu, Dy is a mechanoluminescent material and emits light when stimulated by ultrasound. The emission can be turned ON and OFF by pulsing the ultrasound beam as a function of time. When the ultrasound pulses ON, the spot is visible and exhibits higher emission intensity, and when it is switched OFF the emission decreases and the spot is no longer visible to the naked eye (**Figure 4.2b-c**). Moreover, the luminescence intensity increases by a factor of ~18 when the ultrasound is pulsed ON when compared to the spectra taken while the ultrasound is pulsed OFF.

Upon examination of the spectral data, we noticed a ~10 nm blue shift in the luminescence spectrum of $SrAl_2O_4$:Eu, Dy under ultrasound excitation compared to the afterglow emission seen after UV excitation. Typical afterglow emission spectra of $SrAl_2O_4$:Eu, Dy show an emission maximum at 522 nm, while the spectrum under ultrasound excitation is 512 nm. A blue shift suggests that emission is occurring from a higher energy state than with UV excitation alone. The mechanism for phosphorescence involves absorption of excitation energy, followed by intersystem crossing to an excited triplet state, from which long lived phosphorescence is emitted as electrons transition back to the singlet ground state.[14,15] A possibility is that the introduction of energy from the focused ultrasound beam is sufficient to excite the electrons to a slightly higher energy state before relaxation. This 10 nm blue shift in luminescence emission is noteworthy for optimization of pH sensor film and imaging.

4.4 Target Imaging using ULCI Scanner
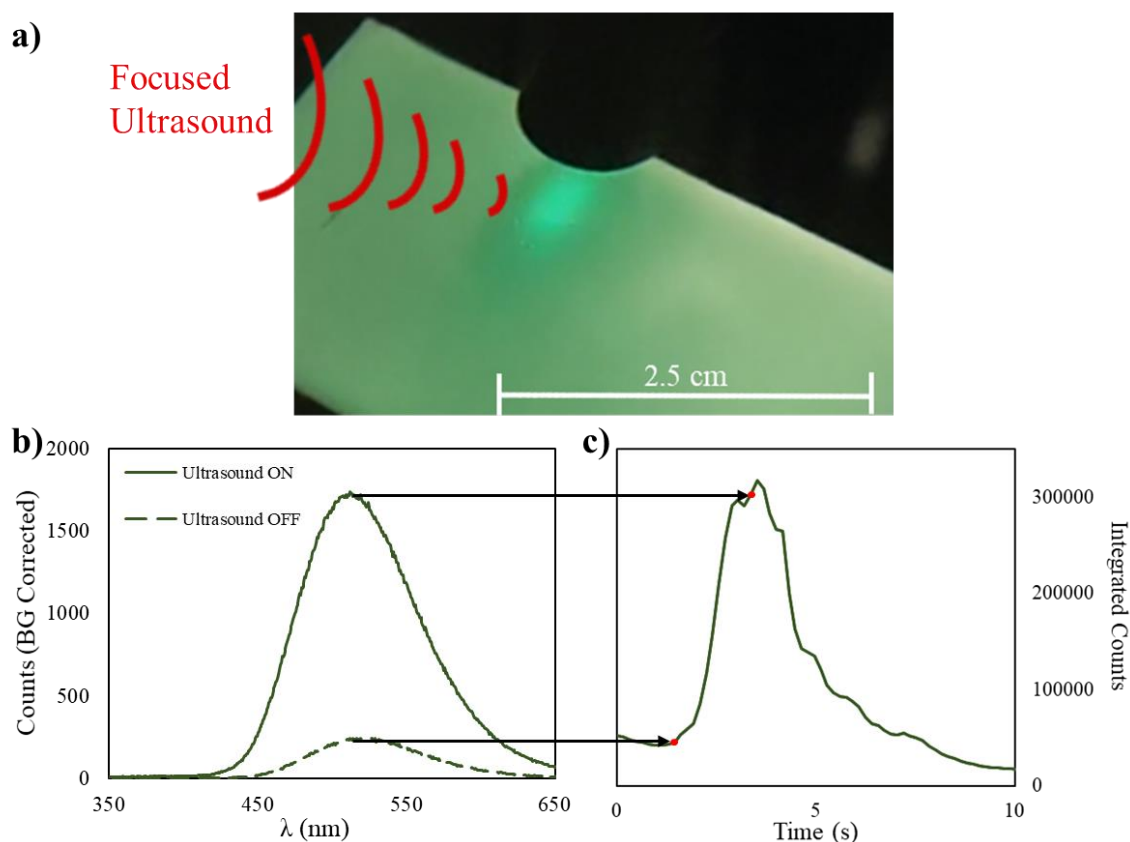
Figure 4.2 a) Depicts ultrasound excited luminescence of SrAl$_2$O$_4$:Eu, Dy embedded in PDMS. The ultrasound source is a focused beam incident on the film, visible as a bright spot. **b)** Plot shows SrAl$_2$O$_4$:Eu, Dy film behavior as ultrasound is pulsed on and off. After initial excitation with 395 nm light, ultrasound excitation produces an 18x increase in luminescence intensity compared to when the ultrasound is switched off.[13] **c)** Shows luminescence intensity as a function of time. Phosphorescence of this material increases rapidly with ultrasound excitation, and decays exponentially once ultrasound is turned off.[13]

The ULCI scanning system is a modified version of the setup used for the X-Ray excited luminescent chemical imaging system, which is described elsewhere.[10,16,17] The SrAl$_2$O$_4$:Eu, Dy film is secured to the bottom of a glass dish, and placed on an X-Y moveable stage (**Figure 4.3a**). The ultrasound probe and liquid light guide are held

stationary while the sample is raster scanned in X-Y directions relative to these components. The ultrasound probe is controlled by a function generator, which pulses the ultrasound at a chosen frequency. The liquid light guide collects light emitted from the $SrAl_2O_4$:Eu, Dy film and delivers it to a 50/50 beam splitter, which splits the signal between two photomultiplier tubes (PMTs) that contain optical filters (625 nm, and 705 nm bandpass filters, in this case). To evaluate knife-edge spatial resolution, shapes are formed with black electrical tape overtop of the $SrAl_2O_4$:Eu, Dy film.

$SrAl_2O_4$:Eu, Dy requires excitation with UV (395 nm) light, and the film emits long lasting afterglow without ultrasound excitation. The afterglow dissipates exponentially with time, and if our ultrasound source were to be continuously ON we would be unable to distinguish between background afterglow luminescence and ultrasound modulated luminescence. This is especially true for targets larger than the ultrasound focal point/spot size. The combined background luminescence can be higher than the luminescence from the ultrasound excited region. By pulsing the ultrasound ON and OFF, we are able to distinguish between the blinking, ultrasound modulated signal, and the signal attributed to background afterglow luminescence. The vertical lines apparent in the ULCI images depict ultrasound modulation. In the intensity vs linear position plot (**Figure 4.3c**) the ultrasound modulation manifests as relative increases and decreases in luminescence intensity, which allow us to distinguish ultrasound modulated luminescence from background luminescence. This modulation pattern is not seen in the regions where black tape is placed. As shown in **Figure 4.3**, triangular and rectangular shapes can be resolved using ultrasound excitation and point-by-point raster scanning. The spatial resolution is essentially limited,

in the current setup, by focused ultrasound spot size. Based on the speed of sound in water (c_s=1530 m s^{-1}) and the ultrasound transducer frequency (v=1.1 MHz), the wavelength (λ) is calculated to be 0.14 cm. We calculate the diffraction limited spot size using the following equations (**equation 1**):

$$BD = 0.62\,\frac{\lambda}{\sin\theta} \tag{1}$$

Where *BD* is the minimum resolvable beam diameter, λ is ultrasound wavelength, and θ is the half-angle.[18] Based on an approximate half angle of 22° (0.38 rad), and the wavelength of our ultrasound in water (λ=0.14 cm), we calculate a diffraction limited spot size of 1.7 mm. Our current focused ultrasound source exhibits a spot size of approximately 0.3 cm (**Figure 4.2**), so we have significant room for imaging resolution improvement. We may also achieve a smaller spot size by using a higher frequency ultrasound source (e.g. 10 MHz ultrasound source would yield a beam diameter of 0.2 mm). However, high-frequency ultrasound waves are more attenuated in biological tissues than lower frequency ultrasound waves.[19]
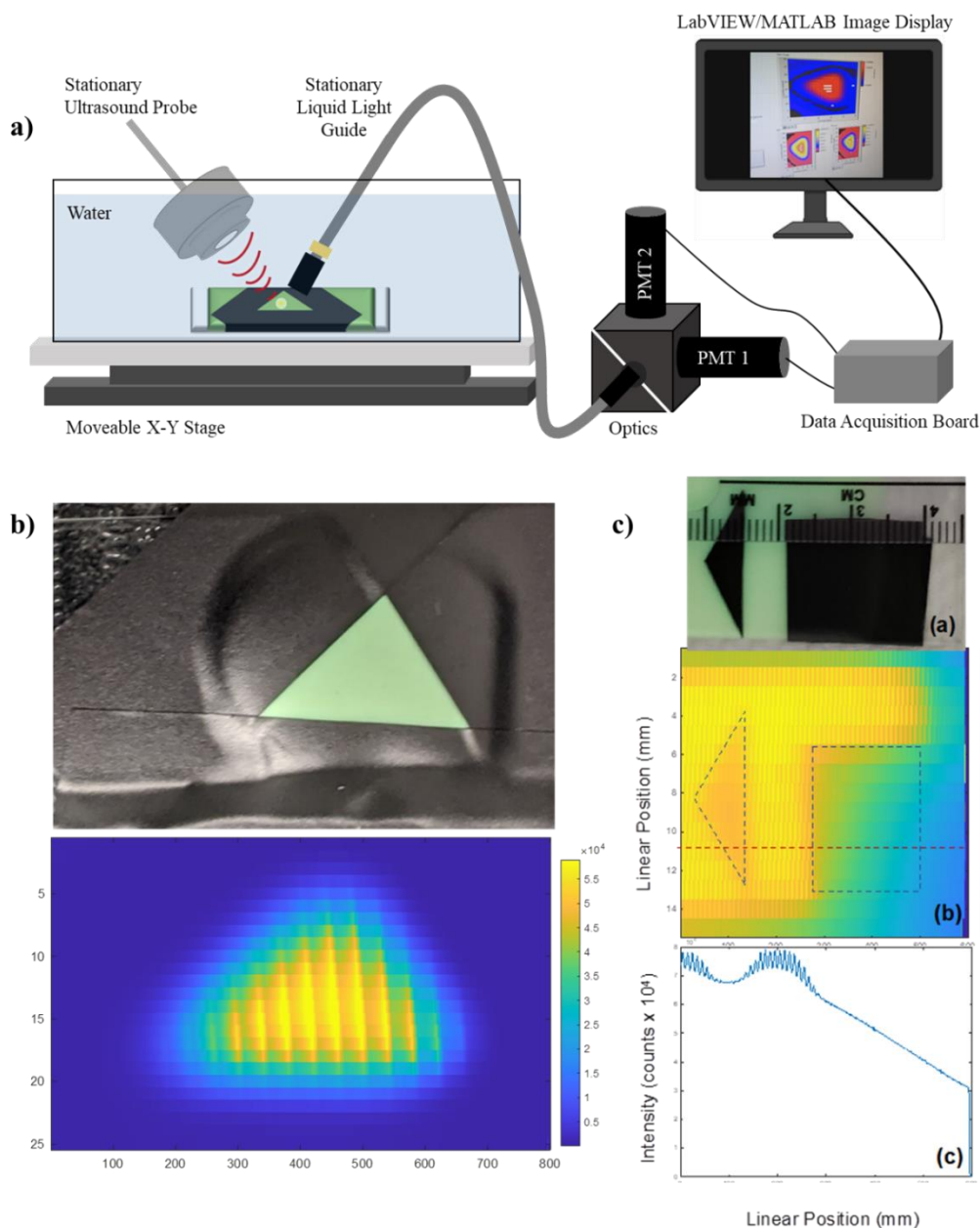
Figure 4.3 a) Depicts ULCI setup for target scanning. The ultrasound probe and liquid light guide are held stationary over the sample, which is attached to a container on the motorized stage. The liquid light guide is fed to the optical filters and PMTs contained in the 50/50 beam splitter. Information from PMTs is fed to a data acquisition board, then sent to a computer for image display using LabVIEW and MATLAB. **b)** Shows triangular $SrAl_2O_4$:Eu, Dy target, created with black electrical tape, and corresponding ULCI image. **c)** Shows triangular and square targets created on a film of $SrAl_2O_4$:Eu, Dy using black electrical tape. Part b) shows the corresponding ULCI image, and c) is a plot of intensity vs. linear position taken from b) in the region indicated by the red dotted line. Ultrasound modulation is seen in this graph as temporary increases in luminescence above background.[13]

4.5 pH Sensing with 2-Layers: UL and pH Sensitive Films

4.5.1 Strontium Aluminate with Krylon™ Paint, and pH Sensitive PEG Hydrogel
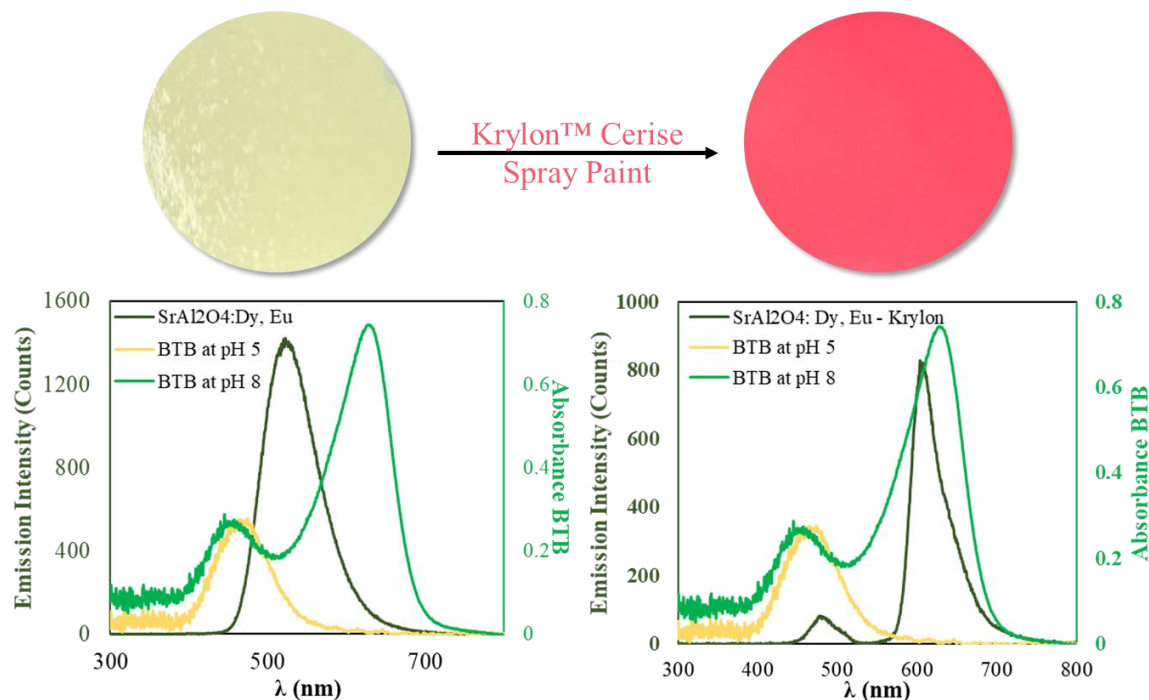
Figure 4.4 PDMS encapsulated SrAl₂O₄:Eu, Dy before and after 3 coats of Krylon™ cerise fluorescent spray paint. Plots depict the UV (395 nm) excited luminescence emission spectra, with emission intensity displayed on the left-most Y-axes. This is overlaid with the absorption profile for bromothymol blue, pH sensitive dye, at pH 5 (yellow) and pH 8 (green). Absorbance values are displayed on the right-most Y-axes. These plots demonstrate that modification of the SrAl₂O₄:Eu, Dy film with Krylon™ spray paint shifts emission to overlap with bromothymol blue absorption at pH 8.[13]

Local acidosis can be an indicator of bacterial growth on biomedical implant surfaces. As a result, we tuned our ultrasound luminescent imaging methodology to be able to detect chemical changes such as pH. As proof of principle, cerise (pink) colored Krylon™ spray paint was coated on top of the SrAl₂O₄:Eu, Dy and PDMS film to shift the luminescence emission to overlap with the absorption of a pH sensitive dye, bromothymol blue (**Figure 4.4**). Bromothymol blue is sensitive to pH range 5-8, which is appropriate for biological application and measurement of localized acidosis. At pH ~8, bromothymol blue appears green, and primarily absorbs light ~627 nm. At pH 4, bromothymol blue appears

yellow, and absorbs light ~ 474 nm. SrAl$_2$O$_4$:Eu, Dy exhibits a luminescence maximum at ~522 nm. When coated with pink Krylon™ spray paint, the luminescence emission is absorbed, and fluorescence is emitted by the paint at ~607 nm. This emission wavelength overlaps with the absorption maximum of bromothymol blue at pH 8 (**Figure 4.4**). When the surrounding medium is at a higher pH, more of the luminescence emission is absorbed by the bromothymol blue dye. As a result, when a hydrogel impregnated with bromothymol blue is placed on top of the Krylon™ coated SrAl$_2$O$_4$:Eu, Dy film, the luminescence intensity decreases as pH increases. This is because when the bromothymol blue film is under acidic conditions, it does not absorb as much of the luminescence emission when compared to more basic conditions. The pH modulated luminescence intensity at a given wavelength (L_{pH}) can be estimated according to the following relationship between percent transmittance of bromothymol blue at a given pH (*%T*) and unmodulated luminescence intensity (*L*) at that wavelength (**Equation 2**). *%T* is related to total absorbance (A_t) and can be written in terms of concentration of deprotonated bromothymol blue (C_{in-}) and protonated bromothymol blue (C_{Hin}), using Beer-Lambert Law (A=εbC, where ε is the molar absorptivity coefficient, b is the path length, and C is the concentration) (**Equations 3 & 4**). Concentrations of protonated and deprotonated pH indicator (BTB) can be calculated using the Henderson-Hasselbalch equation, inputting the pH value and the pK$_a$ (~7.5) (**Equation 5**).

$$L_{pH} = \%T \times L \tag{2}$$

$$\%T = 10^{-A} \tag{3}$$

$$A_t = (\varepsilon_{in-}bC_{in-}) + (\varepsilon_{Hin}bC_{Hin}) \tag{4}$$

$$\frac{C_{in^-}}{C_{Hin}} = 10^{pH-pKa} \tag{5}$$

$$F = C_{in^-} + C_{Hin} \tag{6}$$

$$C_{in^-} = \frac{10^{pH-pKa} \times F}{1+10^{pH-pKa}} \tag{7}$$

$$L_{pH} = \left(10^{-bF\left(\frac{(\varepsilon_{in^-} \times 10^{pH-pKa})+\varepsilon_{Hin}}{1+10^{pH-pKa}}\right)}\right) \times L \tag{8}$$

The total formal concentration of bromothymol blue indicator (F) consists of the sum of deprotonated (C_{in^-}) and protonated (C_{Hin}) components. Equations 5 and 6 are combined to give C_{in^-} as a function of pH, pK_a, and F in **Equation 7**. Equations 2-7 are then combined in **Equation 8** to give luminescence intensity (at a given wavelength) as a function of underlying luminescence spectrum, F, b, ε for protonated and deprotonated BTB, pH, and pK_a. This equation demonstrates that we can calculate the amount of protonated and deprotonated BTB species by measuring pH, and inputting the total formal concentration (F). The signal saturates at low and high pH values, but exhibits sensitive color change (and luminescence modulation) within one pH unit of the pK_a value (~7.5, if we assume one discrete pK_a value). A higher pH yields a higher concentration of deprotonated BTB (C_{in^-}) and will result in a higher absorbance of longer wavelengths. In other words, as pH increases, the $SrAl_2O_4$:Eu, Dy luminescence transmission decreases. This is seen clearly in **Figure 4.5a**, where the luminescence spectra of the Krylon™ coated $SrAl_2O_4$:Eu, Dy film is collected as it passes through the pH sensitive bromothymol blue hydrogel at pH's between 4-9. We note, however, that the response occurs over a wider pH range than expected for the free BTB dye. This suggests that there are a range of microenvironments within the film that cause a spread in local pK_a. This is an advantage

when interested in looking at a wider pH range, but reduces sensitivity near the free dye's

pK$_a$. Nonetheless, the luminescence emission intensity, under consistent UV excitation, is

highest at low pH (pH 4) and lowest at high pH (pH 9).

The pH sensor film, which also contains a control region of hydrogel without

bromothymol blue, was imaged in a solution of coffee creamer (~1.0 g/L) to simulate light

scattering in biological tissue. **Figure 4.5d-e** shows images at pH 4 and pH 9, using

ultrasound modulated frequency of 2 Hz, with a scan speed of 1 mm/s. The pH sensitive
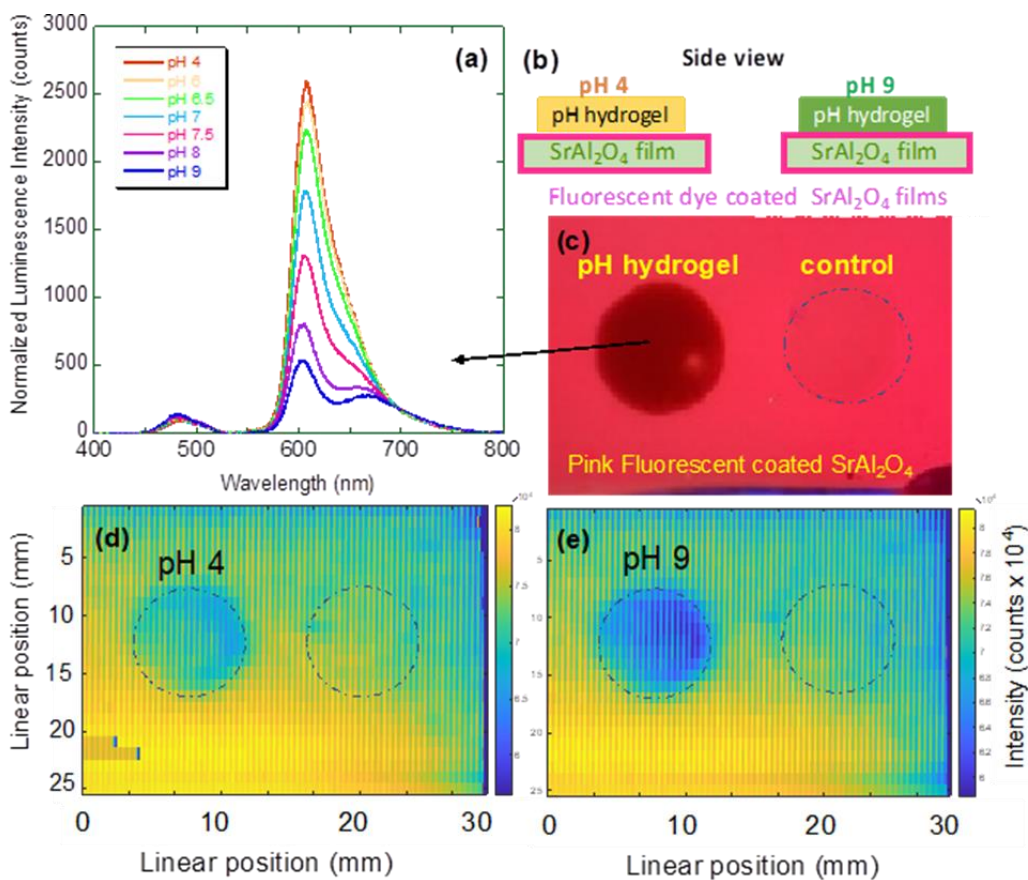
Figure 4.5 a) Plot depicts changes in luminescence intensity of Krylon™ coated SrAl$_2$O$_4$:Eu, Dy film modulated by bromothymol blue pH sensitive dye impregnated PEG hydrogel target at pH 4.0-9.0. **b)** Schematic of film fabrication: SrAl$_2$O$_4$:Eu, Dy film is coated with Krylon™ spray paint, the bromothymol blue PEG hydrogel is attached on top using cyanoacrylate glue. **c)** Image of pH sensor. Left-most hydrogel contains bromothymol blue, and rightmost gel does not (control gel). Hydrogel targets only cover a portion of the Krylon™ coated SrAl$_2$O$_4$:Eu, Dy film. **d)** ULCI image at pH 4. **e)** ULCI image at pH 9. Vertical lines evident in these images are due to ultrasound modulation at 2 Hz (1 mm/s scan rate).[13]

target is clearly distinguishable, in comparison to the control target, from background. Furthermore, the target at pH 9 appears darker, according to the luminescence color map, when compared to the target in the image at pH 4. The decrease is luminescence with increase in pH is consistent with the spectroscopic data shown in **Figure 4.5a**.

The use of Krylon™ spray paint to red shift $SrAl_2O_4$:Eu, Dy film was successful, but impractical for application *in vivo*. Spray paint contains toxic hydrocarbons such as toluene, benzene, and xylene, which are associated with increased risk of renal tubular acidosis, hypokalemic paralysis, and various hematological disorders.[20,21] While it is possible to encapsulate spray paint in the PDMS film with $SrAl_2O_4$:Eu, Dy, thereby circumventing issues associated with leaching and toxicity, the fluorescent dye used in the Krylon™ spray paint is considered proprietary information. This affects the ability to reproduce data in the future, as the exact paint recipe is unknown. As a result, alternative dyes are investigated in the following section(s) that similarly shift the $SrAl_2O_4$:Eu, Dy luminescence emission spectrum.

Another challenge with this approach is the attachment of the hydrogel pH sensitive target to the paint coated $SrAl_2O_4$:Eu, Dy film. The hydrogel is structurally brittle, and difficult to attach to the film without breaking. In the images for **Figure 4.5**, the hydrogel is attached to the luminescent film using household superglue. Occasionally the superglue interacts with the pH sensitive target, preventing reliable pH response and color change. Ideally, the goal is to make a pH sensitive, ultrasound luminescent film, that contains all the necessary components in a single layer. The next section discusses an intermediate step

where an alternative, flexible, hydrophilic polyurethane is used as an alternative to both PDMS and the PEG hydrogel.

4.5.2 Strontium Aluminate with Nile Red, and pH Sensitive Hydrophilic Polyurethane Film
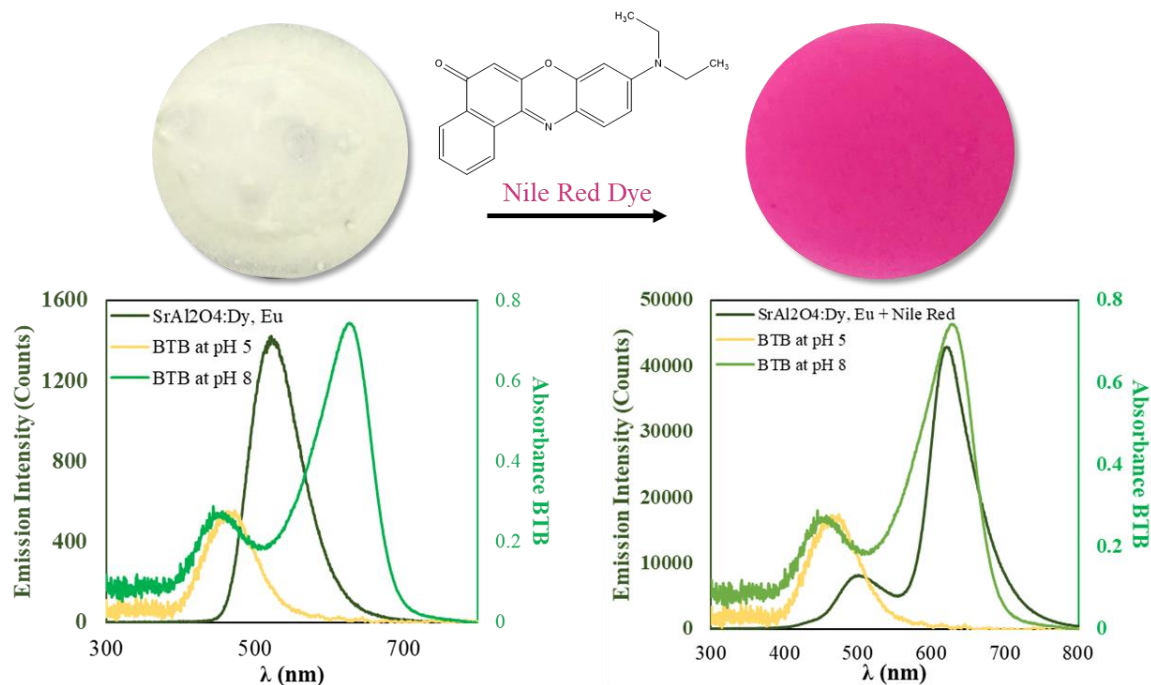
Figure 4.6 HydroMed™ D3 encapsulated SrAl$_2$O$_4$:Eu, Dy with and without nile red fluorescent dye. Plots depict the UV (395 nm) excited luminescence emission spectra, with emission intensity displayed on the left-most Y-axes. This is overlaid with the absorption profile for bromothymol blue, pH sensitive dye, at pH 5 (yellow) and pH 8 (green). Absorbance values are displayed on the right-most Y-axes. These plots demonstrate that modification of the SrAl$_2$O$_4$:Eu, Dy film with nile red shifts emission to overlap with bromothymol blue absorption at pH 8.

Nile red (9-(Diethylamino)-5H-benzo[a]phenoxazin-5-one) is a solvatochromic dye, which means the shape and spectral position of absorption and emission bands vary (up to 100 nm) with solvent. Specifically, nile red excitation and emission spectra shift toward shorter wavelengths as solvent polarity decreases.[22–24] This phenomenon is seen in fluorescent compounds that have aromatic rings with polar substituents, details of which have been explored elsewhere.[25] When a polar solvent (i.e., ethanol) is used to deposit a

film of HydroMed™ D3 (hydrophilic polyurethane), $SrAl_2O_4$:Eu, Dy, and nile red, the absorption of nile red overlaps sufficiently with emission of $SrAl_2O_4$:Eu, Dy. As a result, the fluorescence maximum of nile red in the UL film is observed to be at ~624 nm, compared to ~522 nm luminescence with $SrAl_2O_4$:Eu, Dy alone (**Figure 4.6**). The fluorescence of nile red overlaps with absorption of pH sensitive bromothymol blue at pH 8 (~627 nm), which makes nile red an appropriate replacement for the Krylon™ cerise spray paint.

To impart pH sensitivity, the bromothymol blue film was made using HydroMed™ D3, instead of the PEG hydrogel (described in previous section). As expected, this film is much more flexible and easier to manipulate without tearing or fracturing. Initially this film was directly deposited onto the UL film containing nile red (sealed with PDMS), with the expectation that the two separate films would adhere to one another. However, this was not seen to be the case once the films were submerged in buffer. The topmost film, containing only HydroMed™ D3 and bromothymol blue, detached once the polymer absorbed water. As a result, the film needed to be attached using cyanoacrylate glue on either side of the film. Once secured with glue over-top of the UL film, the bromothymol blue film stayed in place and the color change was uniform after 5 minutes when transferred from PBS buffer at pH 5 (yellow) to new PBS buffer at pH 8 (dark green) (**Figure 4.7c**). While the dye is uniformly distributed throughout the film, the film itself exhibits visible striations and puckering (evident in the photos). However, the emission intensity decreases as pH increases, which is consistent with our expectation (**Figure 4.7a-b**).
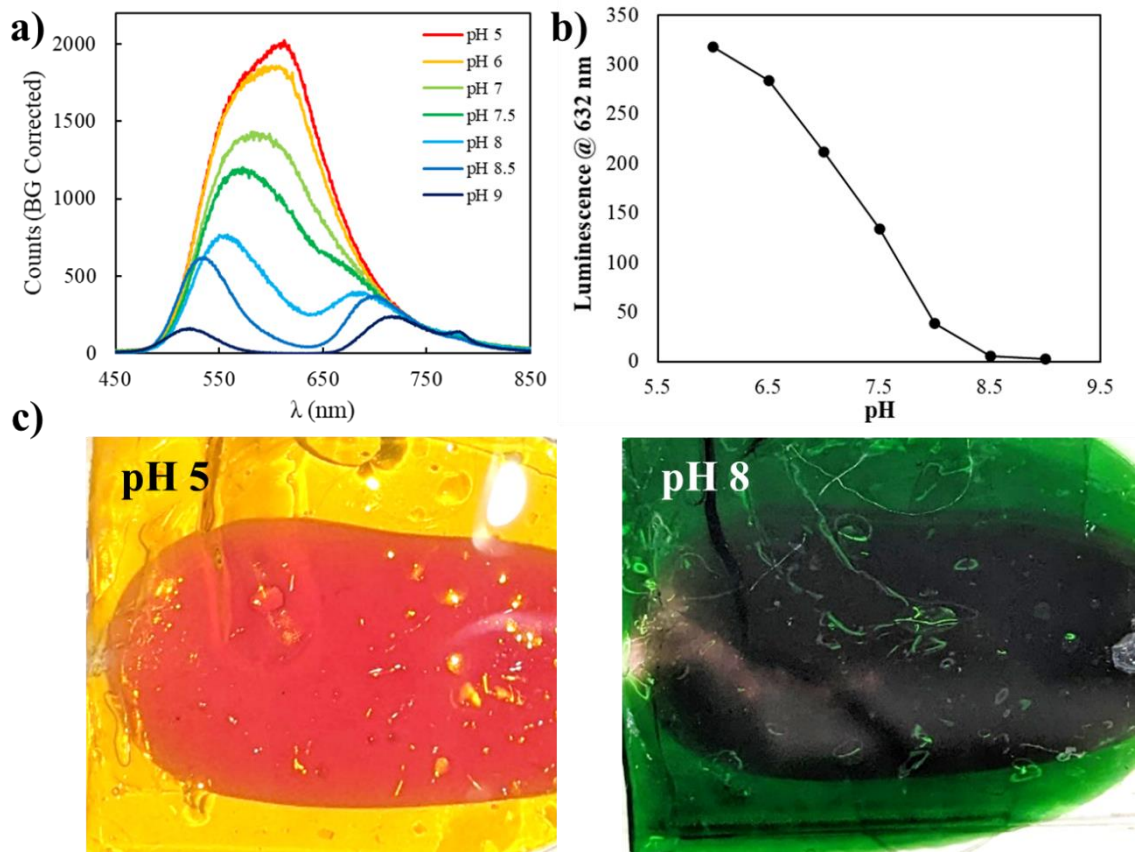
Figure 4.7 a) Plot depicts changes in luminescence intensity of nile red and $SrAl_2O_4$:Eu, Dy film modulated by HydroMed™ D3 film containing bromothymol blue pH sensitive dye at pH 5.0-9.0. **b)** Plot depicting the change in luminescence at 632 nm (the fluorescence maximum for nile red) vs. pH **c)** Images of 2-layer pH sensor. Left-most image shows the yellow color of bromothymol blue at pH 5, and the right-most image shows the green color at pH 8.

4.6 All-In-One pH Sensing Films

4.6.1 Characterization of Nile Red for All-In-One Film
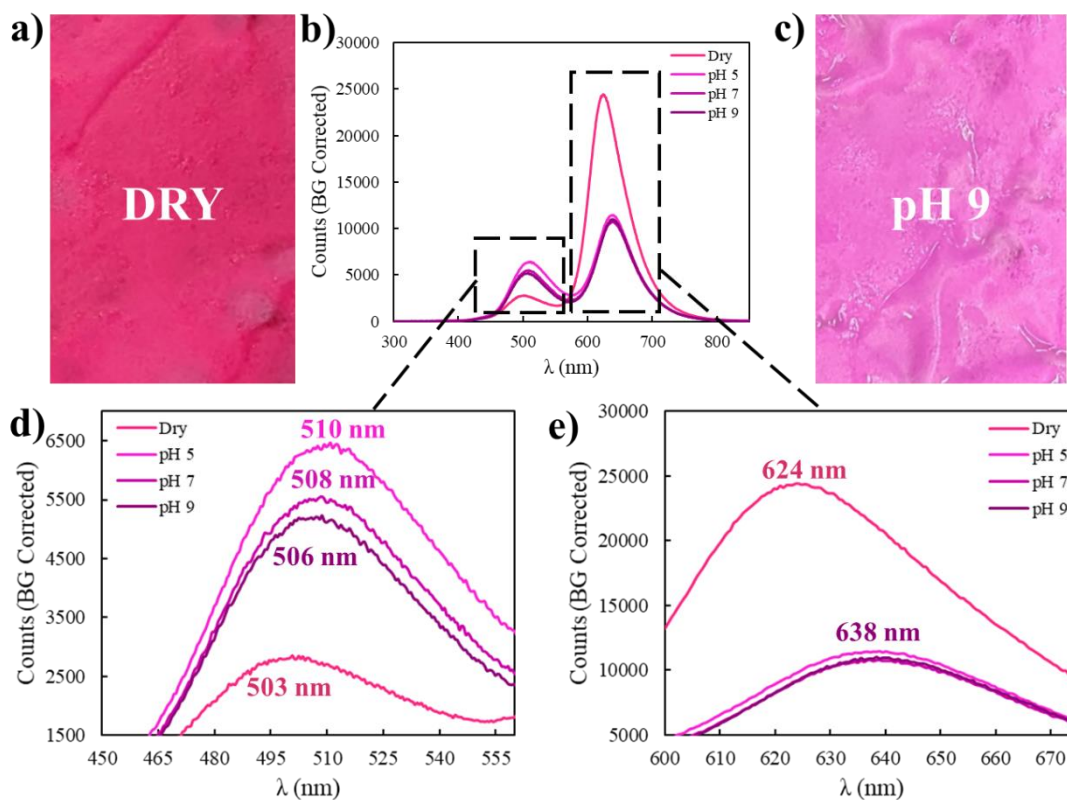
Figure 4.8 Demonstrates the effect of aqueous solution and pH on nile red dye. **a)** HydroMed™ D3 film with nile red before equilibration (dry). **b)** Luminescence spectra of nile red film dry, and at pH 5,7, and 9. Spectra acquired immediately after switching UV excitation source OFF. **c)** nile red film after 30 minutes of equilibration at pH 9. **d)** Wavelength region 450-555 nm from spectrum plotted in b), expanded to see subtle differences. Slight red shift in nile red fluorescence from 503 nm to 510 nm at pH 5, 508 nm at pH 7, and 506 nm at pH 9. **e)** Wavelength region 600-670 nm from spectrum plotted in b), expanded to see subtle differences. Slight red shift in nile red fluorescence from 624 nm to 638 nm at pH 5, 7, and 9.

Due to the solvatochromic properties of nile red, the previous iteration of ULCI film involves sealing the HydroMed^{TM} D3 + SrAl$_2$O$_4$:Eu, Dy + nile red film with PDMS to prevent shifts in the absorption and emission spectra in different aqueous (pH) environments. The pH sensitive bromothymol blue film was attached separately, and the pH sensitive layer is the only layer that needs to change colors. However, to make a pH sensitive film that contains all necessary components within a single layer, the behavior of nile red in HydroMed^{TM} D3 (with SrAl$_2$O$_4$:Eu, Dy) needs to be characterized at different pH's.

The HydroMed™ D3 nile red film, containing SrAl$_2$O$_4$:Eu, Dy, exhibits emission maxima at 503 nm and 624 nm before submersion in buffer (dry). Immediately after submersion in pH 5 buffer, the film changes from a deep pink color to a more pastel purple color. After equilibration in buffer for 30 minutes, the color does not change dramatically from pH from 5 to 9. The 503 nm peak shifts to 510 nm at pH 5, 508 nm at pH 7, and 506 nm at pH 9. The primary peak at 624 nm, which is the region of luminescence modulated by bromothymol blue, shifts to 638 nm at pH 5, then stays at 638 nm from pH 7-9. The absorption maximum for bromothymol blue at pH 8 is ~627 nm, so the red shift in emission maximum of nile red means there is less overlap between the fluorescence and absorption. This could translate to a less dramatic change in luminescence intensity with pH than seen with the nile red film sealed in PDMS. However, the shift is not dramatic enough to prevent this film design from working and the advantages of an all-in-one film outweigh the potential drawbacks. Additionally, once the film is equilibrated in aqueous solution (of any

pH studied), the emission remains consistent at 638 nm. Nile red, within our target pH range, remains an appropriate choice to shift the emission spectrum of SrAl$_2$O$_4$:Eu, Dy.

4.6.2 All-In-One Film
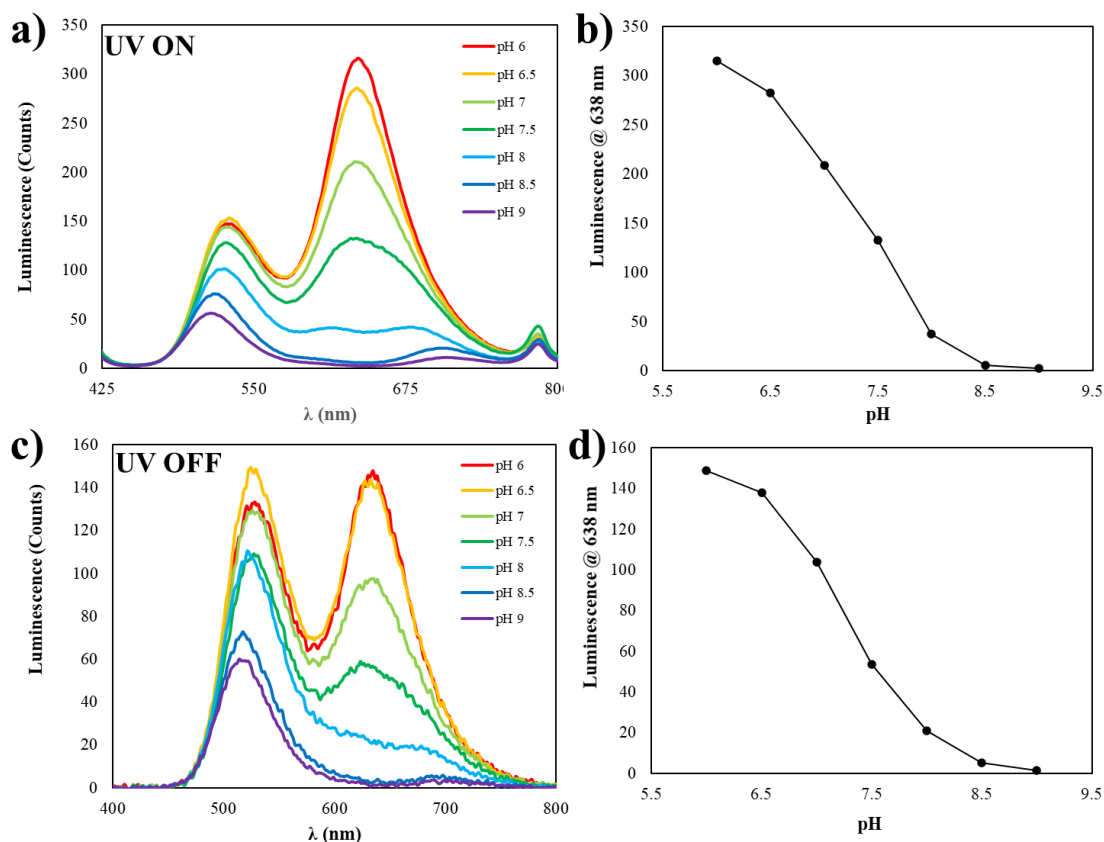
Figure 4.9 a) Plot depicts changes in luminescence intensity of all-in-one HydroMed™ D3, nile red, SrAl$_2$O$_4$:Eu, Dy, bromothymol blue pH sensitive film at pH 6.0-9.0. UV left ON for spectra acquisition **b)** Plot depicting the change in luminescence at 638 nm (the fluorescence maximum for nile red after equilibration in water) vs. pH for UV ON **c)** Plot depicts changes in luminescence intensity of all-in-one HydroMed™ D3, nile red, SrAl$_2$O$_4$:Eu, Dy, bromothymol blue pH sensitive film at pH 6.0-9.0. UV turned OFF for spectra acquisition. **d)** Plot depicting the change in luminescence at 638 nm (the fluorescence maximum for nile red after equilibration in water) vs. pH for UV OFF.

In **Figure 4.9** the all-in-one film response to pH 6.0-9.0 is demonstrated by taking luminescence spectra, with and without UV, after equilibration in various buffer solutions. Spectra acquired with UV OFF have lower emission intensity overall, which is because the

afterglow of $SrAl_2O_4$:Eu, Dy decays exponentially with time (**Figure 4.2c**). Because the pH response of this film is based on changes in luminescence intensity, the time between switching the UV flashlight off and collecting spectrum needs to be consistent for each pH spectrum collected. For this reason, the characterization is compared with spectra taken while the UV light remains ON. For both UV ON and UV OFF, the emission intensity at 638 nm decreases as pH increases. The wavelength 638 nm is chosen because this is the fluorescence maximum determined for nile red within this pH range (section 5.6.1). As expected, the bromothymol blue dye absorbs more of the luminescence emission as it changes from yellow to green (i.e., as pH increases). Despite the 14 nm red shift in nile red fluorescence, the all-in-one film behaves in a similar manner to the 2-part films described in section 5.5 and is most sensitive to changes between pH 6.0 and 8.0. Normal muscle tissues have relatively neutral pH (between 7.0-7.4), and a study of implant surface pH during infection (using microelectrodes) showed that pH dropped to ~6.0.[26] Therefore, this film is sensitive within the correct range to measure biologically relevant pH for localized acidosis.

The film is imaged at pH's 6.0 and 9.0 using ULCI scanner as shown in **figure 4.10**. According to the color map generated in MATLAB, the luminescence intensity is ~5x brighter at pH 6.0, when compared to pH 9.0. The luminescence in the control target remains the same at each pH value. The control target in these experiments contains only HydroMed™ D3 and $SrAl_2O_4$:Eu, Dy, but a more appropriate control should also contain nile red dye. Nile red is intended to impart a consistent red shift in the UL emission of $SrAl_2O_4$, but the subtle solvatochromic shifts (**Figure 4.8**) can be accounted for by adding

nile red to the control region in the future. However, the images acquired in this experiment are more blurred than previously acquired images (i.e. 2-part ULCI film in section 4.5.1**, figure 4.5**). The ultrasound modulation is also difficult to identify if it is present at all. One possible explanation for this is the new target holder made using a laminating pouch. The advantage of this target holder is that the circular window allows circulation of surrounding liquid both above and below the film, without the need for cyanoacrylate adhesive. This design may not hold the UL pH sensor film as rigidly as when a glass slide is beneath the film for support, as is the case for the 2-part films shown in section 5.5. In addition, the behavior of the focused mist-maker ultrasound is inconsistent, and eventually stopped working during experimentation. The ULCI images may not be ultrasound modulated if the ultrasound was not pulsing as it was programmed to, which means the images reflect $SrAl_2O_4$:Eu, Dy afterglow from UV excitation only. This makes distinction between target and background difficult. Nonetheless, the film behaves as expected and the ULCI images still reflect a change in luminescence intensity consistent with increase in surrounding pH.
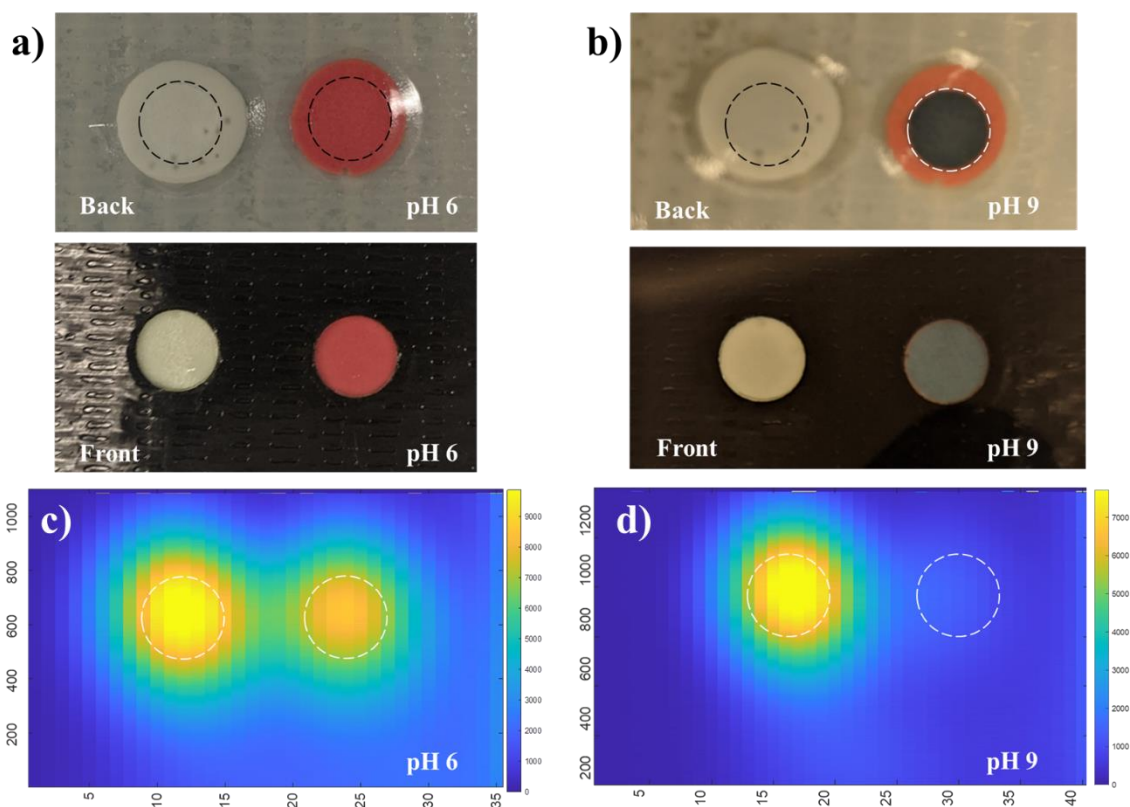
Figure 4.10 Laminating pouch sample holder with windows punched through the front and back layers. Film is held in place around the outer circumference, exposing both films to surrounding medium. The front of the laminating pouch is covered in black duct tape. Left-most film contains only HydroMed[TM] and strontium aluminate. Right-most film contains HydroMed[TM], strontium aluminate, nile red fluorescent dye, and bromocresol blue pH sensitive dye. **a)** Depicts film after equilibration at pH 6. **b)** Depicts film after equilibration at pH 9. Left-most control film does not change color with pH. **c)** ULCI image taken of the sensor at pH 6, from the front side. **d)** ULCI image taken of the sensor at pH 9, from the front side.

4.7 Methods

4.7.1 Preparation of UL film

Polydimethyl siloxane (PDMS) (Sylgard 184 Silicone Elastomer base and curing agent, DOW, Midland, MI, USA) is prepared in a 10:1 ratio (base: curing agent). The PDMS mixture is then combined in a 1:2 ratio, by mass, with $SrAl_2O_4$:Eu, Dy mechanoluminescent powder (756539-25G, Sigma Aldrich, St. Louis, MO, USA). The

mixture is whipped for 10 minutes, then poured onto a substrate, usually a glass microscope slide, for curing. After pouring, the film is placed in a vacuum chamber for 30 minutes to remove excess air bubbles. To cure PDMS, the film is placed in the oven at 80°C for 1 hour. The film, prepared in this way, was used for initial ULCI testing and characterization (**figure 4.2 and 4.3**)

4.7.2 Acquisition of Ultrasound Excited Luminescence Spectra with Time Decay

Film is placed face down on the microscope stage (DMI 5000, Leica Microsystems, Germany), centered over the objective lens. The film is first irradiated from the top with a UV flashlight (395 nm, EscoLite, La Palma, CA, USA), held using a ring stand and clamp, ~ 10 cm from the sample in a perpendicular orientation. For spectra acquisition, a focused ultrasound beam is incident on the UL film, which is generated by a mist-maker removed from a basic humidifier (unknown make and model). Ultrasound spot size is approximately 3 mm in diameter. The ultrasound is pulsed at a frequency of 2 Hz. A 5X objective lens directs light to a spectrometer (DNS 300, DeltaNu, Laramie, WY, USA) to collect spectral data. Kinetic spectra acquisition is used for this experiment with 0.15 s exposure time for a total of 50 seconds.

4.7.3 Application of Krylon™ Spray Paint

To red shift the $SrAl_2O_4$:Eu, Dy emission for overlap with bromothymol blue (pH sensitive dye) absorption, 3 coats of pink, fluorescent spray paint (Krylon Fluorescent

Spray Paint-Cerise, Cleveland, OH, USA) are applied overtop of the cured PDMS/ SrAl$_2$O$_4$:Eu, Dy film. Each coat was dried for 3 hours at room temperature (~25 °C). Before attachment of pH sensitive hydrogel, the painted film was placed in the oven at 80°C for 12 hours to evaporate any remaining solvent.

An alternative method for preparing this film is to incorporate the spray paint into the film, instead of applying paint over top of the film. To do this, 3 coats of paint are applied directly to SrAl$_2$O$_4$:Eu, Dy powder. Once dry, the powder and paint are ground together using a mortar and pestle. The SrAl$_2$O$_4$:Eu, Dy/fluorescent paint mixture can then be added to PDMS in the same ratio as described above. The advantage to this method is that the toxic paint is encapsulated by the biocompatible PDMS.

4.7.4 Preparation of pH Sensitive PEG Hydrogel

The hydrogel is prepared with 35 weight % acrylamide monomer (01696-100G, Sigma-Aldrich, St. Louis, MO, USA), 35 weight % poly(ethylene glycol) diacrylate (PEGDA- Mn 700) chemical cross-linker (455008-100ML, Sigma-Aldrich, St. Louis, MO, USA), 1 weight % 2,2-dimethoxy-2-phenyl acetophenone (DMPA) (196118-50G, Sigma-Aldrich, St. Louis, MO, USA), 0.5 weight % bromothymol blue pH indicator dye (114413-5G, Sigma-Aldrich, St. Louis, MO, USA), and deionized water. All materials are brought to room temperature (~25°C) prior to mixing. Once warmed to room temperature, each component is used as received. An example recipe for 5 g total: 1.75 g acrylamide monomer, 1.75 g PEGDA-700, 25 mg of bromothymol blue, 50 mg DMPA, and 1.425 g

117

deionized water. The mixture is combined using a 360° sample rotator for 3 hours. The solution is then injected into a mold, which is fabricated using a rectangular silicone spacer (400 μm thickness), sandwiched between two 3-inch x 3-inch flint glass plates, clamped together using three binder clips (one on the left, right, and bottom edges). Prior to mold fabrication and injection of polymer solution, the glass plates are soaked in a glass cleaning solution composed of 50 g/L sodium hydroxide (NaOH) in 50% Ethanol for 12 hours, then rinsed with DI water and dried in the oven at 80°C for 30 minutes. The mold, containing polymer solution, is placed into a nitrogen purged glove box (2100-4-C, Cleatech LLC, Santa Ana, CA, USA) for 2 hours. Photo-polymerization is then performed using UV irradiation (~368 nm) for 10 minutes. After polymerization, the hydrogel is removed from the mold by soaking in deionized water. Once removed from the mold, the hydrogel is cycled between 70% ethanol and deionized water each day for four consecutive days (this serves to remove excess monomer, unreacted initiator, and unadhered dye molecules). Once this process is complete, the hydrogel is stored in pH 7 phosphate buffered saline. For preparation of the control hydrogel, the same process is used. The only difference is bromothymol blue is not added to the mixture, and the difference in mass is accounted for by adding additional deionized water (i.e., for the 5 g recipe above, 1.450 g water would be added instead of 1.425 g).

To attach the polymerized hydrogel to the UL film, the gels are cut using a circular hole cutter (3/8 inch diameter), then adhered using cyanoacrylate (Gorilla Super Glue Gel, The Gorilla Glue Company, Cincinnati, OH, USA).

4.7.5 Preparation of HydroMed™ D3 Film with SrAl2O4:Eu, Dy and Nile Red

HydroMed[TM] D3 (AdvanSource Biomaterials Corp, Wilmington, MA, USA) is an ether-based hydrophilic polyurethane designed for coating biomedical implants. This material was chosen because it can be used to immobilize $SrAl_2O_4$:Eu, Dy particles, and is appropriate for incorporation of Nile Red fluorescent dye (N0659, TCI America, Portland, OR, USA). All recipe calculations are based on the total volume of solvent (95% ethanol) chosen and does not account for volume changes due to the addition of individual components. First HydroMed[TM] D3 (120 mg/mL) is added to ethanol. The mixture is placed on a 360° sample rotator for 24 hours to completely dissolve polymer. The following components are added once HydroMed[TM] is dissolved: $SrAl_2O_4$:Eu, Dy (300 mg/mL), and Nile Red (0.08 mg/mL). An example recipe is 0.75 g $SrAl_2O_4$:Eu, Dy, 0.3 g HydroMed[TM] D3, 2.5 mL ethanol (95%), and 200 µL Nile Red (1 mg/mL in acetone). The mixture is then placed on the 360° sample rotator for 3 hours, to ensure homogeneous combination of all components. The mixture is then carefully poured onto a glass microscope slide and placed into a vacuum chamber for 12 hours to evacuate air bubbles and evaporate solvent.

Because Nile Red is a solvatochromic compound, the film must be sealed before placing it into solution to maintain consistent fluorescence properties. PDMS is combined in a 10:1 ratio (base: curing agent) by mass. The mixture is whipped for 10 minutes, then placed in a vacuum chamber to evacuate air bubbles. The PDMS is then thinly spread over top of the $SrAl_2O_4$:Eu, Dy/Nile Red/HydroMed[TM] film using a spatula. The film is then placed in the oven at 80°C for 1 hour to cure.

4.7.6 Preparation of HydroMed™D3 film with pH Sensitive Bromothymol Blue

All recipe calculations are based on the total volume of solvent (95% ethanol) chosen and does not account for volume changes due to the addition of individual components. First HydroMed™ D3 (120 mg/mL) is added to ethanol. The mixture is placed on a 360° sample rotator for 24 hours to completely dissolve polymer. Bromothymol blue is added at a concentration of 1.44 mg/mL. An example recipe is 0.3 g HydroMed™ D3, 2.5 mL 95% ethanol, and 600 µL (6 mg/mL in ethanol) bromothymol blue. The mixture is placed on the 360° sample rotator for an additional 3 hours to ensure homogenous distribution of bromothymol blue throughout the polymer mixture. The mixture is then carefully poured onto a glass microscope slide and placed into a vacuum chamber for 12 hours to evacuate air bubbles and evaporate ethanol.

To detach film from glass slide, it is submerged in pH 5 buffer for 30 minutes. Once detached, film is carefully dried using a Kimwipe (KIMTECH™, Roswell, GA, USA), and secured over-top of the UL film using cyanoacrylate glue on the left and right outer edges.

4.7.7 Characterization of Nile Red Film

Nile red film is prepared as described in 5.4.4 section of Methods. Film is then placed, face down, on the microscope stage (DMI 5000, Leica Microsystems, Germany), centered over the objective lens. The film is irradiated from the top with a UV flashlight (395 nm, EscoLite, La Palma, CA, USA), held using a ring stand and clamp, ~ 10 cm from the sample in a perpendicular orientation. A 5X objective lens directs light to a spectrometer (DNS

300, DeltaNu, Laramie, WY, USA) to collect spectral data. An exposure time of 0.01 s is used, and the spectra is collected immediately after UV flashlight is switched off (to collect fluorescence only from nile red excited by $SrAl_2O_4$:Eu, Dy, and eliminate any direct excitation of the nile red dye by UV). A background spectrum is collected in the same way, and subtracted from the fluorescence spectra, manually, in Microsoft Excel. Each spectrum is plotted as an average of three spectra acquired back-to-back. To obtain spectra of the film at pH 5, 7, and 9, the film is submerged in the corresponding phosphate buffered saline (Standard Buffer, BDH LLC, Minneapolis, MN, USA) solution for 30 minutes prior to acquiring spectra. Measurement of pH is done with a pH electrode (Mettler Toledo InLab® Routine Pro, Columbus, OH) and pH meter (6230 N JENCO, San Diego, CA), calibrated at pH 4.0, 7.0, and 10.0.

4.7.8 Preparation of All-in-One pH Sensitive ULCI film

All recipe calculations are based on the total volume of solvent (dichloromethane) chosen and does not account for volume changes due to the addition of individual components. To fabricate the pH sensitive all-in-one target, HydroMed™ D3 (120 mg/mL) is first added to dichloromethane. The mixture is placed on a 360° sample rotator for 24 hours to completely dissolve polymer. The following components are added once HydroMed™ is dissolved: $SrAl_2O_4$:Eu, Dy (300 mg/mL), Nile Red (0.04 mg/mL), and bromothymol blue (0.6 mg/mL). An example recipe is 3 g $SrAl_2O_4$:Eu, Dy, 1.2 g HydroMed™ D3, 10 mL dichloromethane, 400 µL Nile Red (1 mg/mL in acetone), and 1

mL bromothymol blue in ethanol (6 mg/mL). The mixture is then placed on the 360°

sample rotator for 3 hours, to ensure homogeneous combination of all components. The

mixture is then carefully poured onto a glass microscope slide and placed into a vacuum

chamber for 12 hours to evacuate air bubbles and evaporate solvent. To remove film from

glass slide, the film and slide are placed into a petri dish with pH 7 phosphate buffered

saline for 3 hours. The film automatically detaches from the glass slide as it absorbs water.

To fabricate the control film the same recipe is used, without the addition of Nile

red and bromothymol blue dyes. An example recipe is 3 g $SrAl_2O_4$: Eu, Dy, 1.2 g

HydroMed^{TM} D3, and 10 mL dichloromethane. The mixture is then placed on the 360°

sample rotator for 3 hours, to ensure homogeneous combination of all components. Then

the mixture is carefully poured onto a glass microscope slide and placed into a vacuum

chamber for 12 hours to evacuate air bubbles and evaporate solvent. To remove film from

glass slide, the film and slide are placed into a petri dish with pH 7 phosphate buffered

saline for 3 hours. The film automatically detaches from the glass slide as it absorbs water.

The target holder is fabricated using a self-sealing laminating pouch (LS851-10G.

Scotch^{TM} Self-Sealing Laminating Pouches, Business Card Size, 2-inch x 3.5 inches, 3M,

St. Paul, MN, USA). The target windows are created before placing the films into the

laminating pouch. First, black duct tape is applied to the front side of the laminating pouch

in a single layer (Duck 1265013 Black Color Duct Tape, Duck Brand, Avon, OH, USA).

This serves to block luminescence from any film in the laminating pouch that is not in the

defined target window. To generate the target windows, a single hole punch is used to

create two holes (8 mm in diameter, each). The holes are punched through the front and

back layers of the laminating pouch. The pH sensitive film, and control film, are roughly cut into ~10 mm diameter circles and placed inside the laminating pouch, centered over the target window (on the back side of the laminating pouch). The protective sheet on the inside of the top layer is removed and carefully applied to the bottom layer, over the two films still centered over the target window. This target holder design serves to hold the UL films in place at the edges (without the use of cyanoacrylate glue), hold the targets stationary while they are submerged in pH buffer for ULCI scanning, and expose films to changing pH in surrounding fluid (which permits color change in pH sensitive film).

4.7.9 pH Sensor Response Characterization

ULCI film response to pH was characterized using the same Leica microscope and DeltaNu spectrometer described in section 5.4.7 of Methods. **Figure 4.11** is a schematic of the setup, with the separate UL film and pH sensitive PEG hydrogel target as an example. The target is placed face down on the microscope stage, so the UV flashlight irradiates the UL film from underneath, and the light collected by the objective is only the light that has passed through the pH sensitive target. A black piece of carboard, with a hole the same size and shape as the target, is used to block UV and fluorescent light from the UL film that has not passed through the pH sensitive target.

For the UL film coated with cerise Krylon™ spray paint, and the pH sensitive PEG hydrogel, spectra are acquired at pH's 4.0, 6.0, 6.5, 7.0, 7.5, 8.0, and 9.0. The film was submerged in the corresponding buffer (Standard Buffer, BDH) for 30 minutes prior to

Figure 4.11 Depicts microscope setup for characterization of pH sensitive ultrasound luminescent films. UL film is deposited onto glass slide, followed by deposition of pH sensitive film. Film is centered face down over the microscope objective so that UV excitation is incident on the UL film from above, luminescence passes through the pH sensitive film, and the pH modulated luminescence signal passes through the objective and collected by the spectrometer from below.

spectra acquisition to ensure complete color change of pH sensitive target. An exposure time of 0.005 s was used. Spectra are normalized to 700 nm from pH 4.

For the HydroMed™ D3 2-part film, containing nile red and bromothymol blue layers, spectra are acquired at pH's 5.0, 6.0, 7.0, 7.5, 8.0, 8.5, and 9.0. The film was submerged in the corresponding buffer (Standard Buffer, BDH) for 30 minutes prior to spectra acquisition to ensure complete color change of pH sensitive target. An exposure time of 0.00003 s was used. Spectra are normalized to 750 nm from pH 7.5.

For the all-in-one film, spectra are acquired at pH's 6.0, 6.5, 7.0, 7.5, 8.0, 8.5, and 9.0. The film was submerged in the corresponding b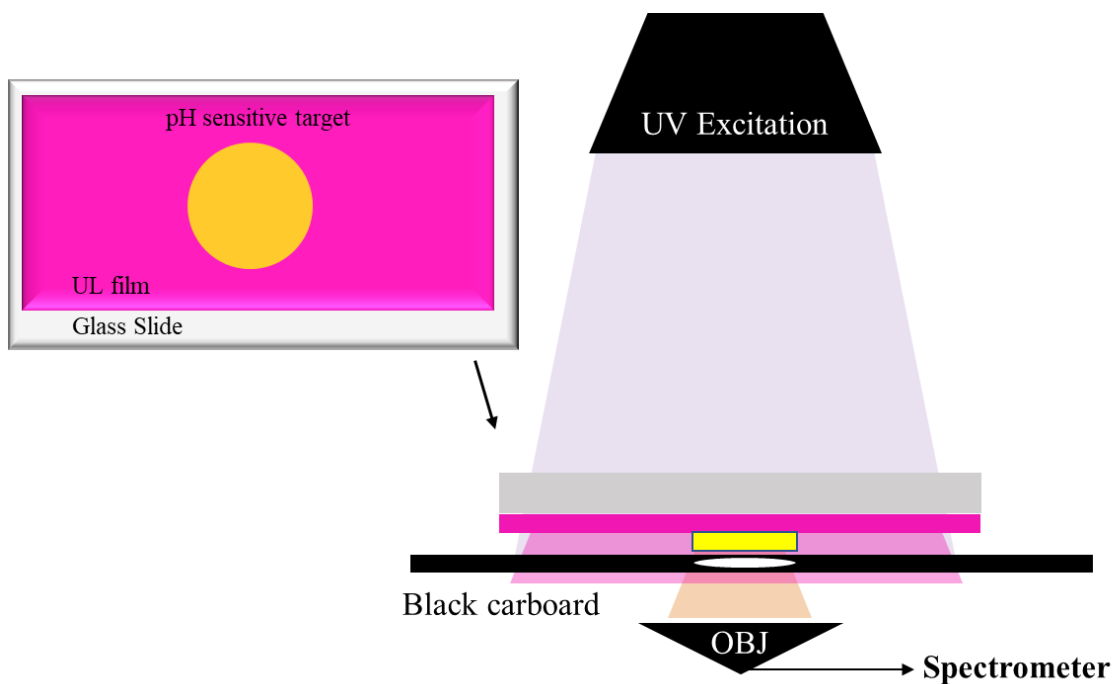uffer (Standard Buffer, BDH) for 30 minutes prior to spectra acquisition to ensure complete color change of pH sensitive target.

An exposure time of 0.05 s was used. Measurement of pH for each experiment is done using the pH electrode and meter described in section 5.4.6 of Methods. Spectra are normalized to the intensity of pH 6.5 at 475 nm, and 3 iterations of gaussian smoothing are performed (averaged over a window size of 3).

4.7.10 ULCI Scanning and pH Mapping

ULCI film is first attached to the bottom of an 8" x 8" glass dish (Easy Grab Baking Dish, Pyrex®, Corning, NY, USA) using Scotch tape, then filled with 1.5 L PBS (P4417-100TAB, Sigma Aldrich, St. Louis, MO, USA). The pH of this solution is adjusted using 0.1 M hydrochloric acid (HCl) and 0.1 M sodium hydroxide (NaOH). Measurement of pH for each experiment is done using the pH electrode and meter described in section 5.4.6 of Methods. To mimic scattering effects of biological tissue, powdered coffee creamer is added to the solution (1 g/L) (Coffee-Mate Original Powder Coffee Creamer, Nestle, Arlington, VA, USA).

The scanning system itself is a modified version of setup used for XELCI.. The glass dish is positioned on an x-y motorized stage (Models: LTS300 and LTS150, Thorlabs Inc., Newton, NJ, USA) such that the sample is aligned with ultrasound focus and light collection optics. Below the transparent platform of the stage, UV LED strip lights (385-400 nm) are taped to charge the UL film prior to scanning (Ontesik 20 ft LED Black Light Strip Kit, Amazon, Seattle, WA, USA) (**figure 4.12**). The collimated ultrasound beam is generated by a mist-maker with approximately 3 mm diameter spot size. Initial testing was done using the mist-maker removed from a basic humidifier (unknown make and model),

and later iterations of testing use a mist/fog maker (Aluminum Mist Maker, AGPTEK, Brooklyn, NY, USA) purchased individually. Light is collected using a liquid light guide (Model 77638, Newport Corporation, Irvine, CA, USA) attached to a 50/50 beam splitter containing photomultiplier tubes (PMTs) (Model P25PC-16, SensTech, Surrey, UK) with 625 nm and 705 nm band-pass filters. The beam splitter is an artifact of the XELCI setup, and the readout from 620 nm filter is the signal used to generate images in this study (**figure 4.12**). PMT pulses are counted with a data acquisition board (DAQ) (NI cDAQ™-9171, National Instruments, Austin, TX, USA). The stage is controlled with a custom program written in LabVIEW (National Instruments, Austin, TX, USA). This program also records PMT output and position of stage versus time, displaying the image as it is being acquired. More nuanced description of the scanning system can be found in previously published work.[16]

For image acquisition and scanning, the film is first charged with the UV strip lights for 1 minute, and imaging is initiated 30 s after switching the UV lights off. The mist-maker/ultrasound and liquid light guide are held stationary while the sample inside the glass dish is raster scanned using the stage beneath (**figure 4.3a**). A scan speed of 1 mm/s is used. All imaging components are housed inside a light tight box, with controls outside the box. Images are exported and analyzed using custom MATLAB scripts.
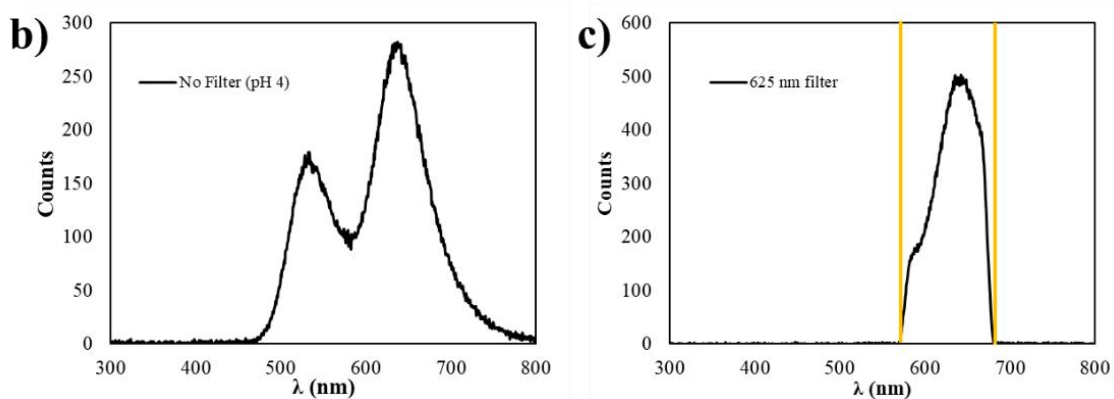
Figure 4.12 a) UV strip lights secured beneath the ULCI scanning setup for consistent excitation before each scan. **b)** and **c)** Depict luminescence spectrum of all-in-one film with and without 625 nm filter. 625

4.7.11 Ultrasound Modulation

Ultrasound output is pulsed by switching the direct current to the transducer on and off, using a field-effect transistor (FET) (IRFP260N, Infineon Technologies, Neubiberg, Germany). The FET is coupled in series on the ground leg of a 24 V, direct current, power supply. This allows the FET to have ground reference, thereby simplifying connection to external function generator (DS345, Stanford Research Systems, Sunnyvale, CA, USA).

The function generator is programmed to output a square wave with 5 V amplitude, and frequency of 2 Hz.[11]

4.8 Conclusions and Future Work

We designed a series of ultrasound luminescent, pH sensitive films, which were imaged in aqueous media using ULCI scanning. 2-layer films, with primary layer containing mechanoluminescent $SrAl_2O_4$:Eu, Dy and either Krylon™ fluorescent spray paint or nile red fluorescent dye, and secondary layer containing pH sensitive bromothymol blue, show sensitive pH response between 6.0 and 8.0. However, attachment of the two layers to one another has proven difficult. As a result, we developed an all-in-one pH sensor film. This film contains HydroMed™ D3, $SrAl_2O_4$:Eu, Dy, nile red, and bromothymol blue. After characterization of solvatochromic nile red at pH's 5, 7 and 9, we found that the shifted signal at 638 nm is modulated effectively by bromothymol blue. This film is sensitive to changes in pH between 6.0-8.0 and is easy to fabricate.

While our findings are promising, there are various avenues for improvement. One example is the challenge of finding a reliable, inexpensive, focused ultrasound source. Initial testing was done using the mist-maker component of a commercial humidifier, but this is not reproducible. We have purchased inexpensive mist-makers, and modified the electronic components for controlled pulsing, but these sources either burn out within a few days, or do not produce a focused spot appropriate for ULCI imaging. We are currently working to identify and fix these issues in the ultrasound sources we have and are also seeking new sources.

For imaging in aqueous scattering media (tissue mimic), we used a concentration of 1 g/L powdered coffee creamer. 1 g/L is an approximate concentration of 0.1%, and literature states that 3.5% milk has a scattering coefficient (25.0 cm^{-1}) comparable to skin epidermis (30.0 cm^{-1}) and well above that of muscle (7.5 cm^{-1}) and whole blood (12.0 cm^{-1}). To have a more accurate representation of the effect of biological tissue, Intralipid (1%) or a higher fat % milk product may be used in the future. In addition, black India Ink (0.3 µL/mL) can be added to mimic absorption properties of tissue.[27]

Lastly, we plan to optimize the optical setup and collection efficiency, as well as determine the best ultrasound pulse frequency for imaging. We are currently using a 50/50 beam splitter with filters optimized for use with $Gd_2O_2S:Eu^{3+}$, which has emission peaks at ~620 nm and 700 nm. The 50/50 beam splitter will be more useful with an alternative filter that collects light within a region of the $SrAl_2O_4:Eu$, Dy spectrum independent of changes in pH. For example, in addition to the 625 nm filter that collects the pH modulated signal, a filter in the 475 nm or 750 nm could potentially serve as a reference. The ratio of reference wavelength emission to pH modulated wavelength emission can be used to account for scattering and absorption due to the presence of biological tissue (or mimics). In addition, positioning of the liquid light guide and ultrasound source can be optimized with respect to excitation and collection efficiency. A custom holder can then be fabricated to maintain optimized positioning and aid reproducibility.

This series of studies demonstrates proof of concept for an ultrasound luminescence based chemical imaging methodology, applied for imaging changes in pH. Localized acidosis is associated with implant associated infection, and an ultrasound-based method

to probe the chemical environment of the implant surface would be useful to detect infection at an early stage. With improvement to sensor design, light collection, and imaging setup, we hope to investigate this sensor in an animal model of infection in the future.

4.9 References

[1]   C. Pan, Z. Zhou, X. Yu, *J. Orthop. Surg.* **2018**, *13*.

[2]   R. M. Mody, M. Zapor, J. D. Hartzell, P. M. Robben, P. Waterman, R. Wood-Morris, R. Trotta, R. C. Andersen, G. Wortmann, *J. Trauma Acute Care Surg.* **2009**, *67*, 758.

[3]   M. Ribeiro, F. J. Monteiro, M. P. Ferraz, *Biomatter* **2012**, *2*, 176.

[4]   B. Li, T. J. Webster, *J. Orthop. Res.* **2018**, *36*, 22.

[5]   P. S. Stewart, *Int. J. Med. Microbiol.* **2002**, *292*, 107.

[6]   P. S. Stewart, *Microbiol. Spectr.* **2015**, *3*.

[7]   N. Høiby, T. Bjarnsholt, M. Givskov, S. Molin, O. Ciofu, *Int. J. Antimicrob. Agents* **2010**, *35*, 322.

[8]   H. Chen, D. C. Colvin, B. Qi, T. Moore, J. He, O. T. Mefford, F. Alexis, J. C. Gore, J. N. Anker, *J. Mater. Chem.* **2012**, *22*, 12802.

[9]   J. C. Gore, T. E. Yankeelov, Todd. E. Peterson, M. J. Avison, *J. Nucl. Med.* **2009**, *50*, 999.

[10]   F. Wang, Y. Raval, H. Chen, T.-R. J. Tzeng, J. D. DesJardins, J. N. Anker, *Adv. Healthc. Mater.* **2014**, *3*, 197.

[11]   S. Bhattacharya, G. Schober, U. Uzair, M. Reel, H. Behlow, L. V. Abbaraju, A. M. Rao, J. Anker, **2020**.

[12] J. Xia, J. Yao, L. V. Wang, *Electromagn. Waves Camb. Mass* **2014**, *147*, 1.

[13] Z. Wang, Y. Liu, Z. Huang, M. Fang, X. Wu, *Mater. Res. Express* **2018**, *5*, 096202.

[14] M. Saleem, R. Neema, M. Mittal, P. K. Sharma, **2015**, *3*, 7.

[15] H. H. Jaffe, A. L. Miller, *J. Chem. Educ.* **1966**, *43*, 469.

[16] D. Benza, U. Uzair, Y. Raval, T.-R. J. Tzeng, C. J. B. M.d, J. N. Anker, In *Frontiers in Biological Detection: From Nanosensors to Systems IX*, SPIE, **2017**, pp. 43–51.

[17] U. Uzair, D. Benza, C. J. Behrend, J. N. Anker, *ACS Sens.* **2019**, *4*, 2367.

[18] C. Li, L. V. Wang, *Appl. Phys. Lett.* **2008**, *93*, 033902.

[19] H. Shankar, P. S. Pagel, D. S. Warner, *Anesthesiology* **2011**, *115*, 1109.

[20] C. M. Vitale, S. Gutovitz, In *StatPearls*, StatPearls Publishing, Treasure Island (FL), **2022**.

[21] J. M. Langman, *Pathology (Phila.)* **1994**, *26*, 301.

[22] P. Greenspan, S. D. Fowler, *J. Lipid Res.* **1985**, *26*, 781.

[23] V. Martinez, M. Henary, *Chem. - Eur. J.* **2016**, *22*, 13764.

[24] S. Liu, Q. Wu, B. Bai, Y. Ma, M. Wei, X. Yin, K. Neeves, In *All Days*, SPE, Tulsa, Oklahoma, USA, **2014**, p. SPE-169111-MS.

[25] N. Ghoneim, *Spectrochim. Acta. A. Mol. Biomol. Spectrosc.* **2000**, *56*, 1003.

[26] Y. T. Konttinen, M. Takagi, J. Mandelin, J. Lassus, J. Salo, M. Ainola, T.-F. Li, I. Virtanen, M. Liljeström, H. Sakai, Y. Kobayashi, T. Sorsa, R. Lappalainen, A. Demulder, S. Santavirta, *J. Bone Miner. Res.* **2001**, *16*, 1780.

[27] M. Z. Vardaki, N. Kourkoumelis, *Biomed. Eng. Comput. Biol.* **2020**, *11*, 1179597220948100.

CHAPTER 5

CONCLUSIONS AND FUTURE DIRECTIONS

In this dissertation we describe methods to make chemical measurements, through tissue, using phosphorescent materials. Crystalline phosphorescent materials, such as $Gd_2O_2S:Eu^{3+}$, emit bright luminescence with high quantum efficiency (60,000 photons per MeV for bulk $Gd_2O_2S:Eu^{3+}$), when excited by ionizing radiation such as X-Ray, UV, or beta-radiation. Luminescence, especially in the red range of wavelengths, is highly suitable for imaging through tissue.[1] In this dissertation luminescence intensity has been used as a quantitative indicator for radiolabeled drug concentration, and as an indicator of pH when paired with appropriate dye combinations.

In chapter 2 we demonstrated a method to image and quantify radiolabeled drug release from a biomedical implant surface using a radioluminescent polymer film composite and CCD camera. We applied this general method in measuring beta-emitting, ^{3}H-vancomycin concentration on the surface of a locking compression plate conformally coated with $Gd_2O_2S:Eu^{3+}$ radioluminescent microparticles. Radioluminescence increases linearly with concentration of ^{3}H-vancomycin (R^2=0.99). As drug is released from the implant surface we are able to quantitatively measure the amount remaining by comparing luminescence changes in the analyte modulated region to a luminescent control region with a known amount of encapsulated ^{3}H.[2]

Monitoring antibiotic release (or accumulation) at the implant surface is useful because biofilm related infections are not usually eradicated with traditional administration

of intravenous or oral antibiotics.[3,4] There is a significant amount of research in developing drug/device combinations that will effectively prevent and/or treat implant associated infection[5–8], but the ability to monitor that drug release in the body is of equal importance. Drug release, in any treatment paradigm, needs to be within a therapeutic dosage window to be effective.[9] As a result, this method may be useful in combination with polymer-based drug release strategies that have already been designed for a variety of different diseases (i.e. prostate cancer[10], breast cancer, Alzheimer's[11], malignant brain tumors[12], osteosarcoma[13], glioblastomas[14], and hepatomas[15]). An advantage of the described approach is the use of tritium as an analyte label. Hydrogen atoms are ubiquitous in any carbon-based structure, which includes most drug molecules. Incorporation of ^{3}H should not interfere with drug action and provides an analyte specific label for tracking via radioluminescence. The primary hurdle for generalizing this method for alternative implant drug release applications will be the incorporation of radioluminescent material.

The ability to monitor drug release from biomedical implant surfaces is of great importance, but nanomaterials for targeted drug delivery also tend to lack quantitative, *in vivo,* monitoring capability. In chapter 3 we extended the work done in chapter 2 to provide proof of principle for monitoring drug release using radioluminescent nanoparticles and radiolabeled drugs. Again, the drug release motif tackled in this work targets implant associated infection. Sodium fluoride (NaF) doped $Gd_2O_2S:Eu^{3+}$ nanoparticles are synthesized and successfully functionalized with silane-PEG5000-biotin. Anti-vancomycin IgM is streptavidin labeled for direct attachment of antibodies to biotin labeled nanoparticles. In dried samples of $Gd_2O_2S:Eu^{3+}$ nanoparticles, there is a linear response

between luminescence intensity and concentration of ^{3}H-vancomycin. Nanoparticles in aqueous suspension did not display the same luminescence response, but this is likely due to unsuccessful functionalization with anti-vancomycin IgM. If anti-vancomycin is not attached to the nanoparticles, we do not expect ^{3}H-vancomycin to bind, and would not expect a luminescence signal.

While the luminescence response of synthesized nanoparticles to ^{3}H-vancomycin is incredibly sensitive (LOD=7.8 nCi=0.4 ng vancomycin), the response needs to be demonstrated and characterized in aqueous suspension to be useful for *in vivo* application. For this reason, the functionalization strategy is the first point of improvement in this project. A simple approach to address this is layer-by-layer alternating deposition of complementary biodegradable polymers (e.g. polyethylene glycol, polysorbate 80, polylactic acid, polyethyleneimine, sodium alginate, or poly-co-glycolide) mixed with radiolabeled analyte.[16–18] For example, negatively charged sodium alginate (AL), and positively charged polyethyleneimine has been coated onto nanoparticles to prevent fusion during annealing, and addition of ^{3}H labeled analyte would be a simple modification.[19] In theory, this simple coating mechanism will bring ^{3}H-analyte in close enough proximity to the nanoparticles to excite luminescence.

Using radioluminescent materials to quantitatively monitor drug release has been the primary objective for chapters 2 and 3, while chapter 4 describes the use of mechanoluminescence for measurement of pH. Bacterial metabolic fermentation produces lactic and carbonic acid through the glycolysis pathway and, as a result, local acidosis is an indication of bacterial infection *in vitro*.[20] Development of a sensor that can probe the

biochemical environment at the implant surface can be used in tandem with drug release coatings to evaluate treatment efficacy. In chapter 4 we describe the design of ultrasound luminescent, pH sensitive films, which are imaged using a stationary ultrasound excitation source and collection optics. $SrAl_2O_4$:Eu, Dy emits luminescence, with a maximum at ~522 nm, and the emission can be red shifted using either Krylon[TM] fluorescent spray paint or Nile red fluorescent dye. By red shifting the emission spectrum of $SrAl_2O_4$:Eu, Dy, pH sensitive bromothymol blue modulates the luminescence intensity as pH changes between 4-8.

One drawback for ultrasound luminescent chemical imaging, as currently designed, is that $SrAl_2O_4$:Eu, Dy (and any mechanoluminescent phosphor) requires UV charging prior to ultrasound imaging. Ultrasound does not directly excite the mechanoluminescent film, to our knowledge, but serves to release trapped electron hole pairs. Release of these trapped electrons (and holes) results in luminescence emission, but the "trapping" process
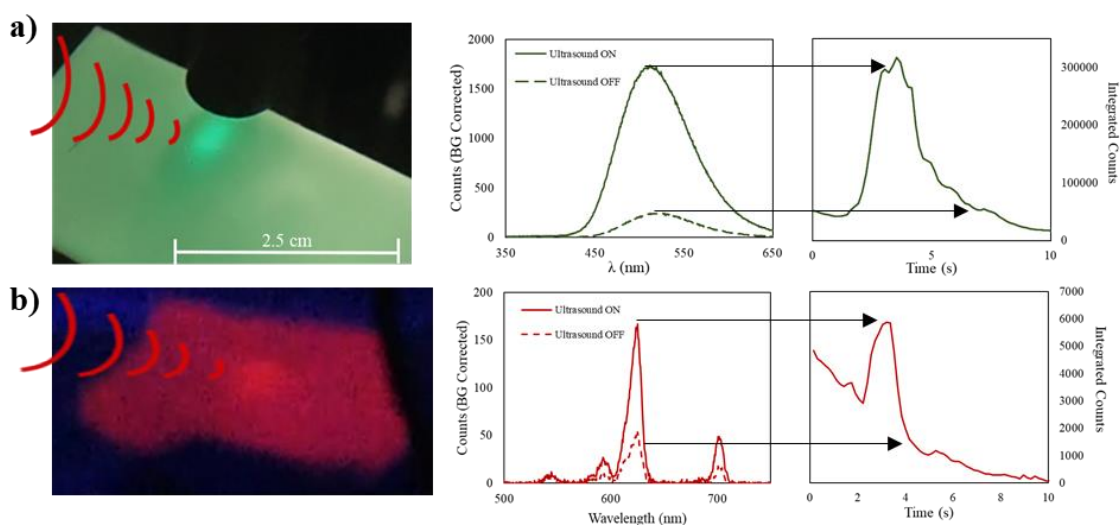

Figure 5.1. a) Ultrasound excited luminescence of $SrAl_2O_4$:Eu, Dy embedded in PDMS. Plots show film behavior as ultrasound is pulsed on and off, after initial excitation with UV (395 nm). b) Ultrasound excited luminescence of Gd_2O_2S:Eu embedded in PDMS. Plots show film behavior as ultrasound is pulsed on and off.

occurs after initial excitation, e.g., from UV/Visible light.[21–23] This sensor is designed for use *in vivo*, and incorporating a UV excitation source poses a significant challenge. Alternatively, we are investigating the possibility that ^3H can serve as an encapsulated excitation source for mechanoluminescent $SrAl_2O_4$:Eu, Dy. This would provide a consistent, internal, excitation source and permit ultrasound imaging without prior UV excitation.

There is reason to suspect that mechanoluminescent phosphors, such as $SrAl_2O_4$:Eu, Dy, may be excited by beta radiation. Radioluminescent Gd_2O_2S:Eu has exhibited mechanoluminescence when exposed to a focused ultrasound source (**Figure 5.1**). Both $SrAl_2O_4$:Eu, Dy and Gd_2O_2S:Eu phosphoresce after exposure to UV, and release luminescence as a direct response to mechanical stimuli (i.e., ultrasound). Besides using ^3H as an internal excitation source to improve pH sensor design, we also plan to image radiolabeled drug release using the ULCI scanning setup. The changes in luminescence intensity can be imaged, point by point, using pulsed ultrasound excitation. In this way, the individual imaging modalities developed in this work may be combined.

Overall, radio- and mechanoluminescent phosphors hold promise in design and development of chemical sensing for biomedical application. The various mechanisms that illicit luminescence in phosphorescent materials are still being investigated. With improvements in light collection, sensor design, and functionalization strategies, the application potential for biomedical application of phosphorescent materials in boundless.

References

[1] S. L. Jacques, *Phys. Med. Biol.* **2013**, *58*, R37.

[2] G. B. Schober, J. N. Anker, *Adv. Funct. Mater.* **2022**, *32*, 2106508.

[3] T.-F. C. Mah, G. A. O'Toole, *Trends Microbiol.* **2001**, *9*, 34.

[4] P. S. Stewart, *Int. J. Med. Microbiol.* **2002**, *292*, 107.

[5] J. A. Lyndon, B. J. Boyd, N. Birbilis, *J. Controlled Release* **2014**, *179*, 63.

[6] E. M. Hetrick, M. H. Schoenfisch, *Chem. Soc. Rev.* **2006**, *35*, 780.

[7] M. Wang, T. Tang, *J. Orthop. Transl.* **2019**, *17*, 42.

[8] C. Pan, Z. Zhou, X. Yu, *J. Orthop. Surg.* **2018**, *13*, 220.

[9] A. Santos, M. Sinn Aw, M. Bariana, T. Kumeria, Y. Wang, D. Losic, *J Mater Chem B* **2014**, *2*, 6157.

[10] H. Brem, S. Piantadosi, P. C. Burger, M. Walker, R. Selker, N. A. Vick, K. Black, M. Sisti, S. Brem, G. Mohr, P. Muller, R. Morawetz, S. C. Schold, *The Lancet* **1995**, *345*, 1008.

[11] R. Mashayekhi, H. Mobedi, J. Najafi, M. Enayati, *DARU J. Pharm. Sci.* **2013**, *21*, 57.

[12] O. Kubo, H. Himuro, N. Inoue, Y. Tajika, T. Tajika, T. Tohyama, M. Sakairi, M. Yoshida, I. Kaetsu, K. Kitamura, *No Shinkei Geka.* **1986**, *14*, 1189.

[13] S. Miura, Y. Mii, Y. Miyauchi, H. Ohgushi, T. Morishita, K. Hohnoki, M. Aoki, S. Tama, Y. Konishi, *Jpn. J. Clin. Oncol.* **1995**, *25*, 61.

[14] H. Brem, M. G. Ewend, S. Piantadosi, J. Greenhoot, P. C. Burger, M. Sisti, *J. Neurooncol.* **1995**, *26*, 111.

[15] R. Yamashita, *Nihon Geka Gakkai Zasshi* **1987**, *88*, 401.

[16] R. Singh, J. W. Lillard, *Exp. Mol. Pathol.* **2009**, *86*, 215.

[17] A. Santos, M. Caldas, P. Pattekari, C. Fontes Ribeiro, A. Jose Ribeiro, Y. Lvov, F. Veiga, In *Design and Development of New Nanocarriers*, Elsevier Science & Technology, **2018**, pp. 595–635.

[18] S. K. Sahoo, V. Labhasetwar, *Drug Discov. Today* **2003**, *8*, 1112.

[19] H. Chen, B. Qi, T. Moore, D. C. Colvin, T. Crawford, J. C. Gore, F. Alexis, O. T. Mefford, J. N. Anker, *Small* **2014**, *10*, 160.

[20] F. Wang, Y. Raval, H. Chen, T.-R. J. Tzeng, J. D. DesJardins, J. N. Anker, *Adv. Healthc. Mater.* **2014**, *3*, 197.

[21] Y. Jia, M. Yei, W. Jia, *Opt. Mater.* **2006**, *28*, 974.

[22] A. J. Walton, *Adv. Phys.* **1977**, *26*, 887.

[23] B. P. Chandra, A. S. Rathore, *Cryst. Res. Technol.* **1995**, *30*, 885.

Appendix A

MATLAB Analysis: Signal vs. Concentration/Dose
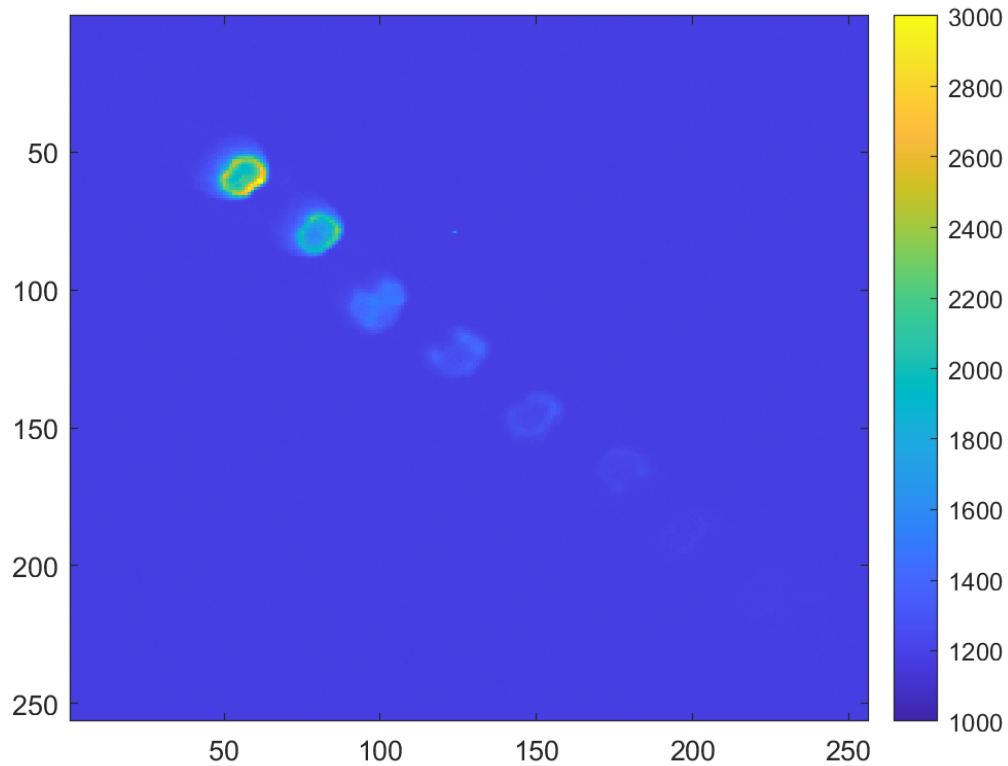
Figure A-1: Luminescence image acquired with IVIS Lumina, displayed in MATLAB. X and Y axes represent pixel number. Color bar represents luminescence intensity, scale adjusted to 1000-3000 counts. Fracture fixation plate oriented diagonally with highest ^{3}H-vancomycin concentration in the upper left-hand corner, decreasing toward the lower right-hand corner.

Use Data Tips in Matlab to determine ROIs:

S_01) X: 35, 65   Y: 40, 70

S_02) X: 65, 95   Y: 60, 90

S_03) X: 85, 115   Y: 90, 120

S_04) X: 110, 140   Y: 105, 135

S_05)   X: 135, 165   Y: 130, 160

S_06)   X: 165, 195   Y: 150, 180

S_07)   X: 180, 210   Y: 170, 200

S_08)   X: 205, 235   Y: 190, 220

S_B)   BLANK (left tip of implant) X: 19, 49   Y: 20, 50

S_RL) Background Left Side   X: 30, 60   Y: 175, 205

S_RR) Background Right Side   X: 170, 200   Y: 30, 60

For Matlab Code list values as (Y1:Y2,X1:X2):
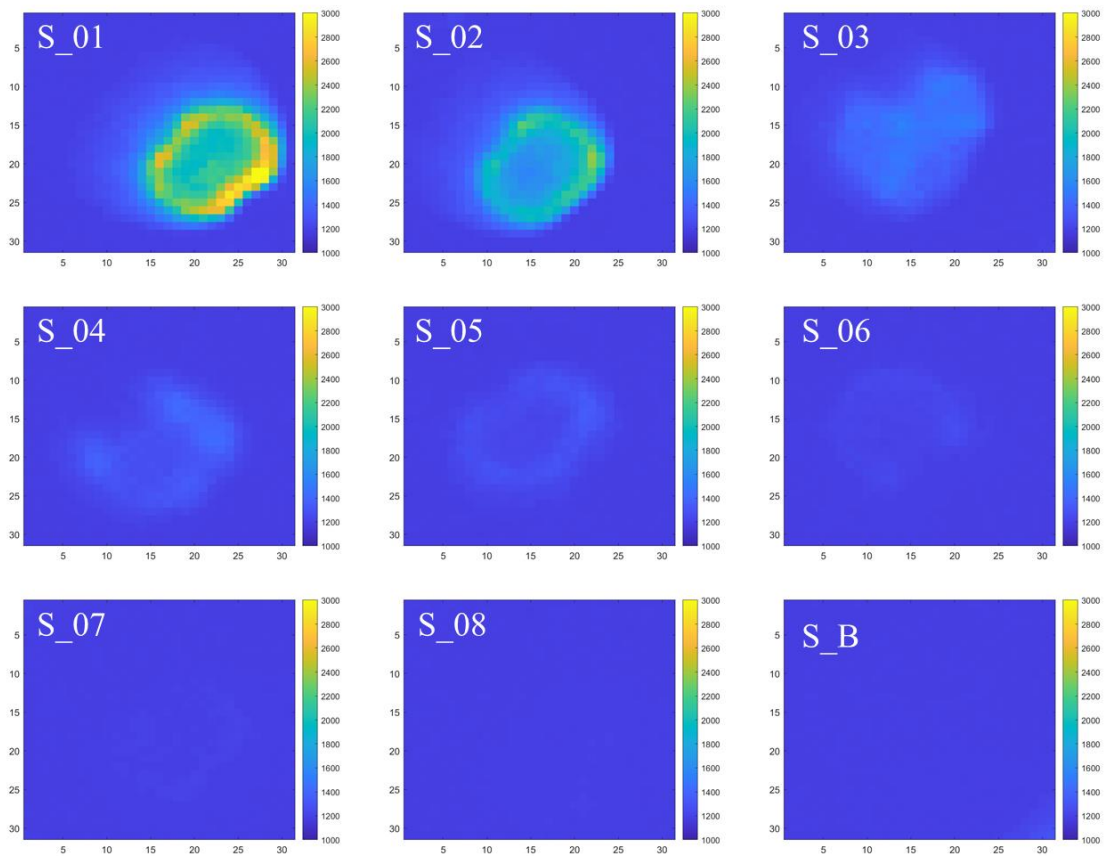
ex)   S_01=sum(sum(I_01(40:70, 35:65)));

Figure A-2: ROIs selected for image analysis, displayed as images.

CODE:

_____

% To open and display the image of interest (as shown in Figure A-1)
% caxis can be adjusted based on luminescence intensity of image

    >>A=imread('filename');
    >>figure; imagesc(A)
    >>caxis([1000 3000])

% Determine regions of interest (ROIs) using **data tips** feature once image is plotted
% Sum feature will add the total counts from each pixel within the defined   ROI

    >> S_01=sum(sum(I_01(40:70,35:65)))

    S_01 =

            1374866

    >> S_02=sum(sum(I_01(60:90,65:95)))

    S_02 =

            1276802

    >> S_03=sum(sum(I_01(90:120,85:115)))

    S_03 =

            1198175

    >> S_04=sum(sum(I_01(105:135,110:140)))

    S_04 =

            1165293

    >> S_05=sum(sum(I_01(130:160,135:165)))

    S_05 =

            1152091

```
>> S_06=sum(sum(I_01(150:180,165:195)))

S_06 =

        1141685

>> S_07=sum(sum(I_01(170:200,180:210)))

S_07 =

        1137329

>> S_08=sum(sum(I_01(190:220,205:235)))

S_08 =

        1135057

>> S_B=sum(sum(I_01(20:50,19:49)))

S_B =

        1134198

>> S_RL=sum(sum(I_01(175:205,30:60)))

S_RL =

        1131240

>> S_RR=sum(sum(I_01(30:60,170:200)))

S_RR =

        1131713
```

MATLAB Analysis: Drug Release
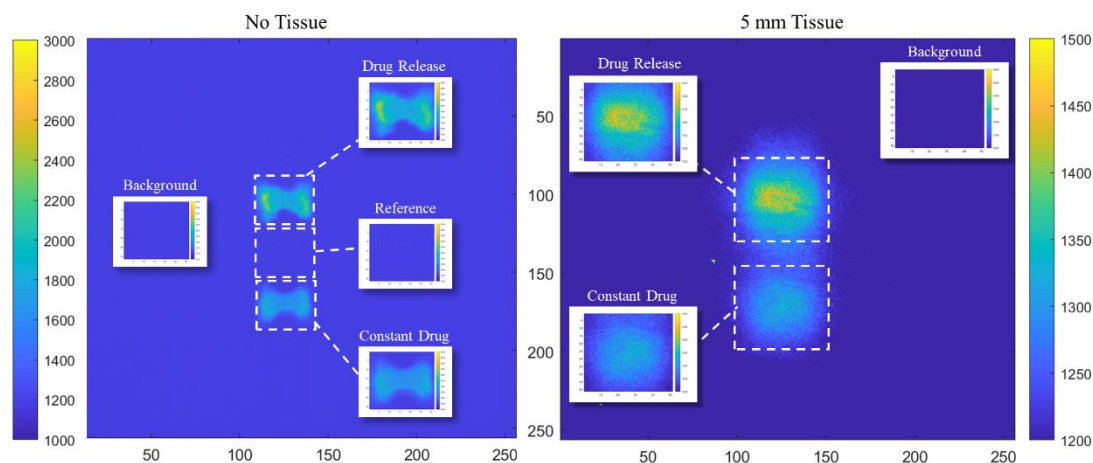
Figure B-1: Luminescence image acquired with IVIS Lumina, displayed in MATLAB. X and Y axes represent pixel number. Left-most image depicts primary drug release image without tissue, with insets depicting analyzed ROIs (30 x 30 pixels). Right-most image depicts primary drug release image through 5 mm tissue, with insets depicting analyzed ROIs (50 x 50 pixels). Color bars represent luminescence intensity, scale adjusted to 1000-3000 counts (on the left), and 1200-1500 (on the right).

Use Data Tips in MATLAB to determine ROIs

No Tissue: 30 x 30 pixel ROIs

Drug Release: X(110, 140)   Y(90, 120)

Reference: X(110, 140)   Y(122, 152)

Constant Drug: X(110, 140)   Y(155, 185)

Background: X(40, 70)   Y(100, 130)

5 mm Tissue: 50 x 50 pixel ROIs

Drug Release: X(100, 150)   Y(80, 130)

Constant Drug: X(100, 150)   Y(145, 195)

Background: X(200, 250)   Y(1, 51)

For MATLAB Code list values as (Y1:Y2,X1:X2):

ex)   S_01=sum(sum(I_01(90:120, 110:140)));

CODE:

% To open and display the image of interest (as shown in Figure B-1)

% caxis can be adjusted based on luminescence intensity of image

```
>>I_dr01=imread('filename');
>>figure; imagesc(I_dr01)
>>caxis([1000 3000])
```

% Determine regions of interest (ROIs) using **data tips** feature once image is plotted

% Sum feature will add the total counts from each pixel within the defined ROI

% 3 images taken at each drug release point. This set of code is repeated for each set of 3 images for every drug release point, with and without tissue

%NO TISSUE

>> S_DR=sum(sum(I_dr01(122:152,110:140)))

S_DR =

   1145889

>> S_REF=sum(sum(I_dr01(122:152,110:140)))

S_REF =

   1145889

>> S_DR=sum(sum(I_dr01(90:120,110:140)))

S_DR =

   1510714

```
>> S_REF=sum(sum(I_dr01(122:152,110:140)))

S_REF =

    1145889

>> S_CON=sum(sum(I_dr01(155:185,110:140)))

S_CON =

    1367173

>> S_BG=sum(sum(I_dr01(100:130,40:70)))

S_BG =

    1136172

%5 MM TISSUE

>> S_5DR=sum(sum(I_tis01(80:130,100:150)))

S_5DR =

    3407745

>> S_5CON=sum(sum(I_tis01(145:195,100:150)))

S_5CON =

    3278816

>> S_5BG=sum(sum(I_tis01(1:51,200:250)))

S_5BG =

    3090638
```
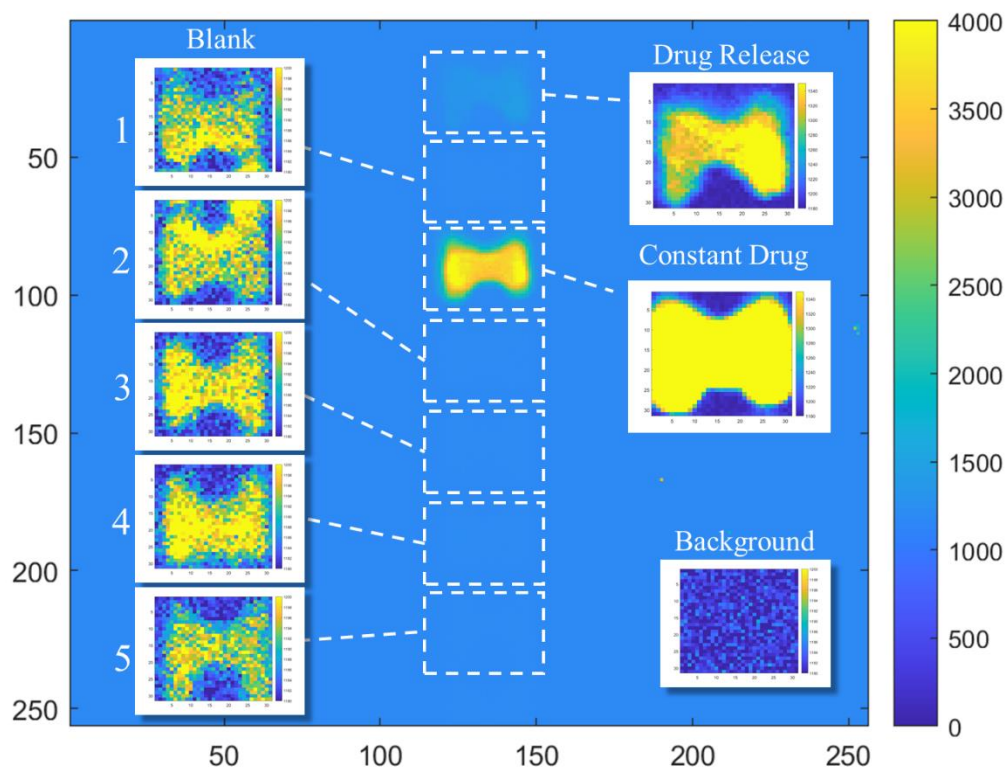
MATLAB Analysis: Analysis of Blank Regions for LOD

Figure C-1: Luminescence image acquired with IVIS Lumina (120 s exposure), displayed in MATLAB. X and Y axes represent pixel number. Primary drug release image with additional blank regions coated along the length of the plate. Insets depicting analyzed ROIs (30 x 30 pixels). Color bars represent luminescence intensity, scale adjusted to 0-4000 counts for main image, 1180-1350 for drug release and constant regions, and 1180-1200 for blanks and background.

Use Data Tips in MATLAB to determine ROIs (30x30 pixels)

Drug Release: X(119, 149)   Y(11, 41)

Blank 1:   X(119, 149)   Y(42, 72)

Constant Drug: X(119, 149)   Y(74, 104)

Blank 2:   X(119, 149)   Y(105, 135)

Blank 3:   X(119, 149)   Y(139, 169)

Blank 4:   X(119, 149)   Y(170, 200)

Blank 5:   X(119, 149)   Y(205, 235)

Background: X(25, 55)   Y(70, 100)

For MATLAB Code list values as (Y1:Y2,X1:X2):

ex)   S_01=sum(sum(I_lod01(11:41, 119:149)));

CODE:
_____

% To open and display the image of interest (as shown in Figure C-1)

% caxis can be adjusted based on luminescence intensity of image

```
>>I_lod01=imread('filename');
>>figure; imagesc(I_lod01)
>>caxis([0 4000])
```


% Determine regions of interest (ROIs) using **data tips** feature once image is plotted

% Sum feature will add the total counts from each pixel within the defined ROI

% 10 images taken consecutively. This set of code is repeated for each image.

>> S120_1DR=sum(sum(I_lod01(11:41,119:149)))

S120_1DR =

    1222609

>> S120_1B1=sum(sum(I_lod01(42:72,119:149)))

S120_1B1 =

    1143948

>> S120_1CON=sum(sum(I_lod01(74:104,119:149)))

S120_1CON =

  2244833

>> S120_1B2=sum(sum(I_lod01(105:135,119:149)))

S120_1B2 =

  1145970

>> S120_1B3=sum(sum(I_lod01(139:169,119:149)))

S120_1B3 =

  1145010

>> S120_1B4=sum(sum(I_lod01(170:200,119:149)))

S120_1B4 =

  1145851

>> S120_1B5=sum(sum(I_lod01(205:235,119:149)))

S120_1B5 =

  1143093

>> S120_1BG=sum(sum(I_lod01(70:100,25:55)))

S120_1BG =

  1135315

Appendix D

Copyright Permission Concerns

For: G. B. Schober, J. N. Anker, *Adv. Funct. Mater.* **2022**, *32*, 2106508.

https://www.wiley.com/network/researchers/latest-content/how-to-clear-permissions-for-a-thesis-or-dissertation